Ph 10
(292/1961)

UDC 533.17:534.213.4-13:621.316.54

ACTA POLYTECHNICA SCANDINAVICA

PHYSICS INCLUDING NUCLEONICS SERIES No. 10

HAAKON FORWALD

Wave Phenomena in Compressed-Air Ducts

Swedish Contribution No. 12
Stockholm 1961

ACTA POLYTECHNICA SCANDINAVICA

. . . a Scandinavian contribution to international engineering sciences

Published under the auspices of the Scandinavian Council for Applied Research

in *Denmark* by the Danish Academy of Technical Sciences

in *Finland* by the Finnish Academy of Technical Sciences, the Swedish Academy of Engineering Sciences in Finland, and the State Institute for Technical Research

in *Norway* by the Norwegian Academy of Technical Science and the Royal Norwegian Council for Scientific and Industrial Research

in *Sweden* by the Royal Swedish Academy of Engineering Sciences, the Swedish Natural Science Research Council, and the Swedish Technical Research Council

Acta Polytechnica Scandinavica consists of the following sub-series:

- *Chemistry including Metallurgy Series, Ch*
- *Civil Engineering and Building Construction Series, Ci*
- *Electrical Engineering Series, El*
- *Mathematics and Computing Machinery Series, Ma*
- *Mechanical Engineering Series, Me*
- *Physics including Nucleonics Series, Ph*

For subscription to the complete series or to one or more of the sub-series and for purchase of single copies, please write to

ACTA POLYTECHNICA SCANDINAVICA PUBLISHING OFFICE

Box 5073
Stockholm 5
Phone 67 09 10

This issue is published by
THE ROYAL SWEDISH ACADEMY OF ENGINEERING SCIENCES
Stockholm, Sweden

UDC 533.17:534.213.4-13:621.316.54

Wave Phenomena in Compressed-Air Ducts

A theoretical and experimental investigation, with special reference to the conditions in air-blast circuit-breakers

By Haakon Forwald

Consulting Engineer for High-voltage Switchgear, ASEA, Ludvika

ACTA POLYTECHNICA SCANDINAVICA

PHYSICS INCLUDING NUCLEONICS SERIES Ph 10

(AP 292 1961)

UPPSALA 1961
APPELBERGS BOKTRYCKERI AB

CONTENTS

Page
Preface 5

A. Introduction 6

B. Introduction to elastic wave phenomena 8

C. Equations of state, motion and change in state 14
    Static-adiabatic change in state 16
    Dynamic-adiabatic change in state 17

D. Front equations 19
    I. Continuous fronts 19
    II. Discontinuous fronts (shock fronts) 25

E. Front propagation 28

F. Front reflection 35

G. Calculation of wave phenomena in conjunction with the rapid discharge of ducts 39
    I. Discharge of a duct only 39
    II. Discharge of a duct connected to a container 45

H. Calculation of wave phenomena in conjunction with the rapid charging of ducts 52
    I. Direct compression period 53
    II. Reflected compression period 56
    III. Direct expansion period 63
    IV. Reflected expansion period 67
    V. Example of calculation regarding the reflected compression period 67

J. Description of experimental arrangements 69
    I. Apparatus arrangements 69
        a. Arrangements for rapid discharge 70
        b. Arrangements for rapid charging 73
        c. Arrangements for free escape 76
        d. Opening members 77
    II. Measuring devices 86

K. Experiments with the rapid discharge of ducts 91
    I. Discharge of a duct only 91
        Arrangement 1: Operation by bursting diaphragms, full discharge opening 91
        Arrangement 2: Operation by bursting diaphragms, throttled discharge opening 93
        Arrangement 3: Operation by valve, throttled discharge opening 95
    II. Discharge of a duct connected to a container 98
        Arrangement 4: Operation by bursting diaphragms, full discharge opening 98
        Arrangement 5: Operation by bursting diaphragms, throttled discharge opening 101

L. Experiments with the rapid charging of ducts 104
  I. Operation by bursting diaphragms, 3″ tubes 104
    Arrangements 6–8: Tube closed at exterior end 104
    Arrangements 9 and 10: Tube open at exterior end 115
  II. Operation with valve, tube closed at exterior end 117
    Arrangements 11–14: 3″ tubes 117
    Arrangements 15–17: 2″ tubes 123
    Arrangement 18: 3″ tube with throttled inlet 124
    Arrangements 19 and 20: 3″ and 2″ tubes in succession 128
    Arrangement 21: 2″ and 3″ tubes in succession 131
    Arrangements 22 and 23: 1½″ and 1¼″ tubes 135

M. Experiments on the acceleration period of escaping air 136
    Arrangements 24 and 25 136

N. General considerations 140

Acknowledgement 141

Summary 141

Résumé 141

Zusammenfassung 142

Bibliography 143

The figures in square brackets refer to the bibliography after the article.

PREFACE

The theoretical investigations and the practical results described in this treatise were originally intended to serve as a basis for the development programme established at Asea for high-voltage air-blast circuit-breakers. Later on, it was ascertained that these investigations were of considerable value also in other technical fields and for this reason, therefore, the publication of this treatise has been considered justifiable. A contributory factor to this decision was that reports about measurements concerning transient pneumatic phenomena in ducts are rather scarce in the technical literature, whereas the number of theoretical investigations is very considerable.

Waves with high amplitudes travelling in ducts are generally subjected to a pronounced damping or attenuation due to friction and turbulence, which causes the wave phenomena to undergo considerable changes in relation to the ideal behaviour. Measurements taken under different conditions are therefore highly desirable also for the purpose of obtaining criteria concerning the influence of the damping factors. For this it is necessary that the ideal theoretical phenomena of the experimental arrangement should be known as exactly as possible. Since these wave phenomena are also rather complicated from the theoretical viewpoint, a relatively large proportion of this treatise has been devoted to the mathematical treatment of these phenomena. A comparison between the experimentally determined phenomena and the calculated ones has given, in several cases, interesting information regarding the influence of the damping. As a rule, the damping is not of great importance immediately after the transient phenomenon has been initiated, and comparisons for this period between results obtained from measurements and estimated results have generally led to good agreement.

This treatise also includes a certain amount of information of historical interest regarding the research into wave phenomena.

A. INTRODUCTION

Wave phenomena in gases have long been the subject of numerous investigations. The first theoretical studies of fundamental importance were presented about 1860 by Earnshaw [3] and Riemann [4] and are concerned mainly with continuous waves. Riemann treated also shock compression and assumed that this, like continuous compression, obeyed the adiabatic law of Poisson. Later on, this supposition was subjected to considerable criticism. Earnshaw maintained in his work that shock compression was a physical impossibility. In 1887 Hugoniot [10] propounded a theory for shock compression based on the conservation of energy and derived formulae for the propagation of shock waves which are still in use to-day. Lord Rayleigh [7] raised an objection in 1896 to Riemann's theory for shock compression, since he had found from energy investigations that such a compression was not physically possible. It does not appear as if Lord Rayleigh knew of the existence of the investigations made by Hugoniot. In a work published in 1910 [26] he refers, however, to an investigation of Rankine [5] from 1870, where the latter has arrived at principally the same results as Hugoniot by applying the laws of thermodynamics. Weber [27] in his work of 1912 (pp. 552–553) defends Riemann's investigations on shock compression and points out that the results obtained by both Riemann and Hugoniot can only be considered as being approximations of the real conditions, since, in the one case, a frictionless motion is assumed and, in the other case, heat transfer is neglected. Furthermore, Weber questions whether the equation of state can be considered as being directly applicable to gases in motion. Becker [29] treated in 1922 shock compression, taking into account both viscosity and heat transfer, and found that the theoretical results are confirmed, inter alia, by the experiments made by Stodola [14]. In addition, Bechert [43] made theoretical investigations in 1941 on shock compression and he has taken into consideration both friction and heat transfer. In this respect, reference can also be made to the works published in 1942 and 1943 by Sauer [53], and a paper presented by Brinkley and Kirkwood [64] in 1947.

Verification of the presence of shock compression from practical experiments was first obtained by Mach and Sommer [6], who described in 1877 measurements of the velocity of explosion waves. Wolff [12] described similar experiments in 1899 and stated that he found values conforming with Riemann's theory. In 1903 Stodola [14] established for the first time by pressure measurements the occurrence of a stationary compression shock in a de Laval nozzle.

The following may be of interest concerning earlier works describing experiments with travelling waves in ducts.

Vieille [13] described in 1899 experiments on waves in a tube having a diameter of 22 mm in which wave propagation was initiated by means of a bursting diaphragm. Pressures of up to about 30 atm abs. were applied to the one side of the diaphragm, with atmospheric pressure on the other side. The length of the experimental tube was about 2 m. The velocity of propagation of the wave front was found to be about 600 m/s at an initial pressure of 29 atm abs. for the outgoing wave front and about 190 m/s for the front after its reflection. The static pressure in the outgoing wave front was found to be 3.7 atm abs. The pressure was recorded by means of a mechanical arrangement with a rotating drum at several fixed points along the tube.

Kobes [24] investigated in 1910 wave velocities measured in train brake conduits having a length of several hundred metres. Experiments with resonance oscillations in pipes were described in papers by Schmidt [36] in 1935, Mayer-Schuchard [37] in 1936, and Lettau [38] in 1939. These oscillations were initiated by means of a pulsating piston at one end of the pipe. Pressure and velocity measurements were made at points spaced out at intervals of 2 m along a 10 to 12 m long pipe with an inner diameter of 70 mm. The maximum pressure amounted to a few tenths of an atmosphere and the maximum velocity of flow to about 50 m/s. The diagrams give evidence of the presence of shock fronts. Pfriem [45] in 1941 states that the above-mentioned resonance experiments have not been able to verify the theoretically derived laws of reflection due to their narrow measuring range and the consequently insufficient accuracy of measurement. In 1946 Payman and Shepherd [57] published results from experiments with shock waves produced by bursting diaphragms in an 1-in. tube with a length of about 1 m. Compressed air having a pressure of up to about 75 atm was applied to the one side of the diaphragm, whereas atmospheric pressure prevailed on the other side. The wave fronts were photographed according to the Schlieren method, which enabled the wave velocities to be determined. It was stated later that these show good conformity with the theoretically derived values.

Results from experiments when discharging to atmosphere from a tube of 2-in. bore were presented in 1948 in a paper by Bannister and Mucklow [76]. A pressure of up to about 10 atm was used and the maximum tube length was about 12 m. The pressure variations were recorded at points along the tube at intervals of about 3 m from one another. The measuring arrangement consisted of mirrors operated by means of diaphragms so as to deflect a beam of light dependent on the pressure. The experiment was initiated by causing a cellophane membrane to burst. The effects of friction were also treated in this paper. The purpose of the investigations was mainly to study the conditions in the exhaust pipes of internal combustion engines.

The experimental treatment of problems of this nature is best carried out in ducts having a constant cross-sectional area, since it is possible then to work with one-dimensional waves, which yield the simplest conditions required for a comparison with the theory. Such waves occur in practice, for example, in brake conduits and in the feed and exhaust pipes of internal combustion engines. More recently a new practical field has emerged, where the study of one-dimensional waves and their reflection has proved to be important. This aspect of the question is concerned with *air-blast circuit-breakers* for electric power installations. With circuit-breakers it is necessary, for example, for ducts having a length of about 10 m and a cross-sectional area of 200 cm^2 to be filled with compressed air having a gauge pressure of 15 atm within a few hundredths of a second. Very pronounced wave phenomena of both a continuous and discontinuous nature occur during this process. In the course of the development of air-blast circuit-breakers at the Asea Ludvika Works considerable research has been devoted to these wave phenomena, and a number of experiments have been made in order to study the wave motions during the filling and discharge of long ducts. Most of these experiments have been performed at an initial gauge pressure of 15 atm with tubes having an inner diameter of 80 mm and a length of up to 11 m. The charges and discharges have been initiated both by opening a high-speed valve, which uncovered the tube area in less than 0.01 s, and by means of bursting diaphragms. These latter experiments resulted in particularly pronounced wave fronts well suited for making a comparison with the theoretical results. The wave motions have been determined by making oscillographic recordings of the pressures at different points along the tubes, generally at intervals of 1 m.

B. INTRODUCTION TO ELASTIC WAVE PHENOMENA

When treating the propagation of elastic changes in a state, it is preferable to refer to a *wave front* rather than to a *wave*, since the term "wave" is associated more closely with a combination of two, or more, wave fronts, for example, one with a rising, and one with a falling, pressure, which do not obey, however, the same equations. The phenomena occurring in this connection display typical front characteristics, that is to say, a given air state ahead of the front is converted into another air state behind the front without the occurrence of maxima or minima of the variable quantities.

Plane fronts will be treated in this paper, that is to say, fronts where the air state is homogeneous within each plane perpendicular to the direction of propagation of the front. Such fronts are experienced with wave phenomena free from losses in ducts having a constant cross-sectional area.

The change in state within a front involves a change in pressure, volume, temperature and mass speed (i.e., speed of flow). It is more suitable, however, to take into account density and speed of sound, that is to say, the propagation velocity of an infinitely small change in state at the temperature in question, instead of the quantities volume and temperature included in the conventional equation of state. As a rule, the changes

Sa 1

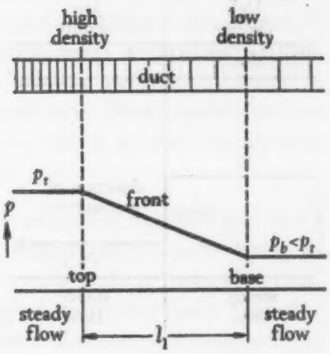

p_t Pressure at top of front
p_b Pressure at base of front
l_1 Range of front

Fig. 1. Graphical representation of continuous front (press front and expansion front).

in pressure are of the greatest interest and the term "front" will hereafter refer to the variation in pressure.

Fig. 1 shows a duct with a given pressure distribution, that is to say, a front, along a range l_1. This front is in a state of motion in the duct, and the Figure shows its appearance at a given instant t_1. It is assumed that a stationary state of flow prevails on each side of the range. Since the front is advancing, a continuous conversion of the one stationary limit condition into the other takes place within this range. The transition from front to stationary state of flow with a lower pressure is called ***front base*** and to a state with higher pressure ***front top***. The temperature rises adiabatically from the base to the top. The propagation of an infinitely small pressure change – an elementary pressure – anywhere in the front takes place relative to the air with the speed of sound corresponding to the temperature of the position in question. The air, however, has a mass speed relative to the duct, and the propagation velocity of the elementary pressure relative to the duct will be equal to the sum of the acoustic speed and the mass speed. Relative to the air the elementary pressure can propagate either towards the base or towards the top. If it propagates towards the base, the range of front l_1 will be reduced; in other words, the front will become "steeper". A front of this nature can suitably be called a *compression front*. If, on the other hand, the elementary pressure propagates towards the top, the range of front is extended and the front becomes less steep. It can then be called an *expansion front*. In the former case it is a question of the propagation of a pressure rise, in the latter case the propagation of a pressure drop.

The mass speed relative to the duct in both cases can be in the same or the opposite direction to that of the propagation of the elementary pressure relative to the air. If it is propagated in the same direction, it is possible to refer to a ***positive front***, and, if it is propagated in the opposite direction, it is a ***negative front***.

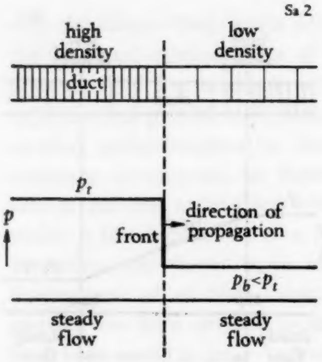

p_t Pressure at top of front
p_b Pressure at base of front

Fig. 2. Graphical representation of discontinuous front (shock front).

By combining the above-mentioned four kinds of front, the following four *front types* are obtained:

Positive compression front, which arises due to the propagation of a compression front in the direction of the flow,

Negative compression front, which arises due to the propagation of a compression front in the opposite direction of the flow,

Positive expansion front, which arises due to the propagation of an expansion front in the direction of the flow,

Negative expansion front, which arises due to the propagation of an expansion front in the opposite direction of the flow.

It is assumed for these four front types that the conversion of the state ahead of the front into the state behind the front takes place during a certain finite time, that is to say, the pressure at a fixed point in the duct during the passage of the front will change *continuously* from the one limit pressure to the other.

As already mentioned above, the range of front of compression fronts is reduced during the propagation. Sooner or later the range, at least for a part of the front, will become zero, that is to say, the change in state will take place instantaneously during the continued propagation. The pressure at a fixed point in the duct will then change *discontinuously* (Fig. 2) during the passage of the front. From the above it is thus apparent that compression fronts may occur in both a continuous and a discontinuous form, whereas expansion fronts can only occur in a continuous form. It is reasonable to suppose that the discontinuous form represents a limiting case for the continuous form and that both forms can consequently be treated on the same theoretical basis. This is, however, not the case. When the range of front becomes zero, or, in other words, when the front becomes "vertical", a fundamental change suddenly takes place, and the propagation obeys thereafter other laws. The conditions are very complicated, particularly at the transition, and extensive theoretical studies have been devoted to their clarification. The viewpoints presented by various research workers are, to some extent, contradictory. An indication of this is to be found in the notes appended to the references in the bibliography. The problem concerning *shock compression* has been the subject of debate for more than 100 years, but it is only recently that acceptable theoretical solutions have been presented.

Pfriem [44] postulated in 1941 in his theoretical investigations that two new wave fronts occur when a compression front reaches the state of discontinuity during its propagation as a continuous front. One of these fronts is a *shock front* ("vertical" front), which moves in the same direction as the original continuous front. The other front is an expansion front, which moves in the opposite direction. It is interesting to note that Stokes [2] already in 1848 surmised that such a returning front might exist. More recent theoretical investigations concerning the propagation of shock fronts also take into consideration internal friction and heat conduction of air. It is difficult, nevertheless, to apply the results of these investigations for practical calculations owing to their complicated nature. Furthermore, friction and heat transfer between the air and the duct walls are generally not taken into account, despite the fact that experimental results have shown that these factors must be considered as being of great importance in the case of travelling wave fronts in ducts. For this reason, therefore, when judging the experimental results in this work as far as shock fronts are concerned, a comparison has been made with the calculated results based on the *Hugoniot curve* or, more correctly, the Rankine–Hugoniot curve, also called the *dynamic adiabate*, which renders possible a relatively simple theoretical treatment of the conditions.

As already mentioned, compression fronts occur in two forms, continuous and discontinuous. The latter form has been known for a long time as *shock front*. No similar short designation is available for the first-mentioned form, and since the expression "continuous compression front" is unwieldy, the term *press front* will be used hereafter for such a front.

The different front types can then be collated in the following manner:

a positive press front
b negative press front
c positive expansion front
d negative expansion front
e positive shock front
f negative shock front

As far as shock fronts are concerned, the rule that the front velocity is equal to the sum of the mass speed and the acoustic speed does not apply, but the velocities are related to one another by rather complicated equations.

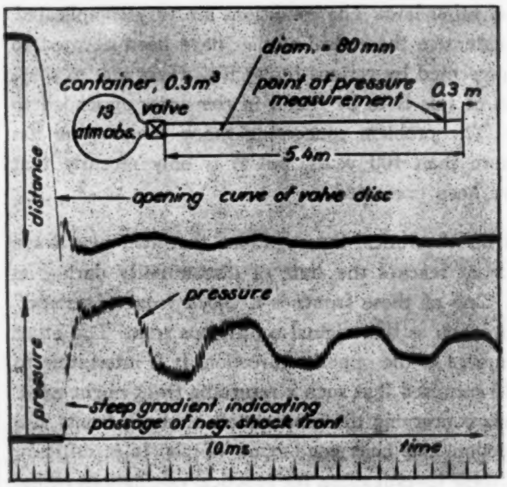

Fig. 3. Oscillogram of pressure variations near the closed end of a duct caused by wave action set up in conjunction with rapid charging (1 scale division on the time sweep = 10 ms). (Z 11778.)

Cases can occur when the mass speeds ahead of and behind the front are of opposite directions. With the above-mentioned classification, which assumes that the velocities are calculated relative to the duct, the front will then comprise a combination of two types obeying different equations. Such a front can, for example, be composed of a positive and a negative press front. By allowing the co-ordinate system to accompany the base or the top of the front combination, the latter can be covered by one single equation system, if both the fronts are of a continuous nature.

Cases also occur when the mass speed is zero on one or other side of the front. This speed can have the value zero *ahead of* the fronts, *a*, *d* and *e* and *behind* the fronts *b*, *c* and *f*.

When a rather long tube, closed at the external end, is being filled with compressed air from a container by means of a rapidly opening device close to the container, oscillations will develop, as illustrated in Fig. 3, which shows an oscillographic recording of the pressure variations near the closed end of the tube. All the above-mentioned front types may occur in a more or less pronounced fashion during such a charging process. After the device has been opened, a positive press front rushes along the tube and manages, before it reaches the end of the tube, generally to be converted into a positive shock front on its head. If a valve having an opening time of a few milliseconds is used, if the pressure in the container is a few atmospheres, and if an initial pressure of 1 atm abs. is maintained in the tube, the conversion will commence a few metres from the valve. The front is reflected at the end of the tube, and a new front, consisting of a negative shock front and a negative press front, moves towards the container through the compressed air flowing with a high velocity from the container towards the front. The velocity of the head of the front, that is to say, the negative shock front, has been found from experiments to be about 200 m/s. Similar results have been established by Payman and Shepherd [57] in experiments performed according to the Schlieren method. The pressure at the end of the tube has risen after the reflection of the front to a value considerably in excess of that in the container, and the air between the end of the tube and the front travelling towards the container lies almost at rest. When the front reaches the container, the entire tube is filled with air having a pressure higher than that in the container. A gradual pressure equalisation then develops in such a way that a negative expansion front commences to propagate towards the closed end of the tube. Within the front a change of pressure into speed takes place, that is to say, air flows from the tube into the container. The negative expansion front is reflected in its turn from the closed end of the tube and is then converted into a positive expansion front, which moves towards the container. The air remains almost at rest between this latter front and the end of the tube and has a lower pressure than that in the container. Thus, when the front reaches the container, charging of the tube commences again, being introduced by a positive press front. The cycle as described above is then repeated several times, although with decreasing amplitude and a slight transformation of the fronts caused by the attenuation due to friction.

If a tube filled with compressed air is suddenly opened at one end, the discharge will have a wave characteristic. When the tube is opened, a negative expansion front is initiated which rushes towards the closed end of the tube and, during its passage, converts the air state from rest to motion in the direction of the outlet. If the entire cross-section of the tube has been uncovered, the front base will remain at the outlet and the front will consequently lie finally along the full length of the tube. The reason for this is that the flowing out when the tube end is fully open takes place with the speed of sound, and thus a change in pressure at the tube end cannot propagate into the tube. If only a part of the cross-section of the tube is uncovered, the base too, on the other hand, will propagate along the tube. The front will be reflected at the closed end of the tube and a positive expansion front will then propagate towards the open end, where, due to reflection, it will be converted again into a negative expansion front. The air behind the positive expansion front will remain practically at rest and at a lower pressure than that of the air ahead of the front. If the pressure is measured at the open and closed tube ends, it is found that the pressure decreases by steps with time.

The theory of wave phenomena is treated in the following to the extent that the results obtained from the measurements may be adequately judged.

The symbols and units given in the following table are used in the calculations.

Symbol	Term	Unit	Relationship or value
F	cross-sectional area	m^2	
m	unit mass	kg/m^2s	
ϱ	density	kg/m^3	$\varrho = \gamma/g = 1/v$
γ	specific weight	Kg/m^3	
v	specific volume	m^3/kg	
p	specific pressure	Kg/m^2	$1\ Kg/cm^2 = 1$ atm
a	speed of sound (acoustic speed)	m/s	
c, u	speed of mass (speed of flow)	m/s	
y, w	front velocity	m/s	
T	absolute temperature	°K	
E	specific internal energy, heat	kcal/Kg	$E = c_v T$
	work	m^2/s^2	$E = A\,gc_v T$
i	specific heat content, heat	kcal/Kg	$i = c_p T$
	work	m^2/s^2	$i = A\,gc_p T$
c_p	specific heat at constant pressure	kcal/Kg degree	$c_p = 0.24$ for air
c_v	specific heat at constant volume	kcal/Kg degree	$c_v = 0.172$ for air
$\varkappa$	adiabatic index	–	$\varkappa = c_p/c_v = 1.4$ for air
R	gas constant	m/°K	$R = 29.27$ for air
A	mechanical equivalent of heat	Kgm/kcal	$A = 427$
g	acceleration due to gravity	m/s^2	$g = 9.81$

The unit kg is the mass unit, defined as the weight divided by the acceleration due to gravity. The unit Kg is the force unit, which is also used here as the weight unit. The units kg and Kg are interrelated by the expression $1\ Kg = 1\ kgm/s^2$.

C. EQUATIONS OF STATE, MOTION AND CHANGE IN STATE

Air can be considered as a perfect gas within the temperature limits normally occurring here. The *equation of state* applies to such a gas:

$$pv = gRT \tag{1}$$

if v is calculated in volume per unit of mass. If v is calculated in volume per unit of weight, g does not appear. The introduction of density instead of specific volume gives

$$p/\varrho = gRT \tag{2}$$

The following expression for the *speed of sound* is known from physics

$$a^2 = dp/d\varrho \tag{3}$$

It is also known that the change in state of a gas at the propagation of sound takes place adiabatically and therefore follows *Poisson's law*

$$p = \text{const.} \times \varrho^{\varkappa} \tag{4}$$

Deriving this equation gives

$$dp/d\varrho = \text{const.} \times \varkappa\varrho^{\varkappa-1} \tag{5}$$

which with Eqs. (3) and (4) yields

$$a^2 = \varkappa p/\varrho \tag{6}$$

With $\varkappa = 1.4$, this constitutes an equation of state for air with the speed of sound as a variable instead of the absolute temperature. This form of the equation of state is very suitable when treating gas dynamic problems.

From Eqs. (2) and (6) it follows that

$$a = \sqrt{\varkappa gRT} \approx 20\sqrt{T} \tag{7}$$

The following three laws apply to motion:

the mass law (also called the continuity law), *the impulse law* and *the energy law*, which can be expressed as follows for one-dimensional phenomena (see, for example, Prandtl [51], pp. 244–246).

The mass law: $m = \varrho u = \text{const.}$ (8)

where m is the *unit mass*, that is to say, the mass flowing per unit of time and per unit of the cross-sectional area.

The impulse law: $\varrho u^2 + p = \text{const.}$ (9)

The energy law: $\frac{u^2}{2} + E + \frac{p}{\varrho} = \text{const.}$ (10)

In this latter expression E denotes *the internal energy*

$$E = A\, gc_v T \tag{11}$$

or, if the equation of state is introduced,

$$E = \frac{1}{\varkappa - 1} \cdot \frac{p}{\varrho} \tag{12}$$

The expression

$$i = E + \frac{p}{\varrho} \tag{13}$$

denotes the *heat content* or the *enthalpy*.

Introducing Eq. (12) in Eq. (13) results in

$$i = \frac{\varkappa}{\varkappa - 1} \cdot \frac{p}{\varrho} = \varkappa E \tag{14}$$

By introducing $\varkappa = c_p/c_v$ and E according to Eq. (11), we obtain

$$i = A\, gc_p T \tag{15}$$

If Eq. (14) is inserted in Eq. (10), the energy law assumes the form

$$\frac{u^2}{2} + \frac{\varkappa}{\varkappa - 1} \cdot \frac{p}{\varrho} = \text{const.} \tag{16}$$

Introducing here the equation of state Eq. (6) gives

$$\frac{u^2}{2} + \frac{a^2}{\varkappa - 1} = \text{const.} \tag{17}$$

or, with $\varkappa = 1.4$,

$$u^2 + 5a^2 = \text{const.} \tag{18}$$

The above energy equations refer to frictionless phenomena. If friction occurs, the following fundamental equation applies (Prandtl [51] p. 245)

$$\frac{u^2}{2} + \int \frac{\mathrm{d}p}{\varrho} + E_f = \text{const.} \tag{19}$$

where E_f is the specific friction work applied to the air between the inlet and outlet cross-sectional area.

The static energy of air, which is normally negligible, has been omitted in all the energy equations.

The *changes in state* which occur with continuous phenomena are assumed to follow the normal *static adiabate* and those which occur with discontinuous phenomena the *dynamic adiabate* (the Rankine-Hugoniot curve).

Static-adiabatic change in state

If the subscript 0 refers to an initial state, we have according to Eq. (4)

$$\frac{p}{\varrho^\varkappa} = \frac{p_0}{\varrho_0{}^\varkappa} \quad \text{or} \quad \frac{\varrho}{\varrho_0} = \left(\frac{p}{p_0}\right)^{\frac{1}{\varkappa}} \tag{20}$$

According to Eq. (2)

$$p/\varrho = gRT \quad \text{and} \quad p_0/\varrho_0 = gRT_0 \tag{21}$$

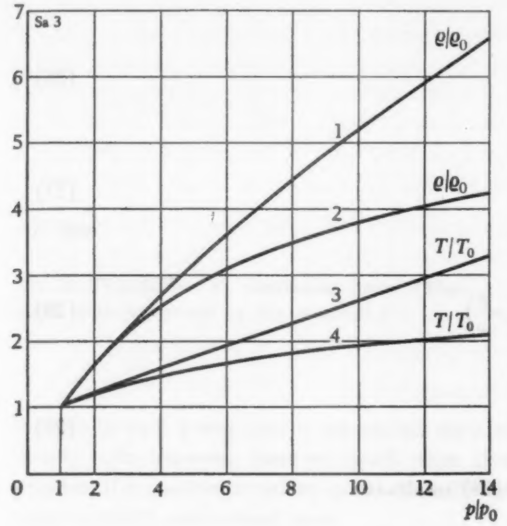

1 Static-adiabatic change in state, see Eq. (20)
2 Dynamic-adiabatic change in state, see Eq. (33)
3 Dynamic-adiabatic change in state, see Eq. (36)
4 Static-adiabatic change in state, see Eq. (22)

Fig. 4. Density, ϱ/ϱ_0, and temperature, T/T_0, of air as functions of pressure, p/p_0.

From Eqs. (20) and (21) it follows that

$$\frac{T}{T_0} = \left(\frac{p}{p_0}\right)^{\frac{\varkappa-1}{\varkappa}} \tag{22}$$

According to Eq. (6)

$$a^2 = \varkappa p/\varrho \quad \text{and} \quad a_0^2 = \varkappa p_0/\varrho_0 \tag{23}$$

From Eqs. (20) and (23) it follows that

$$\frac{a}{a_0} = \left(\frac{p}{p_0}\right)^{\frac{\varkappa-1}{2\varkappa}} = \left(\frac{\varrho}{\varrho_0}\right)^{\frac{\varkappa-1}{2}} \tag{24}$$

The speed of sound within a continuous wave front thus changes with the pressure; a higher pressure consequently corresponds to a higher speed of sound. As will be shown later, a disturbance, in this case an arbitrary point in the front, will always be propagated relative to the air with the speed of sound applicable to the point in question, which means that the front will change form as it propagates along the tube.

Dynamic-adiabatic change in state

The relationship between the pressure and density can be obtained on the basis of the mass law, impulse law and energy law. If the subscript 0 denotes the initial state, and if c and c_0 denote the speeds relative to the discontinuity surface, Eq. (8) gives

$$\varrho c = \varrho_0 c_0 \tag{25}$$

Eq. (9)

$$\varrho c^2 + p = \varrho_0 c_0^2 + p_0 \tag{26}$$

and Eq. (16)

$$c^2 + \frac{2\varkappa}{\varkappa - 1} \cdot \frac{p}{\varrho} = c_0^2 + \frac{2\varkappa}{\varkappa - 1} \cdot \frac{p_0}{\varrho_0} \tag{27}$$

or

$$c^2 - c_0^2 = (c + c_0)(c - c_0) = \frac{2\varkappa}{\varkappa - 1}\left(\frac{p_0}{\varrho_0} - \frac{p}{\varrho}\right) \tag{28}$$

Dividing Eq. (26) by Eq. (25) gives

$$c - c_0 = \frac{p_0}{\varrho_0 c_0} - \frac{p}{\varrho c} \tag{29}$$

The introduction of Eq. (29) in Eq. (28) results in

$$\frac{p_0 c}{\varrho_0 c_0} - \frac{p c_0}{\varrho c} = \frac{\varkappa + 1}{\varkappa - 1}\left(\frac{p_0}{\varrho_0} - \frac{p}{\varrho}\right) \tag{30}$$

If $c/c_0 = \varrho_0/\varrho$ and $c_0/c = \varrho/\varrho_0$ (31)

are introduced according to Eq. (25),

$$\frac{p_0}{\varrho} - \frac{p}{\varrho_0} = \frac{\varkappa + 1}{\varkappa - 1}\left(\frac{p_0}{\varrho_0} - \frac{p}{\varrho}\right) \tag{32}$$

which gives

$$\frac{\varrho}{\varrho_0} = \frac{\dfrac{\varkappa + 1}{\varkappa - 1} + \dfrac{p_0}{p}}{\dfrac{\varkappa + 1}{\varkappa - 1} \cdot \dfrac{p_0}{p} + 1} = \frac{\dfrac{\varkappa + 1}{\varkappa - 1} \cdot \dfrac{p}{p_0} + 1}{\dfrac{\varkappa + 1}{\varkappa - 1} + \dfrac{p}{p_0}} = \frac{6 \cdot \dfrac{p}{p_0} + 1}{6 + \dfrac{p}{p_0}} \tag{33}$$

This is an expression for the Rankine–Hugoniot curve. Replacing density by specific volume, this is also expressed in the literature by

$$\frac{1}{2}(p + p_0)(v - v_0) = -\frac{p v - p_0 v_0}{\varkappa - 1} \tag{34}$$

In 1942 Schultz-Grunow [50] derived Eq. (33) in a slightly different manner by introducing the front speed.

From Eq. (33) it is apparent that ϱ/ϱ_0 approaches the maximum value 6 (at $\varkappa = 1.4$), if p/p_0 approaches infinity. For high values of p/p_0 and correspondingly high temperatures, the specific heat cannot, however, be considered any longer as being constant.

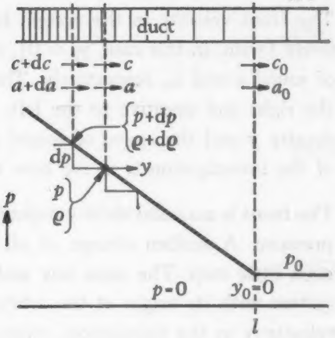

l Base

Fig. 5. Propagation of continuous front. (The initial state is denoted by the subscript 0.)

It alters in such a way that $\varkappa$ approaches unity when p/p_0 approaches infinity. The density ratio increases, however, much more slowly than for static-adiabatic compression. It is possible to reckon upon with sufficient accuracy $\varkappa = 1.4$ for the pressure ratios normally encountered here.

The variation of the temperature and the speed of sound with pressure can be found in the following way.

From the equations of state (2) and (6) can be derived

$$T/T_0 = (a/a_0)^2 = p\varrho_0/p_0\varrho \tag{35}$$

Introducing Eq. (33) in Eq. (35) gives

$$\frac{T}{T_0} = \left(\frac{a}{a_0}\right)^2 = \frac{\dfrac{\varkappa+1}{\varkappa-1} + \dfrac{p}{p_0}}{\dfrac{\varkappa+1}{\varkappa-1} + \dfrac{p_0}{p}} = \frac{6 + \dfrac{p}{p_0}}{6 + \dfrac{p_0}{p}} \tag{36}$$

D. FRONT EQUATIONS

I. Continuous fronts

Fig. 5 shows a front having an initial state denoted by 0. It is assumed that the front propagates in a duct having a constant cross-sectional area, that is to say, the phenomenon is one-dimensional. The pressure p within the front rises from the lower limit value p_0 in the base. The front equations are first suitably determined for a co-ordinate system in the base l. The equations are transformed later on so as to apply to a co-ordinate system which is fixed relative to the duct. The base l moves in this latter system at constant velocity and it is consequently a simple matter to transform the equations.

The front velocity in the system having its origin at l is designated y and y_0, respectively (with, in this case, $y_0 = 0$), the mass speed c and c_0, respectively, and the speed of sound a and a_0, respectively. They are all treated as directed quantities, positive to the right and negative to the left. The static adiabatic law is assumed to apply. The density ϱ and the speed of sound a are functions only of the pressure p. The object of the investigation is to see how the speeds c and y vary with a and p, respectively.

The front is assumed to be composed of infinitely small, sudden step-like changes in the pressure. A sudden change of all the state variables and speeds takes place within each little step. The mass law and impulse law apply to each change. A co-ordinate system with its origin at the arbitrary point is assumed in order to include the front velocity y in the calculations when establishing the fundamental equations.

According to the mass law Eq. (8) we have then

$$(\varrho + \mathrm{d}\varrho)(y - c - \mathrm{d}c) = \varrho(y - c) \tag{37}$$

and according to the impulse law Eq. (9)

$$(\varrho + \mathrm{d}\varrho)(y - c - \mathrm{d}c)^2 + p + \mathrm{d}p = \varrho(y - c)^2 + p \tag{38}$$

Eq. (37) gives

$$\frac{\mathrm{d}\varrho}{\varrho} = \frac{\mathrm{d}c}{y - c} \tag{39}$$

and Eq. (38)

$$(y - c)\left(y - c - 2\varrho\frac{\mathrm{d}c}{\mathrm{d}\varrho}\right) + \frac{\mathrm{d}p}{\mathrm{d}\varrho} = 0 \tag{40}$$

Inserting Eq. (39) in Eq. (40) and, according to Eq. (3), with $\mathrm{d}p/\mathrm{d}\varrho = a^2$, we have

$$y = c \pm a \tag{41}$$

The velocity of a point, that is to say, an arbitrary pressure within the front, is thus equal to the arithmetic sum of, or difference between, the mass speed and the acoustic speed for the point in question.

Inserting Eq. (41) in Eq. (39) gives

$$\frac{\mathrm{d}\varrho}{\varrho} = \pm\frac{\mathrm{d}c}{a} \tag{42}$$

Logarithmic differentiation of Eq. (24) results in

$$\frac{\mathrm{d}\varrho}{\varrho} = \frac{2}{\varkappa - 1}\cdot\frac{\mathrm{d}a}{a} \tag{43}$$

which with Eq. (42) yields

$$\frac{dc}{da} = \pm \frac{2}{\varkappa - 1} \tag{44}$$

Integrating Eq. (44) gives

$$c \mp \frac{2}{\varkappa - 1} a = \text{const.} \tag{45}$$

From Eqs. (41) and (45) it follows that, if the state 0 is introduced,

$$c = \pm \frac{2}{\varkappa - 1}\left(a - \frac{\varkappa + 1}{2} a_0\right); \text{ limiting case: } c_0 = \mp a_0 \tag{46}$$

and

$$y = \pm \frac{\varkappa + 1}{\varkappa - 1}(a - a_0); \text{ limiting case: } y_0 = 0 \tag{47}$$

Since $p > p_0$, a is numerically larger than a_0. For point l then, a_0 is negative if c_0 is positive and vice versa will apply. Numerically, a_0 and c_0 are equally large. It is therefore obvious that a is negative if c is positive and vice versa will also apply for that part of the front lying nearest to point l. If c in Eq. (46) is to become positive for *negative values of a and a_0*, the positive sign must be used. In this case c decreases with an increasing numerical value of a and becomes zero when $a = [(\varkappa + 1)/2]a_0$. If the numerical value of a increases still further, c becomes negative. According to Eq. (47), where the corresponding sign, that is to say, the plus sign, must be used, y becomes negative if a and a_0 are negative. The numerical value of y increases continuously with an increasing numerical value of a.

It is apparent from the above that the front during the propagation becomes *less steep*, that is to say, a given pressure drop along the duct will spread out over a range of front increasing with time. A front of this nature where the density in *the normal range* (see below) drops in the direction of flow is called an *expansion front*.

If c in Eq. (46) is to become negative for *positive values of a and a_0*, the plus sign must also be used in this case, as far as the front nearest to point l is concerned. Consequently c becomes zero when the numerical value of a is equal to $[(\varkappa + 1)/2]a_0$, and becomes positive if a increases still more. The plus sign in Eq. (47) and positive values of a and a_0 will give a positive value of y, that is to say, the front will become *steeper* during the propagation. The density of this front will increase in the normal range in the direction of flow. Such a front is called a *compression front* or, as has already been stated, more suitably a *press front*.

From the above it follows that the plus sign must be used in Eqs. (41), (46) and (47) if the acoustic speeds are considered as directed quantities. If, on the other hand, a and a_0 are only inserted with their numerical values, that is to say, always as positive quantities, the plus sign is used in the above-mentioned formulae for press fronts and the minus sign for expansion fronts.

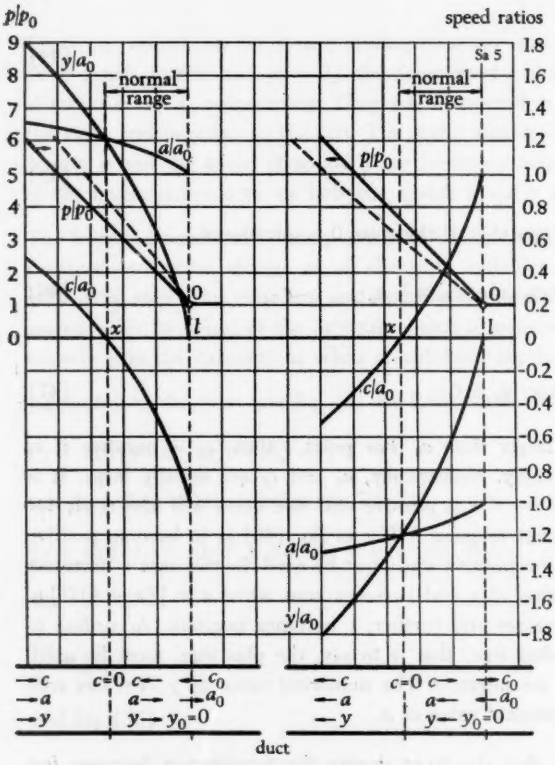

a) Press front b) Expansion front

Fig. 6. Graphical representation of continuous fronts, the base of front being at rest ($y_0 = 0$).

Fig. 6 shows the conditions prevailing with continuous fronts at an arbitrary point of time during the propagation. The front, that is to say, the pressure curve, has been plotted as a straight line for the sake of simplicity. The broken line shows the front an instant later. In the Figure it can also be seen how the velocities are distributed within the range of front. They are calculated in relation to the acoustic speed at point *l*.

With the above-mentioned *normal range* is meant the range between the points *l* and *x*. At point *x* the direction of *c* changes and the state variables have here certain characteristic values. Waves generally occur within the normal range for one-dimensional phenomena. The front will extend beyond the normal range for flow velocities which, relative to the duct, exceed the local speed of sound.

Expressions will now be derived which apply to a co-ordinate system fixed in relation to the duct. The mass speed is designated in this system by *u* and the front velocity by w. The acoustic speed is still a. The initial state is denoted by the subscript 0. The following will then apply to a press front:

$$u = u_0 + a_0 + c \tag{48}$$

and

$$w = u_0 + a_0 + y \tag{49}$$

The following applies to an expansion front:

$$u = u_0 + a_0 - c \tag{50}$$

and

$$w = u_0 + a_0 - y \tag{51}$$

In Eqs. (48) and (49) the expressions for c and y according to Eqs. (46) and (47) will be introduced with a plus sign, but, on the other hand, with a minus sign in Eqs. (50) and (51). The expressions for u and w will then be the same for press fronts and expansion fronts. This gives

$$u = u_0 + \frac{2}{\varkappa - 1}(a - a_0) \tag{52}$$

and

$$w = u_0 + \frac{\varkappa + 1}{\varkappa - 1}a - \frac{2}{\varkappa - 1}a_0 \tag{53}$$

or

$$\frac{u - u_0}{a_0} = \frac{2}{\varkappa - 1}\left(\frac{a}{a_0} - 1\right) = 5\left(\frac{a}{a_0} - 1\right) \tag{54}$$

and

$$\frac{w - u_0}{a_0} = \frac{\varkappa + 1}{\varkappa - 1} \cdot \frac{a}{a_0} - \frac{2}{\varkappa - 1} = 6\frac{a}{a_0} - 5 \tag{55}$$

Eqs. (54) and (55) include the mass speeds u and u_0, which are directed quantities. They have a plus sign if the speed is in the same direction as the front velocity and a minus sign if it is in the opposite direction. If it is assumed that only the numerical values of the mass speeds are to be introduced in the formulae, irrespective of the direction, formulae (54) and (55) will apply directly to *positive* fronts. The corresponding formulae for *negative* fronts will have the following appearance:

$$\frac{u_0 - u}{a_0} = 5\left(\frac{a}{a_0} - 1\right) \tag{56}$$

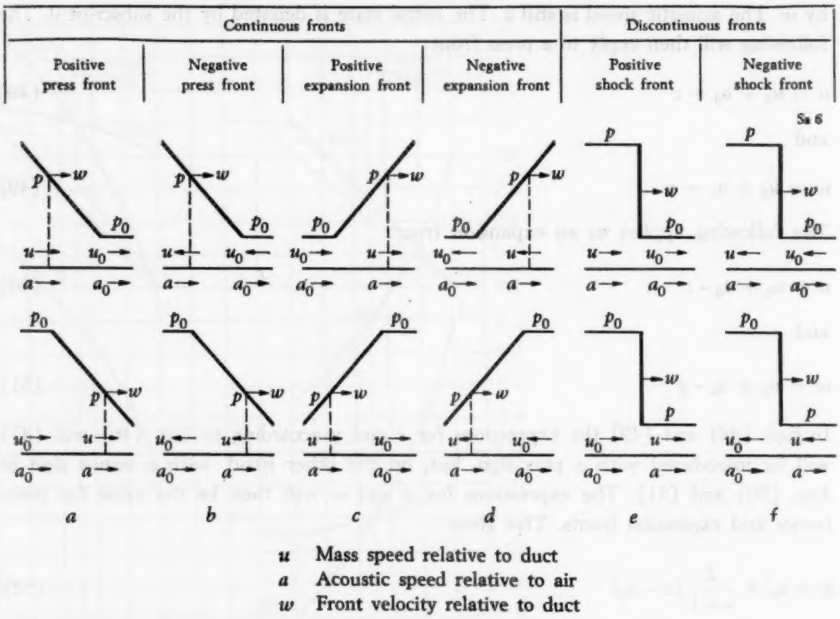
Continuous fronts
Discontinuous fronts
Positive press front
Negative press front
Positive expansion front
Negative expansion front
Positive shock front
Negative shock front
p
w
p_0
u
u_0
a
a_0
a
b
c
d
e
f
u Mass speed relative to duct
a Acoustic speed relative to air
w Front velocity relative to duct

Fig. 7. Diagram of front types. (The subscript 0 denotes the initial state.)

and

$$\frac{w + u_0}{a_0} = 6\,\frac{a}{a_0} - 5 \tag{57}$$

A necessary condition for this is naturally that u and u_0 have the same direction. If they have opposite directions, one of the speeds must be introduced with a minus sign.

The initial state denoted by the subscript 0 can lie anywhere in the front, for example, at the top or on the base, as is apparent from the diagram of front types shown in Fig. 7.

Eqs. (54) to (57) are plotted in the form of curves in Fig. 8, which is intended to cover the range concerned in this investigation. The relationship between the pressure and the acoustic speed is given by Eq. (24). As can be seen, the equations and curves are given in a dimensionless form, since they express quotients between the mass speed or the front velocity and the acoustic speed in the initial state. The equations show that the front is determined only by the difference between the mass speeds and not by their absolute values in relation to the duct.

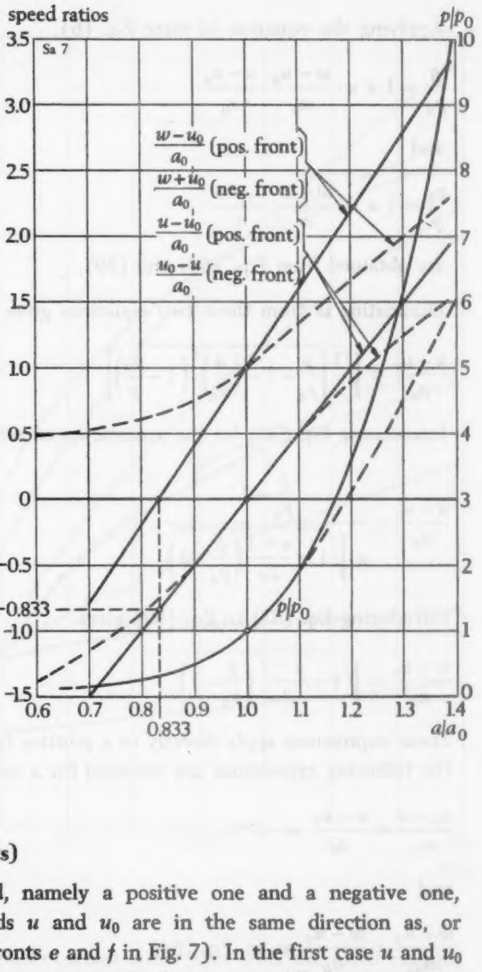

Fig. 8. Front curves as function of the acoustic speed with the adiabatic index $\varkappa = 1.4$.

II. Discontinuous fronts (shock fronts)

Two front types must be considered, namely a positive one and a negative one, according to whether the mass speeds u and u_0 are in the same direction as, or counteract, the front velocity w (the fronts e and f in Fig. 7). In the first case u and u_0 are considered as being positive, and negative in the latter case. All the speeds are treated relative to the duct.

When arranging the equations, it is assumed that there is a co-ordinate system accompanying the front with the velocity w. According to the mass law Eq. (8) this system will have

$$(w-u)\varrho = (w-u_0)\varrho_0 \tag{58}$$

and according to the impulse law Eq. (9)

$$(w-u)^2\varrho + p = (w-u_0)^2\varrho_0 + p_0 \quad . \tag{59}$$

Applying the equation of state Eq. (6),

$$\frac{p}{p_0} = 1 + \varkappa \cdot \frac{w - u_0}{a_0} \cdot \frac{u - u_0}{a_0} \tag{60}$$

and

$$\frac{p_0}{p} = 1 + \varkappa \cdot \frac{w - u}{a} \cdot \frac{u_0 - u}{a} \tag{61}$$

are obtained from Eqs. (58) and (59).

Eliminating w from these two equations gives

$$\frac{u - u_0}{a_0} = \sqrt{\frac{1}{\varkappa}\left[\frac{p}{p_0} - 1 - \left(\frac{a}{a_0}\right)^2\left(1 - \frac{p_0}{p}\right)\right]} \tag{62}$$

Introducing Eq. (36) for the acoustic-speed relationship results in

$$\frac{u - u_0}{a_0} = \frac{\frac{p}{p_0} - 1}{\varkappa\sqrt{1 + \frac{\varkappa + 1}{2\varkappa}\left(\frac{p}{p_0} - 1\right)}} \tag{63}$$

Introducing Eq. (63) in Eq. (60) gives

$$\frac{w - u_0}{a_0} = \sqrt{1 + \frac{\varkappa + 1}{2\varkappa}\left(\frac{p}{p_0} - 1\right)} \tag{64}$$

These expressions apply directly to a *positive* front. By altering the signs for u and u_0, the following expressions are obtained for a *negative* front:

$$\frac{u_0 - u}{a_0} = \frac{u - u_0}{a_0} \text{ as in Eq. (63)} \tag{65}$$

and

$$\frac{w + u_0}{a_0} = \frac{w - u_0}{a_0} \text{ as in Eq. (64)} \tag{66}$$

The dependence of the acoustic speed a on pressure is found from Eq. (36). Curves for shock fronts are also reproduced in Fig. 8.

The curves in Fig. 8 are based on $\varkappa = 1.4$ for both continuous fronts and shock fronts. Results from more recent investigations concerning the dependence of the specific heat on temperature seem to indicate that $\varkappa$ decreases relatively greatly with increasing temperature. If the thermodynamic data given by Keenan and Kaye [55] are taken into consideration, curves are obtained for continuous fronts which, with increasing values of a/a_0, deviate to a certain extent from those shown in Fig. 8. The differences, however, within the range covered by Fig. 8 are so small that they do not

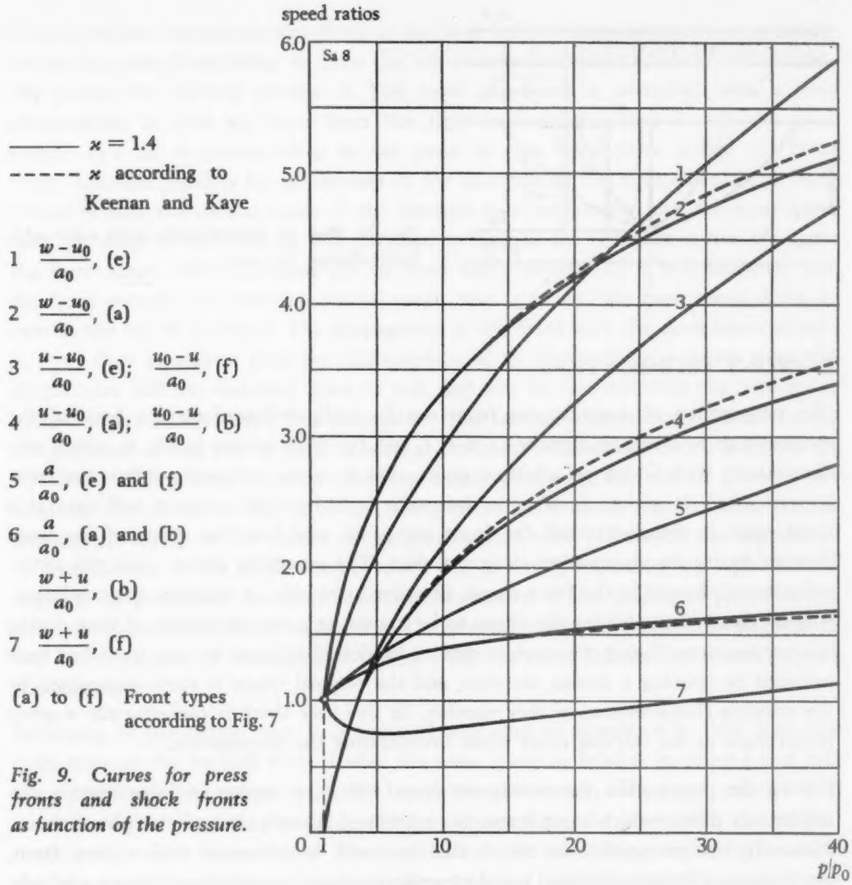

Fig. 9. Curves for press fronts and shock fronts as function of the pressure.

have any practical importance. It is not so certain either that with the rapid changes in state occurring in conjunction with wave phenomena it is possible to assume that the results from measurements concerning specific heat will provide sufficiently reliable data for calculating wave fronts. The reason for this is that the measurements appear to have been performed with air at rest or in a steady flow.

A comparison between the front quantities of press fronts and shock fronts within a wider range is to be found in Fig. 9, where the curves for the velocities are shown depending upon the pressure ratio. The curves for press fronts are based both on $\varkappa = 1.4$ and on varying values of $\varkappa$ according to Keenan and Kaye ([55], p. 36, Table 3). The curves do not noticeably change for shock fronts within the range shown in Fig. 9, if they are based on the temperature-dependent $\varkappa$.
]

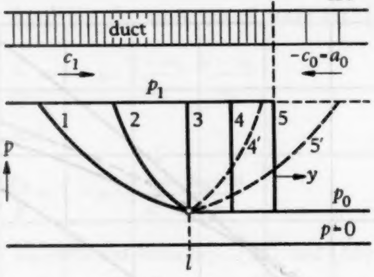

Fig. 10. Rise of discontinuity with static-adiabatic change in state.

E. FRONT PROPAGATION

The propagation of a continuous front can be easily followed on the basis of the equations to be found in chapter D, part I, and the front curves in Fig. 8, which give the velocity with which an arbitrary point, that is to say, pressure, within the front is propagated. It is then possible to determine both how the pressure will vary at a fixed point in the duct while the front passes by, and how the shape of the front changes during its propagation along the duct. The equations permit only the determination of *changes* in the front shape. In order to be able to calculate the conditions, it is necessary therefore for the shape to be known at a certain instant of time during the propagation. During the experiments to be described later on, the front has been initiated by opening a closing member, and the original shape is then determined by the opening characteristics of this member. In this case there is consequently a given *initial front* as the starting point when investigating the propagation.

During the propagation the continuous front will enter sooner or later upon a discontinuous phase, which complicates the continued investigation of the phenomenon. Naturally, the prerequisite for this is that it should be concerned with a press front. An expansion front is flattened out during the propagation and discontinuous phenomena do not thus occur with such a front. During the propagation of a press front the transition to a discontinuous phase, that is to say, a conversion of the press front into a shock front, may take place suddenly or gradually. A sudden conversion occurs when all the pressures within the front appear simultaneously at one and the same point in the duct. This is a special case which probably occurs very seldom in practice, since it requires a fully defined shape of the initial front for the given conditions. The treatment of this case, however, is fruitful from the theoretical viewpoint and is therefore included below. The conversion of the press front into a shock front usually commences first on its foremost part and the conversion then continues gradually.

Fig. 10 serves to illustrate how a sudden conversion of a press front into a shock front takes place during the simplest conditions, that is to say, assuming a static-adiabatic change in state, also after the occurrence of discontinuity, and assuming that the pressure p_1 maintains the same value after as well as before the instant of discontinuity.

The co-ordinate system remains fixed at the base l of the press front. At an arbitrary instant the press front rising up from the left assumes the shape 1, and it will eventually occupy the vertical position 3. This front movement is associated with a flow phenomenon in that air flows from the right towards the base l with the mass speed $-c_0 = a_0$. A gradual drop in the speed to zero takes place within the front range, followed possibly by an increase in the direction to the right, should the front extend beyond the normal range. If the pressure p_1 is sufficiently low, the mass speed does not drop to zero, but air will continue to flow to the left once it has left again the front range. The conditions can be most easily understood if it is assumed that the front extends just over the normal range, that is to say, the mass speed drops to zero to the left of the front. The propagation of the front with the co-ordinate system in l can then be said to have the characteristic of an elastic filling – elastic since the air particles will not suddenly come to rest, but will be retarded from the velocity a_0 to zero within a finite time. This retardation time becomes continuously shorter during the propagation and will be zero as soon as the front attains the vertical position. At this instant filling does not take place any longer elastically, but the air particles are suddenly slowed down, that is to say, the process has a shock characteristic. An instantaneous change in the nature of the process thus takes place with the appearance of discontinuity. It is a simple matter to see that in reality secondary wave phenomena ought to be generated. An exact theoretical treatment of the conditions proves to be, however, extremely difficult to perform. The general opinion is that a drop in pressure will be propagated to the left, and Pfriem [46] has made calculations which support this supposition.

Returning to the simple case, it is assumed now that air continues to flow from the right towards the vertical front 3 with the mass speed a_0 relative to point l and that the air to the left of point l is at rest having the pressure p_1. The front, relative to l, must thereafter move to the right, which is assumed to take place with the vertical shape and pressure p_1 unaltered. The front cannot continue rising to the right around the base point l as indicated by the broken curves 4′ and 5′, since this would mean that different pressures would prevail simultaneously at the same point in the duct, which is physically impossible. If it is assumed now, in conformity with Riemann [4], that the change in state within the front continues according to the static adiabate, the following calculations can be made.

The vertical front, that is to say, the shock front, moves with velocity y to the right relative to point l. The air flowing from the right meets the front with the velocity $y + a_0$. Since the mass speed behind the front in the system l is zero, the air will leave the front with the velocity y. With $c = 0$, Eq. (46) gives the acoustic speed ratio $a/a_0 = 1.2$. When a change of state occurs according to the static adiabate, and with $c = 0$, the following relationship applies

$$\frac{y+a_0}{y} = \frac{\varrho}{\varrho_0} = \left(\frac{a}{a_0}\right)^{\frac{2}{\varkappa-1}} , \qquad (67)$$

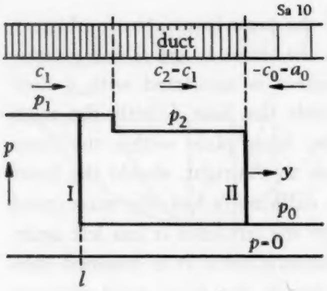

Fig. 11. Rise of discontinuity with dynamic-adiabatic change in state.

which gives

$y/a_0 = 0.67$ or, relative to the duct, $w/a_0 = 1.67$ (68)

Furthermore, we have

$$\frac{p}{p_0} = \left(\frac{a}{a_0}\right)^{\frac{2\varkappa}{\varkappa-1}} = 3.60 \tag{69}$$

The front is thus propagated at $c = 0$ with a velocity $y = 0.67\ a_0$ to the right relative to point l, that is to say, with about 56 per cent of the velocity with which the propagation takes place at the top of the original press front.

If c has a finite value, positive or negative, the initial equation becomes

$$\frac{y-a_0}{y-c} = \frac{y+a_0}{y-\frac{2}{\varkappa-1}\left(a-\frac{\varkappa+1}{2}a_0\right)} \tag{70}$$

which gives

$$\frac{y}{a_0} = \frac{\frac{2}{\varkappa-1}\left(\frac{a}{a_0}-\frac{\varkappa+1}{2}\right)\left(\frac{a}{a_0}\right)^{\frac{2}{\varkappa-1}}+1}{\left(\frac{a}{a_0}\right)^{\frac{2}{\varkappa-1}}-1} \tag{71}$$

and relative to the duct

$$\frac{w}{a_0} = \frac{1+\frac{2}{\varkappa-1}\left(\frac{a}{a_0}-\frac{\varkappa+1}{2}\right)}{1-\left(\frac{a}{a_0}\right)^{-\frac{2}{\varkappa-1}}} \tag{72}$$

Hence it follows that all the state quantities maintain their values after discontinuity has occurred, including also the temperature.

The case where the change in state, after discontinuity has occurred, takes place according to the *dynamic* adiabate will now be treated. The conditions are presented in Fig. 11, where the vertical line I shows the front just at the moment of discontinuity and the line II an instant later. The pressure p_2 after the moment of discontinuity must be assumed here to differ from the pressure p_1 before this moment. It is assumed that the sudden change in pressure $p_1 - p_2$ remains at the same place relative to the air during the continued propagation of the front in order to simplify the calculations of this case. Air flows from the right towards the front with the mass speed $y + a_0$ and leaves the front with the velocity $y - c_1$, since it follows for reasons of continuity that the mass speed c_2 after the shock front must have the same value as the original mass speed c_1.

Before discontinuity occurs,

$$c_1 = \frac{2}{\varkappa - 1}\left(a_1 - \frac{\varkappa + 1}{2} a_0\right) \quad \text{or} \quad \frac{c_1}{a_0} = \frac{2}{\varkappa - 1}\left(\frac{a_1}{a_0} - \frac{\varkappa + 1}{2}\right) \tag{73}$$

applies as in the previous case.

According to Eq. (65) the following expression applies to the shock front

$$\frac{c_1 + a_0}{a_0} = \frac{c_1}{a_0} + 1 = \frac{\frac{p_2}{p_0} - 1}{\varkappa \sqrt{1 + \frac{\varkappa + 1}{2\varkappa}\left(\frac{p_2}{p_0} - 1\right)}} \tag{74}$$

or, after inserting Eq. (73),

$$\frac{a_1}{a_0} = \left(\frac{p_1}{p_0}\right)^{\frac{\varkappa - 1}{2\varkappa}} = \frac{\varkappa + 1}{2} + \frac{\varkappa - 1}{2} \cdot \frac{\frac{p_2}{p_0} - 1}{\varkappa \sqrt{1 + \frac{\varkappa + 1}{2\varkappa}\left(\frac{p_2}{p_0} - 1\right)} - 1} \tag{75}$$

from which p_2/p_0 can be found as a function of p_1/p_0.

The relationship between these quantities is shown graphically in Fig. 12. With $c_1 = 0$, that is to say, at the limit of the normal range, $a_1/a_0 = 1.2$ according to Eq. (73). Introducing this value in Eq. (75) gives $p_2/p_0 = 3.48$ and $p_1/p_0 = 3.58$, that is to say, $p_2/p_1 = 0.97$. The sudden change in pressure $p_1 - p_2$ is limited, as can be seen, within the normal range to relatively very low values. Actually the sudden change does not of course remain as a discontinuity at the same point in the air, but must be assumed to be divided already from the beginning into a shock front moving to the right and an expansion front moving to the left. Theoretically it ought to be possible to treat this phenomenon in the same way as for a sudden removal of a partition separating air of different densities, studied previously by Schardin [35]. When assessing the experimental results described later on, it is unnecessary, how-

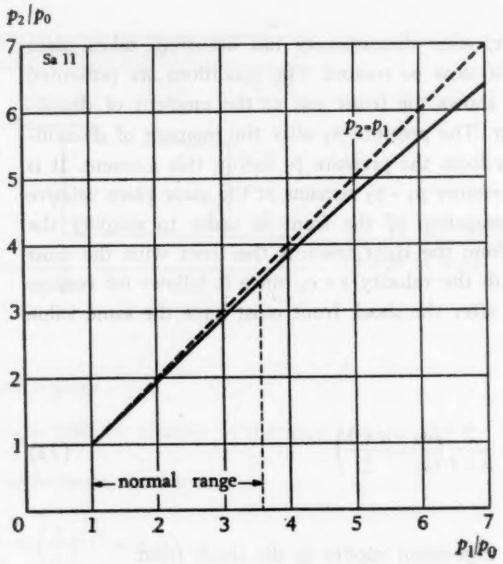

Fig. 12. Graphical representation of the relationship between p_1 and p_2 in Eq. (75).

ever, to investigate more closely these conditions, since the pressures occurring are generally of the magnitude valid for the normal range.

The fundamental equation

$$\frac{y+a_0}{y-c_1} = \frac{\dfrac{y}{a_0}+1}{\dfrac{y}{a_0}-\dfrac{c_1}{a_0}} = \frac{\varrho_2}{\varrho_0} = \frac{\dfrac{\varkappa+1}{\varkappa-1}\cdot\dfrac{p_2}{p_0}+1}{\dfrac{\varkappa+1}{\varkappa-1}+\dfrac{p_2}{p_0}} \tag{76}$$

applies to the front velocity.

Hence, in the special case $c_1 = 0$

$$\frac{y}{a_0} = \frac{(\varkappa-1)\dfrac{p_2}{p_0}+\varkappa+1}{2\left(\dfrac{p_2}{p_0}-1\right)} \tag{77}$$

As has already been shown above, p_2/p_0 in this case is equal to 3.48, and thus $y/a_0 = 0.765$ and $w/a_0 = 1.765$. The velocity of the shock front relative to the duct will thus be about 6 per cent higher for a dynamic-adiabatic change in state than for a static-adiabatic change, this occurring at the limit of the normal range. It is assumed then that the air ahead of the front is at rest ($u_0 = 0$), that is to say, the original base l moves with the velocity a_0 to the right.

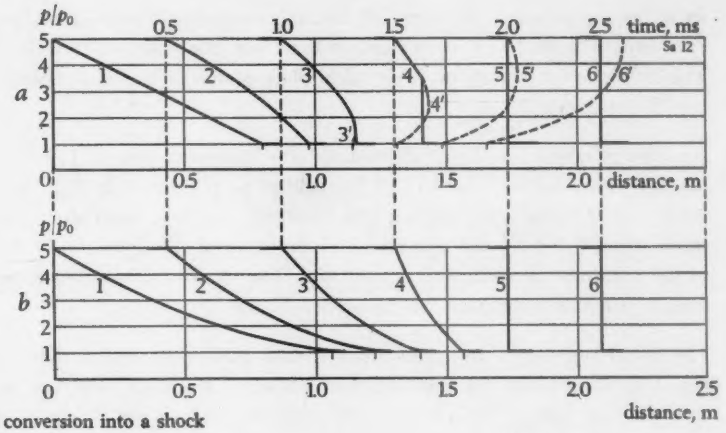

a Gradual conversion into a shock front
b Instantaneous conversion into a shock front
c Method of determining the conversion into shock front in case a

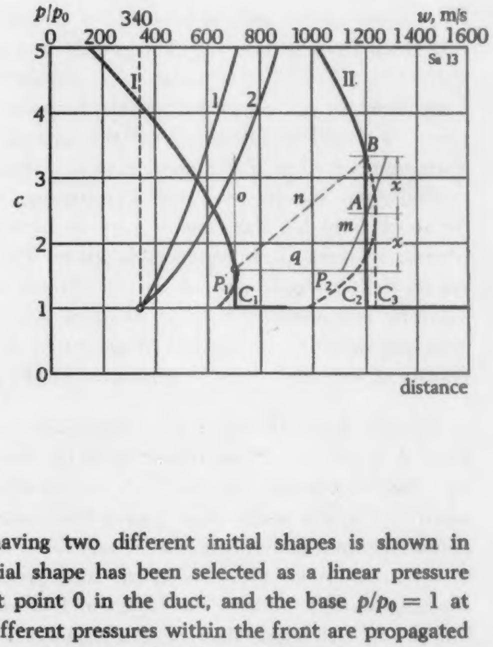

1 w as function of p/p_0 for shock front
2 w as function of p/p_0 for press front
(Applies only to Fig. 13c)

Fig. 13. Propagation of a press front and its conversion into a shock front.

The propagation of a press front having two different initial shapes is shown in Figs. 13a and b. In Fig. 13a the initial shape has been selected as a linear pressure distribution with the top $p/p_0 = 5$ at point 0 in the duct, and the base $p/p_0 = 1$ at the distance 0.8 m in the duct. The different pressures within the front are propagated with front velocities w according to the curves in Fig. 13c, which are based on the curves in Fig. 8 and on an acoustic speed of 340 m/s at $p/p_0 = 1$, corresponding to an approximate temperature ahead of the front of $T = 288$ °K (15 °C). The mass speed ahead of the front has been assumed to be zero. The time interval is 0.5 ms between two adjacent front positions 1 to 6. Since the front velocity increases with an increasing pressure, the front will become steeper as it propagates, and somewhere between positions 2 and 3 the head of the front, the base, starts to become vertical. The conversion into a shock front takes place gradually and is completed when position 5 is reached.

Another principle has been adopted for the representation in Fig. 13b. Position 5 has been assumed to be given – it is identical to position 5 in Fig. 13a – and it has been assumed that this position has resulted, not from a gradual formation of a shock front, but from the attainment of the state of discontinuity by the press front at the same instant along the entire front. The front positions 1–4 have been determined with this assumption by calculating backwards.

The initial shape 1 of the press front is thus quite different in these two cases; in Fig. 13a, for example, it extends over 0.8 m of the duct, whereas in Fig. 13b it extends over 1.06 m. Both fronts give identical shock fronts 5, however, after 2 ms and the distance 1.73 m.

Fig. 13c shows the method adopted for determining the transition from press front into shock front in Fig. 13a. The propagation of front 1 in this latter Figure leads to the fronts 3′–6′, if the formation of a shock front is completely disregarded. These front forms are not physically possible, however, since they signify that two different pressures prevail simultaneously in the same point of the duct. The shock front is often represented in the literature as a vertical tangent to the curves 3′–6′. This method yields, however, too high a propagation velocity, since it is then assumed that the shock front has the same velocity as a press front with the same top pressure, whereas in reality it is considerably lower. The method based on Fig. 13c includes the arithmetic mean value of the shock-front velocity between two front positions following one another. If these positions are situated at not too large a distance from one another, the method yields rather exact results, since the curve for the velocity of the shock front as a function of the pressure is nearly linear.

In Fig. 13c, I and II denote two front positions, roughly corresponding to positions 3 and 4 in Fig. 13a. If the formation of the shock front is not taken into consideration, the front shapes I-P_1 and II-P_2 are obtained. The vertical tangent to P_2 is denoted by C_3. The shock front C_1 has been extended upwards in the axis *o* of the co-ordinate system shown in colour, and the distances which a shock front according to the curve for *w* covers during the corresponding time intervals have been plotted along its abscissa, which gives curve *m*. If a vertical line C_2 intersecting II and *m* is drawn in such a way that the two distances *x* will have the same length, the point of intersection *B* on the front II will represent the limit point between the continuous and the discontinuous part of front II. The line C_2 up to point *B* represents the shock front. In this method the approximation is made that the pressure in the shock front during its propagation between C_1 and C_2 rises linearly with distance and time, corresponding to line *n* in the Figure.

F. FRONT REFLECTION

Only the states before and after a completed reflection and not the reflection itself will be treated here. Theoretical investigations concerning the latter are to be found in several sources in the literature. Reference can be made, for example, to Pfriem [45]. The changes in state during the reflection itself are rather complicated and difficult to grasp as far as continuous fronts are concerned.

Fronts can be reflected in different ways as, for example,

(a) against a rigid wall in the duct,
(b) against a fully or partly open duct end,
(c) in conjunction with constriction of the duct,
(d) in conjunction with expansion of the duct,
(e) against a boundary surface between air columns of different states.

In addition, reflection phenomena resulting from the conversion of a press front into a shock front in a duct having a constant cross-sectional area must also be included.

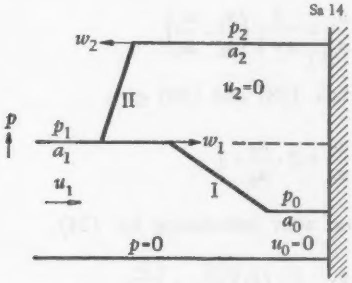

Fig. 14. Reflection against a rigid wall of a positive press front (I), *changing into a negative press front* (II).

Fig. 14 indicates the conditions for reflection of a positive press front I against a rigid wall. If the mass speed u_1 is lower than the acoustic speed a_1, the base of the reflected front II can propagate towards the left, and the front may then possibly have a continuous character also after the reflection, that is to say, it is converted into a negative press front. If $u_1 \geq a_1$, the original press front changes over immediately at the reflection into a negative shock front, since the base of the press front in this case has no possibility of propagating towards the left.

A calculation is made in the following of the pressure p_2 behind the reflected front II. It is first assumed that the front is a negative press front (Fig. 14). The initial state ahead of front I is air at rest having a pressure of p_0 and the acoustic speed a_0. The air between the front and the wall remains at rest also after the reflection, but has a higher pressure p_2 and a higher acoustic speed a_2. All the changes in state take place according to the static adiabate. The following applies to front I according to Eq. (54)

$$\frac{u_1}{a_0} = \frac{2}{\varkappa - 1}\left(\frac{a_1}{a_0} - 1\right) \qquad (78)$$

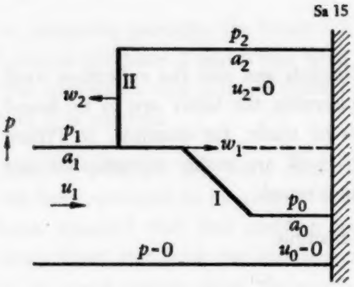

Fig. 15. Reflection against a rigid wall of a positive press front (I), changing into a negative shock front (II).

and for front II according to Eq. (56)

$$-\frac{u_1}{a_2} = \frac{2}{\varkappa - 1}\left(\frac{a_1}{a_2} - 1\right) \tag{79}$$

which divided by a_0 gives

$$\frac{u_1}{a_0} = \frac{2}{\varkappa - 1}\left(\frac{a_2}{a_0} - \frac{a_1}{a_0}\right) \tag{80}$$

Eqs. (78) and (80) give

$$\frac{a_2}{a_0} = 2 \cdot \frac{a_1}{a_0} - 1 \tag{81}$$

or, after introducing Eq. (24),

$$\frac{p_2}{p_0} = \left[2\left(\frac{p_1}{p_0}\right)^{\frac{\varkappa-1}{2\varkappa}} - 1\right]^{\frac{2\varkappa}{\varkappa-1}} \tag{82}$$

For the case shown in Fig. 15 where the reflected front II is a negative shock front, Eq. (78) applies to front I, whereas front II obeys Eq. (65), which with the notation in Fig. 15 gives

$$\frac{u_1}{a_1} = \frac{\dfrac{p_2}{p_1} - 1}{\varkappa\sqrt{1 + \dfrac{\varkappa+1}{2\varkappa}\left(\dfrac{p_2}{p_1} - 1\right)}} \tag{83}$$

Eqs. (78) and (83) give

$$\frac{a_1}{a_0} = \left(\frac{p_1}{p_0}\right)^{\frac{\varkappa-1}{2\varkappa}} = \left[1 - \frac{\dfrac{\varkappa-1}{2\varkappa}\left(\dfrac{p_2}{p_1} - 1\right)}{\sqrt{1 + \dfrac{\varkappa+1}{2\varkappa}\left(\dfrac{p_2}{p_1} - 1\right)}}\right]^{-1} \tag{84}$$

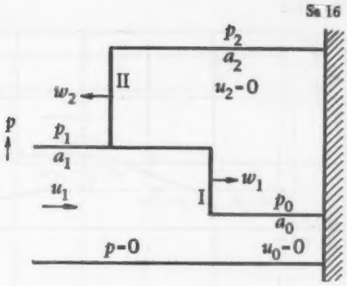

Fig. 16. Reflection against a rigid wall of a positive shock front (I), changing into a negative shock front (II).

According to Eq. (66) we have

$$\frac{w_2+u_1}{a_1}=\sqrt{1+\frac{\varkappa+1}{2\varkappa}\left(\frac{p_2}{p_1}-1\right)} \tag{85}$$

If u_1/a_1 from Eq. (83) is introduced,

$$\frac{w_2}{a_1}=\frac{\dfrac{\varkappa-1}{2\varkappa}\cdot\dfrac{p_2}{p_1}+\dfrac{\varkappa+1}{2\varkappa}}{\sqrt{1+\dfrac{\varkappa+1}{2\varkappa}\left(\dfrac{p_2}{p_1}-1\right)}} \tag{86}$$

or, with Eq. (84),

$$\frac{w_2}{a_0}=\frac{\dfrac{\varkappa-1}{2\varkappa}\cdot\dfrac{p_2}{p_1}-\dfrac{\varkappa+1}{2\varkappa}}{\sqrt{1+\dfrac{\varkappa+1}{2\varkappa}\left(\dfrac{p_2}{p_1}-1\right)}-\dfrac{\varkappa-1}{2\varkappa}\left(\dfrac{p_2}{p_1}-1\right)} \tag{87}$$

If front I is also a shock front, as shown in Fig. 16, we have for this latter according to Eq. (63)

$$\frac{u_1}{a_0}=\frac{\dfrac{p_1}{p_0}-1}{\varkappa\sqrt{1+\dfrac{\varkappa+1}{2\varkappa}\left(\dfrac{p_1}{p_0}-1\right)}} \tag{88}$$

Front II obeys Eq. (83). Considering Eq. (36), Eqs. (83) and (88) give the following relationship between the pressures

$$\frac{\left(\dfrac{p_2}{p_1}-1\right)^2}{1+\dfrac{\varkappa+1}{2\varkappa}\left(\dfrac{p_2}{p_1}-1\right)}=\frac{\left(\dfrac{\varkappa+1}{\varkappa-1}+\dfrac{p_0}{p_1}\right)\left(\dfrac{p_1}{p_0}-1\right)^2}{\left(\dfrac{\varkappa+1}{\varkappa-1}+\dfrac{p_1}{p_0}\right)\left[1+\dfrac{\varkappa+1}{2\varkappa}\left(\dfrac{p_1}{p_0}-1\right)\right]} \tag{89}$$

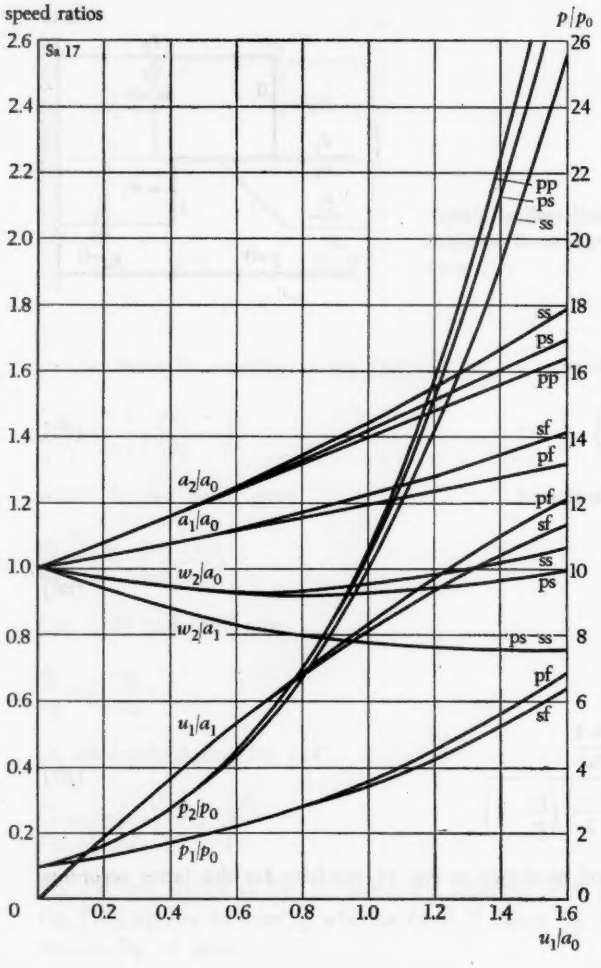

pf	Press front
sf	Shock front
pp	Press front changing into press front
ps	Press front changing into shock front
ss	Shock front changing into shock front

Fig. 17. Pressure and speed curves for reflection of a front against a rigid wall. (The symbols refer to Figs. 14–16.)

Eq. (86) applies to the front velocity w_2/a_1 which, with Eq. (36), gives

$$\frac{w_2}{a_0} = \left(\frac{\varkappa-1}{2\varkappa}\cdot\frac{p_2}{p_1}+\frac{\varkappa+1}{2\varkappa}\right)\sqrt{\frac{\dfrac{\varkappa+1}{\varkappa-1}+\dfrac{p_1}{p_0}}{\left(\dfrac{\varkappa+1}{\varkappa-1}+\dfrac{p_0}{p_1}\right)\left[1+\dfrac{\varkappa+1}{2\varkappa}\left(\dfrac{p_2}{p_1}-1\right)\right]}} \qquad (90)$$

The reflection of a shock front against a rigid wall is treated theoretically by Pfriem [45]. He has found that the ratio between the pressure rises after and before the

Sa 18

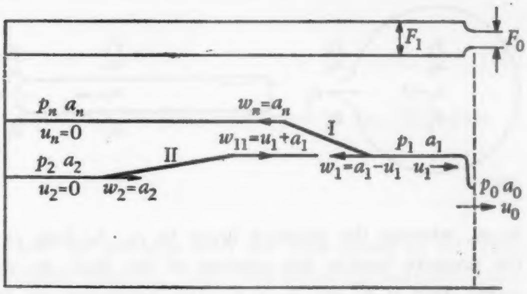

Fig. 18. Calculation of fronts in conjunction with the rapid discharge of a duct alone.

reflection, $(p_2-p_0)/(p_1-p_0)$, becomes 2 at $p_1/p_0=1$ and approaches a maximum value of 8 when p_1/p_0 is increased. If, for example, $p_1/p_0=3$, $(p_2-p_0)/(p_1-p_0)=$ $=3.25$.

Fig. 17 shows curves for pressures and velocities when a front is reflected against a rigid wall for the three cases treated above. The speed ratio u_1/a_0 has been selected as the abscissa so as to facilitate the comparison between the results obtained from measurements. The curves have been plotted with the aid of the front curves shown in Fig. 8. They do not display, at least within the normal range $(u_1/a_0 \leq 1)$, any pronounced differences between one another.

Fronts which are reflected in the ways (b)–(e), described at the beginning of this chapter, will be treated in a later chapter in so far as they are of interest when judging the results obtained from the measurements.

G. CALCULATION OF WAVE PHENOMENA IN CONJUNCTION WITH THE RAPID DISCHARGE OF DUCTS

I. Discharge of a duct only

Let us assume a duct having a constant cross-sectional area F_1 and at one end an opening with an area of F_0, being closed from the beginning. The other end of the duct may be closed or may open out into a large container. The case where the duct is *closed* will first be treated. The duct is filled with air having the state n. The pressure p_n within the duct is higher than the external pressure. The opening F_0 is rapidly uncovered and air starts to flow out. The change in state of the air in the duct from rest to motion takes place as a wave front, which moves from the opening F_0 into the duct. The front, which is denoted I in Fig. 18, is a negative expansion front. The air ahead of the front is in a state of rest and has the pressure p_n. Behind the front there is air flowing towards the opening with the mass speed u_1 and the pressure p_1. In the minimum cross-sectional area F_0 of the opening the speed increases

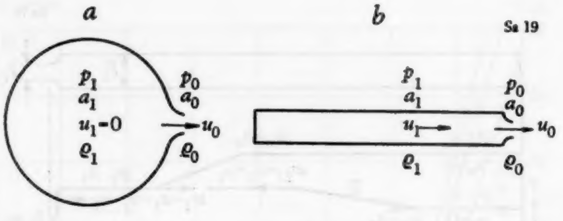

Fig. 19. Calculation of static nozzle pressure for discharge from a large container (a) and from a long duct (b). Initial mass speed $u_1 = 0$ (a) and $u_1 > 0$ (b).

to u_0, whereas the pressure drops to p_0. As long as the pressure p_0 is higher than the pressure outside the opening of the duct, air will flow out with the speed of sound, that is to say, $u_0 = a_0$. The conditions are treated in the following making this assumption. The first step is to determine how the state 1 varies with the change in the cross-sectional area ratio F_0/F_1. The state 1 is calculated relative to the initial state n. What is to be determined is consequently the pressure ratio p_1/p_n, the mass-speed ratio u_1/a_n and the acoustic-speed ratio a_1/a_n as a function of the cross-sectional area ratio F_0/F_1.

Before treating the wave phenomena, equations must be derived for the static pressure in the opening F_0. This pressure deviates in fact from the normal critical pressure which is 0.53 times the container pressure. This latter value applies to air flowing directly out of a container, which is so large that the air velocity within it can be considered as being zero. In a duct, however, the air flows with a considerable velocity towards the opening, and this velocity influences the static pressure in the opening. Fig. 19 shows schematically the discharge from a large container and from a long duct.

The law of energy Eq. (16) gives the following relationship between the states 1 and 0.

$$\frac{u_1^2}{2} + \frac{\varkappa}{\varkappa - 1} \cdot \frac{p_1}{\varrho_1} = \frac{u_0^2}{2} + \frac{\varkappa}{\varkappa - 1} \cdot \frac{p_0}{\varrho_0} \tag{91}$$

Introducing

$$\frac{p_1}{\varrho_1} = \frac{a_1^2}{\varkappa} \quad \text{and} \quad \frac{p_0}{\varrho_0} = \frac{a_0^2}{\varkappa} \tag{92}$$

according to the equation of state (6) and

$$a_0^2 = a_1^2 \left(\frac{p_0}{p_1}\right)^{\frac{\varkappa - 1}{\varkappa}} \tag{93}$$

according to the adiabate law Eq. (24), we obtain

$$\frac{p_0}{p_1} = \left(1 + \frac{\varkappa - 1}{2} \cdot \frac{u_1^2 - u_0^2}{a_1^2}\right)^{\frac{\varkappa}{\varkappa - 1}} \tag{94}$$

When air flows out from a large container, the mass speed $u_1 = 0$. We then have

$$\frac{p_0}{p_1} = \left[1 - \frac{\varkappa - 1}{2}\left(\frac{u_0}{a_1}\right)^2\right]^{\frac{\varkappa}{\varkappa - 1}} \tag{95}$$

For a supercritical pressure ratio ($u_0 = a_0$) Eq. (93) introduced in Eq. (95) gives

$$\frac{p_0}{p_1} = \left(\frac{2}{\varkappa + 1}\right)^{\frac{\varkappa}{\varkappa - 1}} = 0.53 \tag{96}$$

For a duct with air flowing towards the opening with the mass speed u_1 Eq. (94) directly applies to a subcritical pressure ratio ($u_0 < a_0$). The following *nozzle-pressure equation* is obtained for a supercritical pressure ratio, which is of interest here, if Eq. (93) is inserted in Eq. (94)

$$\frac{p_0}{p_1} = \left[\frac{2}{\varkappa + 1} + \frac{\varkappa - 1}{\varkappa + 1}\left(\frac{u_1}{a_1}\right)^2\right]^{\frac{\varkappa}{\varkappa - 1}} \tag{97}$$

or

$$\frac{p_0}{p_1} = \left(\frac{2}{\varkappa + 1}\right)^{\frac{\varkappa}{\varkappa - 1}}\left[1 + \frac{\varkappa - 1}{2}\left(\frac{u_1}{a_1}\right)^2\right]^{\frac{\varkappa}{\varkappa - 1}} = 0.53\left[1 + 0.2\left(\frac{u_1}{a_1}\right)^2\right]^{3.5} \tag{98}$$

When treating again the wave phenomena, we obtain for the conditions in Fig. 18 according to the mass law

$$u_1 F_1 \varrho_1 = u_0 F_0 \varrho_0 \tag{99}$$

and, according to the adiabate law,

$$\frac{\varrho_1}{\varrho_0} = \left(\frac{p_1}{p_0}\right)^{\frac{1}{\varkappa}} \tag{100}$$

With $u_0 = a_0$, the latter two equations give

$$\frac{u_1}{a_0} = \frac{F_0}{F_1}\left(\frac{p_0}{p_1}\right)^{\frac{1}{\varkappa}} \tag{101}$$

Introducing according to the adiabate law

$$\frac{a_1}{a_0} = \left(\frac{p_1}{p_0}\right)^{\frac{\varkappa - 1}{2\varkappa}} \tag{102}$$

results in

$$\frac{p_0}{p_1} = \left(\frac{u_1}{a_1} \cdot \frac{F_1}{F_0}\right)^{\frac{2\varkappa}{\varkappa + 1}} \tag{103}$$

The nozzle-pressure equation (97) is now introduced, which gives

$$\frac{F_1}{F_0}=\frac{a_1}{u_1}\left[\frac{2}{\varkappa+1}+\frac{\varkappa-1}{\varkappa+1}\left(\frac{u_1}{a_1}\right)^2\right]^{\frac{\varkappa+1}{2(\varkappa-1)}} \tag{104}$$

According to the adiabate law

$$\frac{a_1}{a_n}=\left(\frac{p_1}{p_n}\right)^{\frac{\varkappa-1}{2\varkappa}} \tag{105}$$

which, together with Eq. (104), yields

$$\frac{F_1}{F_0}=\frac{a_n}{u_1}\left(\frac{p_1}{p_n}\right)^{\frac{\varkappa-1}{2\varkappa}}\left[\frac{2}{\varkappa+1}+\frac{\varkappa-1}{\varkappa+1}\left(\frac{u_1}{a_n}\right)^2\left(\frac{p_1}{p_n}\right)^{-\frac{\varkappa-1}{\varkappa}}\right]^{\frac{\varkappa+1}{2(\varkappa-1)}} \tag{106}$$

The equation for a negative expansion front is according to Eqs. (56) and (105)

$$\left(\frac{p_1}{p_n}\right)^{\frac{\varkappa-1}{2\varkappa}}=1-\frac{\varkappa-1}{2}\cdot\frac{u_1}{a_n} \tag{107}$$

Introducing this in Eq. (106) results in

$$\frac{F_1}{F_0}=\frac{1-\frac{\varkappa-1}{2}\cdot\frac{u_1}{a_n}}{\frac{u_1}{a_n}}\left[\frac{2}{\varkappa+1}+\frac{\varkappa-1}{\varkappa+1}\left(\frac{\frac{u_1}{a_n}}{1-\frac{\varkappa-1}{2}\cdot\frac{u_1}{a_n}}\right)^2\right]^{\frac{\varkappa+1}{2(\varkappa-1)}} \tag{108}$$

The calculation of u_1/a_n can be simplified by introducing

$$x=\frac{\frac{u_1}{a_n}}{1-\frac{\varkappa-1}{2}\cdot\frac{u_1}{a_n}} \tag{109}$$

Making this substitution, Eq. (108) assumes the form

$$\frac{F_0}{F_1}=\frac{x}{\left(\frac{2}{\varkappa+1}+\frac{\varkappa-1}{\varkappa+1}x^2\right)^{\frac{\varkappa+1}{2(\varkappa-1)}}}=\frac{x}{(0.833+0.167\,x^2)^3} \tag{110}$$

This equation has been plotted as a curve in Fig. 20. If Eq. (109) is solved with regard to u_1/a_n,

$$\frac{u_1}{a_n}=\frac{x}{1+\frac{\varkappa-1}{2}x}=\frac{x}{1+0.2\,x} \tag{111}$$

from which u_1/a_n can be found, after the value of x for a given ratio of F_0/F_1 has been taken from the curve in Fig. 20.

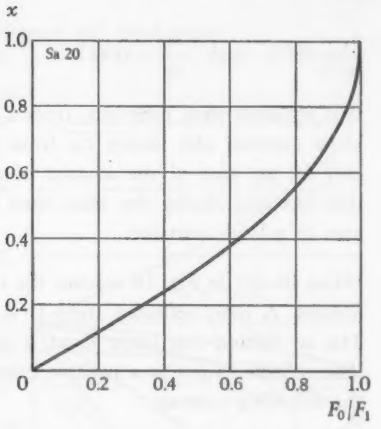

Fig. 20. Graphical representation of Eq. (110) with x as function of the cross-sectional area ratio, F_0/F_1.

The pressure ratio p_1/p_n can then be found from Eq. (107) and the acoustic-speed ratio a_1/a_n from Eq. (105).

The *front velocities* for the base and top of front I (Fig. 18), respectively, are $w_1 = a_1 - u_1$ and $w_n = a_n$, which are both directed from the opening F_0 inwards into the duct, thus causing this front to move to the left. The base has a lower velocity than the top, and consequently the steepness will decrease with the propagation, that is to say, the front range along the duct increases with the propagation. By varying the pressure ratio in Eqs. (105) and (107), the change in the shape of the front with the propagation can be followed.

For the limit case $F_0 = F_1$, when the entire cross-sectional area of the duct is uncovered, $p_0 = p_1$, $u_0 = u_1$, and $a_0 = a_1$. If the discharge takes place at the speed of sound, that is to say, $u_1 = a_1$, we have then according to Eqs. (105) and (107)

$$\frac{p_1}{p_n} = \left(\frac{2}{\varkappa+1}\right)^{\frac{2\varkappa}{\varkappa-1}} = 0.278 \tag{112}$$

The front velocity of the base becomes in this case $w_1 = a_1 - u_1 = a_1 - a_1 = 0$, that is to say, the base remains at the opening, whereas the top moves into the duct with the velocity a_n. The front will thus finally lie along the entire duct. The mass speed becomes according to Eqs. (104), (107) and (112)

$$\frac{u_1}{a_n} = \frac{2}{\varkappa+1} = 0.833 \tag{113}$$

It may be of interest to compare these values for a discharge front with the critical state in an opening which is fed direct from a large container filled with air having the state n. For the latter case Eqs. (95) and (96) give

$$\frac{p_1}{p_n} = 0.53 \quad \text{and} \quad \frac{u_1}{a_n} = 0.913 \tag{114}$$

It is apparent that, inter alia, from a tube filled with compressed air which is opened at its external end, during the front movement away from and towards the opening only 58 per cent of the amount of air by weight is flowing out as compared with that obtained during the same time from an opening with the same cross-sectional area in a large container.

When front I in Fig. 18 reaches the closed end of the duct, a reflection process commences. A new, reflected front II is formed, which moves towards the opening F_0. The air behind this latter front is in a state of rest having a pressure of $p_2 < p_1$. The reflected front is a positive expansion front. The state 2 can be determined in the following manner.

According to Eqs. (24) and (54) the front equation is

$$\left(\frac{p_1}{p_2}\right)^{\frac{\kappa-1}{2\kappa}} = 1 + \frac{\kappa-1}{2} \cdot \frac{u_1}{a_2} \tag{115}$$

The adiabate law Eq. (24) gives

$$\frac{a_2}{a_n} = \left(\frac{p_2}{p_n}\right)^{\frac{\kappa-1}{2\kappa}} \tag{116}$$

which, introduced in Eq. (115), results in

$$\frac{p_2}{p_n} = \left[\left(\frac{p_1}{p_n}\right)^{\frac{\kappa-1}{2\kappa}} - \frac{\kappa-1}{2} \cdot \frac{u_1}{a_n}\right]^{\frac{2\kappa}{\kappa-1}} \tag{117}$$

If Eq. (107) is introduced here, this yields

$$\frac{p_2}{p_n} = \left[2\left(\frac{p_1}{p_n}\right)^{\frac{\kappa-1}{2\kappa}} - 1\right]^{\frac{2\kappa}{\kappa-1}} \tag{118}$$

which is, in principle, the same expression as Eq. (82) for a reflected press front.

It should be readily perceived that the steepness of the front diminishes also after the reflection. Fig. 21 shows the pressure and speed ratios, as functions of the cross-sectional area ratio for the expansion fronts I and II. When front II reaches the opening F_0, a reflection is also initiated here. The reflected front III can be treated in the same way as front I. The initial state is, in this case, air at rest having a pressure of p_2 and an acoustic speed of a_2. The condition for this, however, is that the pressure at F_0 should be still higher than the pressure outside the opening, that is to say, the discharge should take place with the acoustic speed. If this is not so, the calculation must be based on a nozzle-pressure equation which takes into consideration the velocity at F_0. It would be too laborious, however, to treat also this case here

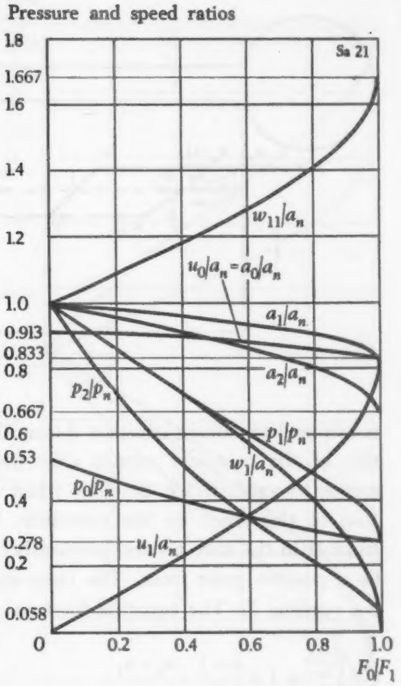

Fig. 21. Front curves for the rapid discharge of a duct alone. (The symbols refer to Fig. 18.)

and it is not necessary when making the comparison with the measured results described later on, since the measurements have been performed at relatively high pressures.

A reservation must be made as far as the calculated state 2 is concerned in the case of high values of the cross-sectional area ratio F_0/F_1. It has already been shown that the base of front I remains at the opening if $F_0/F_1 = 1$, which means that the top of the front II will not encounter air of state 1 until it reaches the opening. Previous to this, the top has moved in air having a pressure which has dropped gradually to the value p_1 at the opening. Consequently, p_2 has obtained a higher value than that resulting from the method of calculation. The pressure behind front II is unable to drop to the calculated value at sufficiently high values of F_0/F_1, since front III reflected from the opening has already commenced to change the state 2.

II. Discharge of a duct connected to a container

The case where the duct is not closed at the inner end but runs out into a *large container* (Fig. 22) will now be treated. It is assumed that the container and the duct are filled with compressed air of the state *n*. The pressure p_n in the container

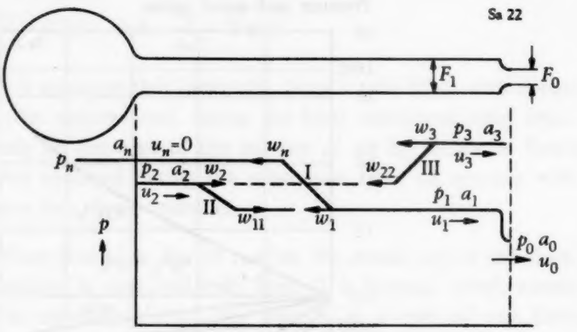

Fig. 22. Calculation of fronts in conjunction with the rapid discharge of a duct with container.

is assumed to remain constant during the experiment. It is evident that the introduction of the container cannot alter the conditions with regard to the first front I moving inwards which develops when the opening F_0 is uncovered. After the reflection of this front by the container, however, a front II develops, differing from front II in the case treated previously. It is apparent that the reflected front II must be a positive press front. The mass speed behind the front is also directed towards the opening F_0. The equation for front II is then according to Eqs. (24) and (54)

$$\left(\frac{p_2}{p_1}\right)^{\frac{\varkappa-1}{2\varkappa}} = 1 + \frac{\varkappa-1}{2} \cdot \frac{u_2 - u_1}{a_1} \tag{119}$$

State 1 is given from Eqs. (105), (107) and (111), and the sought state 2 can therefore be determined on the basis of state 1. Introducing state n in Eq. (119) gives

$$\frac{\left(\frac{p_2}{p_n}\right)^{\frac{\varkappa-1}{2\varkappa}}}{\left(\frac{p_1}{p_n}\right)^{\frac{\varkappa-1}{2\varkappa}}} = 1 + \frac{\frac{\varkappa-1}{2}\left(\frac{u_2}{a_n} - \frac{u_1}{a_n}\right)}{\frac{a_1}{a_n}} \tag{120}$$

A further two equations are required when determining state 2, that is to say, p_2/p_n, u_2/a_n and a_2/a_n. These are obtained by applying the energy law and the adiabate law to states n and 2. The energy law (17) gives

$$\frac{\varkappa-1}{2}\left(\frac{u_2}{a_n}\right)^2 + \left(\frac{a_2}{a_n}\right)^2 = 1 \tag{121}$$

According to the adiabate law Eq. (24)

$$\left(\frac{a_2}{a_n}\right)^2 = \left(\frac{p_2}{p_n}\right)^{\frac{\varkappa-1}{\varkappa}} \tag{122}$$

which, inserted in Eq. (121), gives

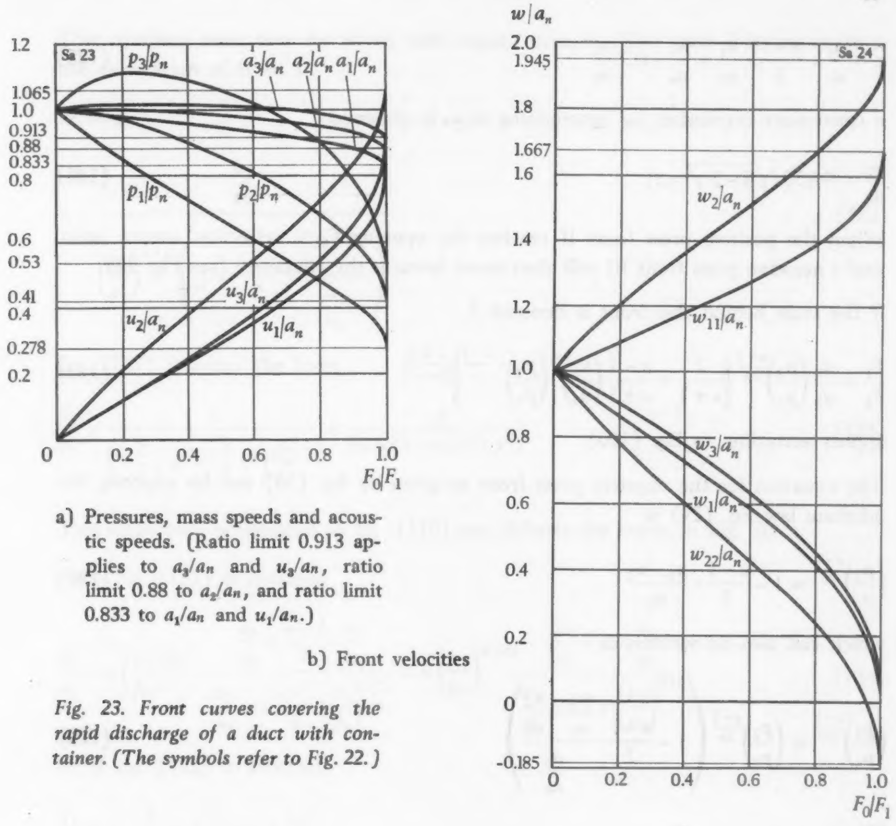

a) Pressures, mass speeds and acoustic speeds. (Ratio limit 0.913 applies to a_3/a_n and u_3/a_n, ratio limit 0.88 to a_2/a_n, and ratio limit 0.833 to a_1/a_n and u_1/a_n.)

b) Front velocities

Fig. 23. Front curves covering the rapid discharge of a duct with container. (The symbols refer to Fig. 22.)

$$\left(\frac{p_2}{p_n}\right)^{\frac{\varkappa-1}{2\varkappa}} = \sqrt{1-\frac{\varkappa-1}{2}\left(\frac{u_2}{a_n}\right)^2} \tag{123}$$

which, inserted in Eq. (120), gives

$$1-\frac{\varkappa-1}{2}\left(\frac{u_2}{a_n}\right)^2 = \left[\frac{1+\frac{\varkappa-1}{2}\cdot\left(\frac{u_2}{a_n}-\frac{u_1}{a_n}\right)}{\frac{a_1}{a_n}}\right]^2\left(\frac{p_1}{p_n}\right)^{\frac{\varkappa-1}{\varkappa}} \tag{124}$$

from which u_2/a_n can be determined on the basis of state 1. Then p_2/p_n is found from Eq. (123) and a_2/a_n from Eq. (122).

Curves for state 2 are plotted in Figs. 23a and b as a function of the ratio F_0/F_1. Introducing the acoustic speed in Eq. (24) instead of the pressure according to Eq. (105) and then writing

$$z = \frac{a_1}{a_n} - \frac{\varkappa - 1}{2} \cdot \frac{u_1}{a_n} = \frac{a_1}{a_n} - 0.2\,\frac{u_1}{a_n} \tag{125}$$

a convenient expression for determining u_2/a_n is obtained

$$\frac{u_2}{a_n} = 0.833\,(\sqrt{6 - 5\,z^2} - z) \tag{126}$$

When the positive press front II reaches the opening F_0, a reflection occurs again, and a negative press front III will then move towards the container (see Fig. 22).

If the state behind this front is denoted 3,

$$\frac{F_1}{F_0} = \frac{a_n}{u_3}\left(\frac{p_3}{p_n}\right)^{\frac{\varkappa-1}{2\varkappa}} \left[\frac{2}{\varkappa + 1} + \frac{\varkappa - 1}{\varkappa + 1}\left(\frac{u_3}{a_n}\right)^2 \left(\frac{p_3}{p_n}\right)^{-\frac{\varkappa-1}{\varkappa}}\right]^{\frac{\varkappa+1}{2(\varkappa-1)}} \tag{127}$$

applies according to Eq. (106)

The equation for the negative press front as given by Eq. (56) and by applying the adiabate law Eq. (24) is

$$\left(\frac{p_3}{p_2}\right)^{\frac{\varkappa-1}{2\varkappa}} = 1 - \frac{\varkappa - 1}{2} \cdot \frac{u_3 - u_2}{a_2} \tag{128}$$

which can also be written as

$$\left(\frac{p_3}{p_n}\right)^{\frac{\varkappa-1}{2\varkappa}} = \left(\frac{p_2}{p_n}\right)^{\frac{\varkappa-1}{2\varkappa}} \left(1 - \frac{\varkappa - 1}{2} \cdot \frac{\frac{u_3}{a_n} - \frac{u_2}{a_n}}{\frac{a_2}{a_n}}\right) \tag{129}$$

or

$$\left(\frac{p_3}{p_n}\right)^{-\frac{\varkappa-1}{\varkappa}} = \left(\frac{p_2}{p_n}\right)^{-\frac{\varkappa-1}{\varkappa}} \left(1 - \frac{\varkappa - 1}{2} \cdot \frac{\frac{u_3}{a_n} - \frac{u_2}{a_n}}{\frac{a_2}{a_n}}\right)^{-2} \tag{130}$$

Introducing Eqs. (129) and (130) in Eq. (127) results in

$$\frac{F_1}{F_0} = \frac{\left(\frac{p_2}{p_n}\right)^{\frac{\varkappa-1}{2\varkappa}}}{\frac{u_3}{a_n}} \left(1 - \frac{\varkappa - 1}{2} \cdot \frac{\frac{u_3}{a_n} - \frac{u_2}{a_n}}{\frac{a_2}{a_n}}\right) \times$$

$$\times \left[\frac{2}{\varkappa + 1} + \frac{\varkappa - 1}{\varkappa + 1}\left(\frac{u_3}{a_n}\right)^2 \left(\frac{p_2}{p_n}\right)^{-\frac{\varkappa-1}{\varkappa}} \left(1 - \frac{\varkappa - 1}{2} \cdot \frac{\frac{u_3}{a_n} - \frac{u_2}{a_n}}{\frac{a_2}{a_n}}\right)^{-2}\right]^{\frac{\varkappa+1}{2(\varkappa-1)}} \tag{131}$$

This equation must now be solved with regard to u_3/a_n. The state 2 is known from the calculation of front II.

Putting

$$x = \frac{\dfrac{u_3}{a_n}}{\left(\dfrac{p_2}{p_n}\right)^{\frac{\varkappa-1}{2\varkappa}} \left(1 - \dfrac{\varkappa-1}{2} \cdot \dfrac{\dfrac{u_3}{a_n} - \dfrac{u_2}{a_n}}{\dfrac{a_2}{a_n}}\right)} \tag{132}$$

Eq. (131) assumes the form

$$\frac{F_0}{F_1} = \frac{x}{\left(\dfrac{2}{\varkappa+1} + \dfrac{\varkappa-1}{\varkappa+1}\,x^2\right)^{\frac{\varkappa+1}{2(\varkappa-1)}}} = \frac{x}{(0.833 + 0.167\,x^2)^3} \tag{133}$$

This expression is identical to Eq. (110) and follows the curve in Fig. 20.

From Eq. (132) is obtained

$$\frac{u_3}{a_n} = x\left(\frac{p_2}{p_n}\right)^{\frac{\varkappa-1}{2\varkappa}} \cdot \frac{\dfrac{a_2}{a_n} + \dfrac{\varkappa-1}{2}\cdot\dfrac{u_2}{a_n}}{\dfrac{a_2}{a_n} + x\dfrac{\varkappa-1}{2}\left(\dfrac{p_2}{p_n}\right)^{\frac{\varkappa-1}{2\varkappa}}} = x\left(\frac{p_2}{p_n}\right)^{0.143} \frac{\dfrac{a_2}{a_n} + 0.2\dfrac{u_2}{a_n}}{\dfrac{a_2}{a_n} + 0.2\,x\left(\dfrac{p_2}{p_n}\right)^{0.143}} \tag{134}$$

or, if Eq. (122) is inserted,

$$\frac{u_3}{a_n} = \frac{x}{1 + 0.2\,x}\left(\frac{a_2}{a_n} + 0.2\,\frac{u_2}{a_n}\right) \tag{135}$$

from which u_3/a_n can be determined for given F_0/F_1, if x is introduced according to Fig. 20 and u_2/a_n and a_2/a_n according to Fig. 23a.

Eq. (129) gives the pressure ratio

$$\frac{p_3}{p_n} = \frac{p_2}{p_n}\left(1 - \frac{\varkappa-1}{2}\cdot\frac{\dfrac{u_3}{a_n} - \dfrac{u_2}{a_n}}{\dfrac{a_2}{a_n}}\right)^{\frac{2\varkappa}{\varkappa-1}} = \frac{p_2}{p_n}\left(1 - 0.2\,\frac{\dfrac{u_3}{a_n} - \dfrac{u_2}{a_n}}{\dfrac{a_2}{a_n}}\right)^7 = \left[\frac{a_2}{a_n} - 0.2\left(\frac{u_3}{a_n} - \frac{u_2}{a_n}\right)\right]^7 \tag{136}$$

In addition, the adiabate law Eq. (24) gives

$$\frac{a_3}{a_n} = \left(\frac{p_3}{p_n}\right)^{\frac{\varkappa-1}{2\varkappa}} = \left(\frac{p_3}{p_n}\right)^{0.143} \tag{137}$$

State 3 is also included in the curves in Figs. 23a and b.

A reservation similar to that for case I for a duct without a container must also be made here in the case of higher values of the cross-sectional area ratio F_0/F_1. Since the low pressure p_1 in this case does not propagate – or only slowly – along the duct, p_2 will become higher than according to the calculations. It is not possible to formulate any general equations for these conditions, because the states ahead of and behind the fronts in these extreme cases are variable. If a concrete case of this nature is to be treated, a step-by-step method must be adopted.

Front I in Fig. 22 will become less steep during the propagation, whereas the reflected front II becomes steeper. This latter phenomenon leads one to ask whether front II can be converted into a shock front. The greatest possibility of this occurring is if front I from the beginning is vertical, that is to say, if F_0 has been uncovered instantaneously. The range of the front I along the duct at the reflection by the container has then attained a length of

$$l_2 = (w_n - w_1)\,t_{\text{I}} \tag{138}$$

where t_{I} signifies the time required by the middle point of the range to cover the distance from the opening F_0 to the container. Assuming that front II has the initial length l_2, and if t_{II} is the time taken for its mid-point to move from the container to F_0 and if l_3 is its range when the mid-point has reached F_0, we have

$$l_3 = l_2 - (w_2 - w_{11})\,t_{\text{II}} \tag{139}$$

The condition for front II to be fully converted into a shock front ($l_3 = 0$) is thus

$$(w_2 - w_{11})\,t_{\text{II}} \geq l_2 \tag{140}$$

or, if Eq. (138) is introduced,

$$\frac{t_{\text{II}}}{t_{\text{I}}} \geq \frac{w_n - w_1}{w_2 - w_{11}} \tag{141}$$

If L denotes the length of the duct between F_0 and the container,

$$L = \tfrac{1}{2}(w_n + w_1)\,t_{\text{I}} = \tfrac{1}{2}(w_2 + w_{11})\,t_{\text{II}} \tag{142}$$

applies, which gives

$$\frac{t_{\text{II}}}{t_{\text{I}}} = \frac{w_n + w_1}{w_2 + w_{11}} \tag{143}$$

According to Eqs. (141) and (143), the condition for front II to be fully converted into a shock front is

$$\frac{w_n + w_1}{w_2 + w_{11}} \geq \frac{w_n - w_1}{w_2 - w_{11}} \tag{144}$$

or

$$w_1 w_2 \geq w_n w_{11} \tag{145}$$

or, if the mass and acoustic speeds are introduced,

$$\frac{a_2 + u_2}{a_n} \geq \frac{a_1 + u_1}{a_1 - u_1} \tag{146}$$

Thus

$$\frac{a_2}{a_n} + \frac{u_2}{a_n} \geq \frac{\dfrac{a_1}{a_n} + \dfrac{u_1}{a_n}}{\dfrac{a_1}{a_n} - \dfrac{u_1}{a_n}} \tag{147}$$

According to the curves in Fig. 23, the expressions on both sides of the unequality sign will be equal to unity for $F_0/F = 0$. With increasing values of F_0/F, both the expressions increase, but more rapidly on the right-hand side than on the left-hand one. When $F_0/F = 1$, the expression on the left-hand side will be 1.945 and on the right-hand side ∞. The reflected front II cannot therefore reach the state of discontinuity for any cross-sectional area ratio. It is probable, however, that this may happen with the reflected front III.

The condition for this front being a press front is that $w_3 > w_{22}$, or, in other words, that $(a_3/a_n - u_3/a_n) > (a_2/a_n - u_2/a_n)$. Fig. 23 shows, that this is the case for all cross-sectional area ratios, since a_3/a_n is always larger than a_2/a_n and u_3/a_n always smaller than u_2/a_n. It is assumed that front III has the length l_3 at the instant of reflection. The time taken for its mid-point to move along the length L of the duct is denoted t_{III} and its length when the mid-point reaches the container l_4. We then have

$$l_4 = l_3 - (w_3 - w_{22})t_{III} \tag{148}$$

The condition for the formation of a shock front is

$$(w_3 - w_{22})t_{III} \geq l_3 \tag{149}$$

or, with Eqs. (138) and (139),

$$(w_3 - w_{22})\, t_{III} \geq (w_n - w_1)\, t_I - (w_2 - w_{11})\, t_{II} \tag{150}$$

With

$$t_I = \frac{2L}{w_n + w_1}; \quad t_{II} = \frac{2L}{w_2 + w_{11}} \quad \text{and} \quad t_{III} = \frac{2L}{w_3 + w_{22}} \tag{151}$$

the condition for the formation of a shock front becomes

$$\frac{w_3 - w_{22}}{w_3 + w_{22}} \geq \frac{w_n - w_1}{w_n + w_1} - \frac{w_2 - w_{11}}{w_2 + w_{11}} \tag{152}$$

or, after introducing the mass and acoustic speeds,

$$\frac{\left(\frac{a_3}{a_n}-\frac{u_3}{a_n}\right)-\left(\frac{a_2}{a_n}-\frac{u_2}{a_n}\right)}{\left(\frac{a_3}{a_n}-\frac{u_3}{a_n}\right)+\left(\frac{a_2}{a_n}-\frac{u_2}{a_n}\right)} \geq \frac{1-\left(\frac{a_1}{a_n}-\frac{u_1}{a_n}\right)}{1+\left(\frac{a_1}{a_n}-\frac{u_1}{a_n}\right)} - \frac{\left(\frac{a_2}{a_n}+\frac{u_2}{a_n}\right)-\left(\frac{a_1}{a_n}+\frac{u_1}{a_n}\right)}{\left(\frac{a_2}{a_n}+\frac{u_2}{a_n}\right)+\left(\frac{a_1}{a_n}+\frac{u_1}{a_n}\right)} \tag{153}$$

An investigation carried out on the basis of Eq. (153) and the curves in Fig. 23 indicates that front III can be converted into a shock front, if the cross-sectional area ratio F_0/F_1 does not exceed about 0.8.

H. CALCULATION OF WAVE PHENOMENA IN CONJUNCTION WITH THE RAPID CHARGING OF DUCTS

A large container, which is filled with compressed air having the state n (Fig. 24), is connected via a closing member to a duct with a constant cross-sectional area. The duct is closed at the outer end. The closing member is to begin with closed, and the pressure p_0 (for example, atmospheric pressure) prevails along the entire duct. The initial temperature and the acoustic speed are assumed to be the same in both the container and the duct ($a_0 = a_n$). If the closing member is suddenly opened, oscillations will arise, as has already been briefly described in chapter B. It was apparent there that the phenomena encountered during a complete cycle can be divided into four groups displaying rather varying conditions. It is desirable to treat these four groups individually so as to make the presentation more lucid. The following distinction can be made:

I. The *direct compression period*, reckoned from the opening of the closing member until the resultant compression front formed by this has reached the closed end of the duct.

II. The *reflected compression period*, reckoned from the reflection of the compression front from the outer end until the front has returned again to the container.

III. The *direct expansion period*, reckoned from the instant when air has commenced to flow back again from the duct to the container until the associated negative expansion front has reached the end of the duct.

IV. The *reflected expansion period*, reckoned from the instant when this latter front has been reflected from the outer end until the positive front resulting from the reflection has returned to the container.

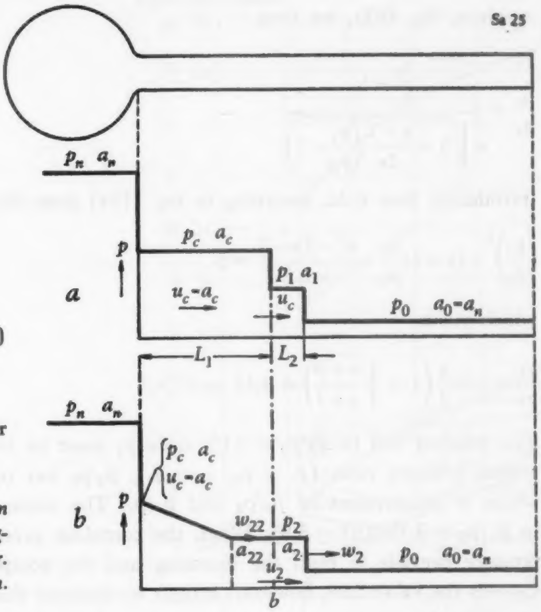

- · - · - · Boundary layer (*b*)

L_1 Length of incoming air column

L_2 Length of compressed air column

Fig. 24. Calculation of fronts in conjunction with the rapid charging of a duct from a container. Supercritical pressure condition.

1. Direct compression period

If it is assumed that the closing member uncovers instantaneously the entire cross-sectional area of the duct, it is reasonable to suppose that the following phenomenon takes place for a supercritical pressure condition (Fig. 24a).

Air of critical state flows from the container into the duct, that is to say, with the speed of sound (cf. Eqs. (95) and (96))

$$u_c = a_c = a_n \sqrt{\frac{2}{\varkappa + 1}} = 0.913\, a_n \tag{154}$$

and with the static pressure (cf. Eq. (96))

$$p_c = p_n \left(\frac{2}{\varkappa + 1}\right)^{\frac{\varkappa}{\varkappa - 1}} = 0.53\, p_n \tag{155}$$

The air flowing in acts as a piston which moves along the duct with the velocity a_c. The air originally present in the duct is compressed ahead of this piston in a discontinuous way. At a given instant the length of the incoming air column is L_1 and the length of the compressed column L_2.

Applying Eq. (63), we have

$$\frac{u_c}{a_n} = \frac{\frac{p_1}{p_0} - 1}{\varkappa \sqrt{1 + \frac{\varkappa+1}{2\varkappa}\left(\frac{p_1}{p_0} - 1\right)}} \tag{156}$$

Introducing here u_c/a_n according to Eq. (154) gives the following equation for p_1/p_0

$$\left(\frac{p_1}{p_0}\right)^2 - (\varkappa+2)\frac{p_1}{p_0} - \frac{\varkappa^2 - 2\varkappa - 1}{\varkappa+1} = 0 \tag{157}$$

which yields

$$\frac{p_1}{p_0} = 1 + \frac{\varkappa}{2}\left(1 \pm \sqrt{\frac{\varkappa+9}{\varkappa+1}}\right) = 3.15 \text{ or } 0.243 \tag{158}$$

The solution will be $p_1/p_0 = 3.15$, since p_1 must be higher than p_0. For the supercritical pressure ratio ($p_c > p_0$, $u_c = a_c$), p_1/p_0 has consequently a constant value, which is independent of p_n/p_0 and p_c/p_0. The value of $p_c/p_0 = p_1/p_0$ corresponds to $p_n/p_0 = 3.15/0.53 = 5.95$. When the container pressure has this value, the same pressure prevails in both the incoming and the compressed air. As soon as p_n/p_0 exceeds the value 5.95, however, it must be assumed that a sudden change in pressure occurs in the boundary layer between L_1 and L_2. Such a sudden change in pressure is not, however, of a permanent nature, which should be apparent from the following discussion.

If it is assumed that the pressure is distributed at a given instant as shown in Fig. 24a and that a co-ordinate system follows the flow with the velocity u_c, the conditions will be similar to those for a duct with air at rest having different pressures on each side of a plane perpendicular to the longitudinal direction of the duct. Such a state can only be maintained if this plane consists of a fixed partition. In the case being treated, however, such a partition does not exist and thus a levelling-out phase is initiated immediately in such a way that a positive shock front is propagated to the right, and a negative expansion front to the left (cf. Schardin [35]). When treating the present problem, it is therefore necessary to assume that such a levelling-out phase occurs already from the beginning, that is to say, from the instant when the closing member opens. In this case for a supercritical pressure condition the period will comprise a positive shock front followed by an expansion front (see Fig. 24b). This latter front moves, relative to the air, towards the container. Since the flow of air from the container into the duct must be assumed to take place with the speed of sound, the top of the expansion front will remain at the inlet. The base, on the other hand, will be propagated along the duct, as the calculations will show later on, with a front velocity of $w_{22} = u_2 - a_{22}$. This means that the flow along the expansion front takes place with a supersonic speed increasing towards the base and attaining its maximum value u_2 at the base.

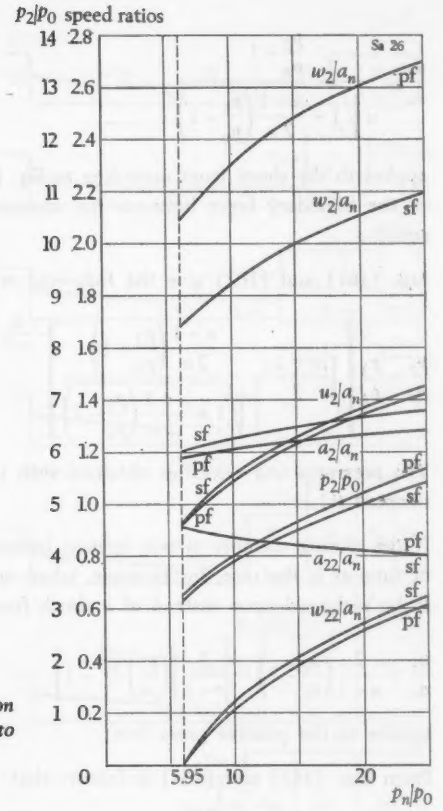

pf Press front
sf Shock front

Fig. 25. Front curves for the direct compression period of rapid charging. (The symbols refer to Fig. 24.)

The following equation

$$\frac{u_2-u_c}{a_c}=\frac{2}{\varkappa-1}\left(1-\frac{a_{22}}{a_c}\right) \tag{159}$$

applies to the expansion front, or, with Eq. (154) and $u_c = a_c$

$$\frac{u_2}{a_n}=\frac{\sqrt{2(\varkappa+1)}}{\varkappa-1}-\frac{2}{\varkappa-1}\cdot\frac{a_{22}}{a_n}=5.477-5\cdot\frac{a_{22}}{a_n} \tag{160}$$

With Eq. (24), this becomes

$$\frac{u_2}{a_n}=\frac{\sqrt{2(\varkappa+1)}}{\varkappa-1}-\frac{2}{\varkappa-1}\left(\frac{p_2}{p_n}\right)^{\frac{\varkappa-1}{2\varkappa}} \quad . \tag{161}$$

$$\frac{u_2}{a_n} = \frac{\frac{p_2}{p_0} - 1}{\varkappa \sqrt{1 + \frac{\varkappa+1}{2\varkappa}\left(\frac{p_2}{p_0} - 1\right)}} \tag{162}$$

applies to the shock front according to Eq. (63), since the mass speeds on both sides of the boundary layer between the incoming air and the compressed air must be equal.

Eqs. (161) and (162) give the following relationship between the pressures

$$\frac{p_n}{p_0} = \frac{p_2}{p_0}\left[\sqrt{\frac{\varkappa+1}{2}} - \frac{\frac{\varkappa-1}{2\varkappa}\left(\frac{p_2}{p_0} - 1\right)}{\sqrt{1 + \frac{\varkappa+1}{2\varkappa}\left(\frac{p_2}{p_0} - 1\right)}}\right]^{-\frac{2\varkappa}{\varkappa-1}} \tag{163}$$

The pressures and velocities obtained with this method are shown in Fig. 25 (curves denoted sf).

If the closing member is not opened instantaneously, but within a certain interval of time as is the case, for example, when opening a valve, a positive press front has to be reckoned upon instead of a shock front. From Eq. (54) it follows that

$$\frac{u_2}{a_n} = \frac{2}{\varkappa - 1}\left(\frac{a_2}{a_n} - 1\right) = \frac{2}{\varkappa - 1}\left[\left(\frac{p_2}{p_0}\right)^{\frac{\varkappa-1}{2\varkappa}} - 1\right] \tag{164}$$

applies to the positive press front.

From Eqs. (161) and (164) it follows that

$$\frac{p_n}{p_0} = \frac{p_2}{p_0}\left[1 + \sqrt{\frac{\varkappa+1}{2}} - \left(\frac{p_2}{p_0}\right)^{\frac{\varkappa-1}{2\varkappa}}\right]^{-\frac{2\varkappa}{\varkappa-1}} \tag{165}$$

According to Eqs. (154) and (164) we have for the case $p_1 = p_c$

$$\frac{p_1}{p_0} = \left[1 + \frac{\varkappa - 1}{\sqrt{2(\varkappa+1)}}\right]^{\frac{2\varkappa}{\varkappa-1}} = 3.24, \text{ i.e., } \frac{p_n}{p_0} = 6.12 \tag{166}$$

which is slightly higher than for a shock front.

Curves for pressures and velocities when the closing member is being gradually opened are also plotted in Fig. 25 (curves denoted pf).

II. Reflected compression period

When the shock front 2 has reached the outer end of the duct, the second stage commences and develops as shown in Fig. 26. After the reflection, the shock front

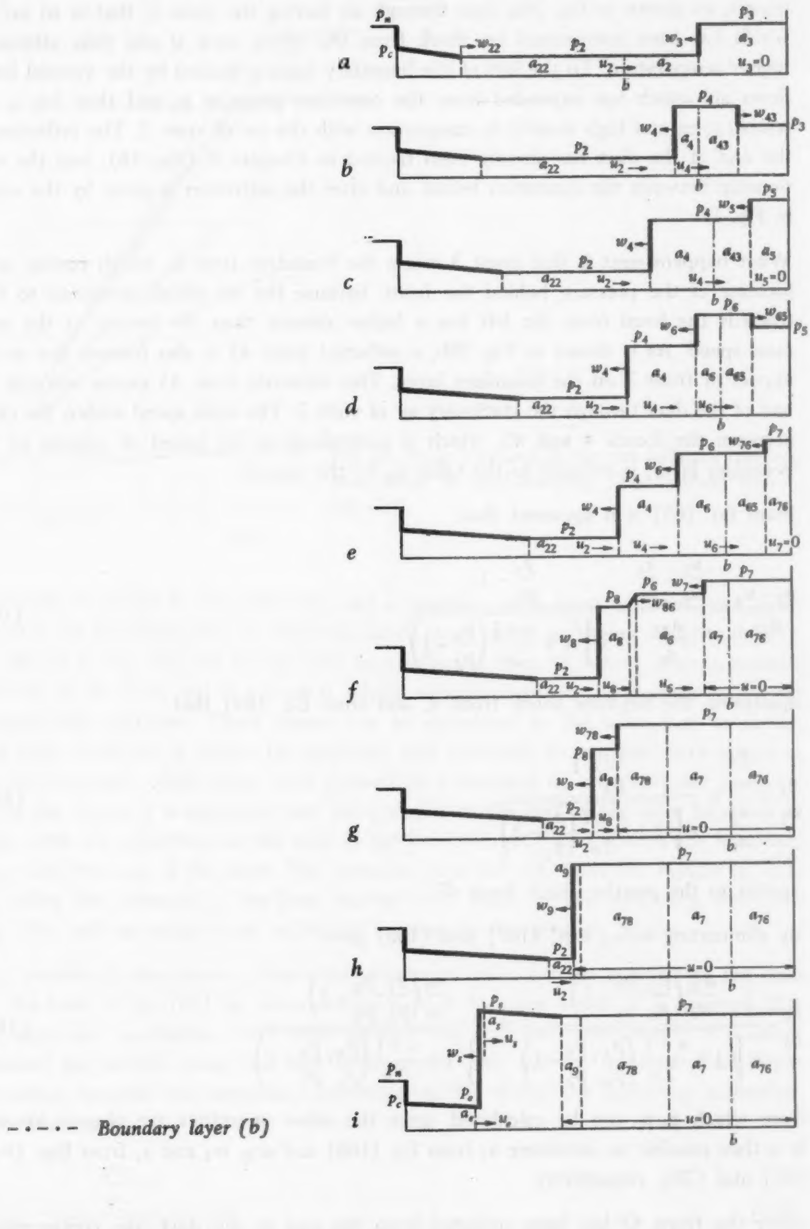
a
b
c
d
e
f
g
h
i
p_a
p_c
p_2
p_3
p_4
p_5
p_6
p_7
p_8
w_{22}
w_3
w_4
w_{43}
w_5
w_6
w_{65}
w_{76}
w_7
w_{86}
w_8
w_{78}
w_9
a_{22}
a_2
a_3
a_4
a_{43}
a_5
a_6
a_{65}
a_{76}
a_7
a_8
a_{78}
a_9
u_2
$u_3=0$
u_4
$u_5=0$
u_6
$u_7=0$
u_8
$u=0$
b
- · - · - Boundary layer (b)

Fig. 26. Calculation of fronts in conjunction with the rapid charging of a duct.

travels, as shown in Fig. 26a, first through air having the state 2, that is to say, air which has been compressed by shock from the initial state 0 and thus attained a higher temperature. To the left of the boundary layer indicated by the vertical line *b* flows air which has expanded from the container pressure p_n and thus has a low temperature and high density in comparison with the air of state 2. The reflection at the end of the duct has already been treated in Chapter F (Fig. 16), and the relationship between the quantities before and after the reflection is given by the curves in Fig. 17.

What happens next is that front 3 meets the boundary layer *b*, which results in an increase of the pressure behind the front, because the air which continues to flow towards the front from the left has a higher density than the former at the same mass speed. As is shown in Fig. 26b, a reflected front 43 is also formed due to the impact of front 3 on the boundary layer. This reflected front 43 moves towards the end of the duct through the stationary air of state 3. The mass speed within the range between the fronts 4 and 43, which is equivalent to the speed of motion of the boundary layer, is reduced to the value u_4 by the impact.

From Eq. (65) it is apparent that

$$\frac{u_2 - u_4}{a_{22}} = \frac{\frac{u_2}{a_n} - \frac{u_4}{a_n}}{\frac{a_{22}}{a_n}} = \frac{\frac{p_4}{p_2} - 1}{\varkappa \sqrt{1 + \frac{\varkappa + 1}{2\varkappa}\left(\frac{p_4}{p_2} - 1\right)}} \tag{167}$$

applies to the negative shock front 4, and from Eq. (63) that

$$\frac{u_4}{a_3} = \frac{\frac{u_4}{a_n}}{\frac{a_3}{a_n}} = \frac{\frac{p_4}{p_3} - 1}{\varkappa \sqrt{1 + \frac{\varkappa + 1}{2\varkappa}\left(\frac{p_4}{p_3} - 1\right)}} \tag{168}$$

applies to the positive shock front 43.

By eliminating u_4/a_n, Eqs. (167) and (168) give

$$\frac{u_2}{a_n} - \frac{\frac{a_{22}}{a_n}\left(\frac{p_4}{p_0} \cdot \frac{p_0}{p_2} - 1\right)}{\varkappa \sqrt{1 + \frac{\varkappa + 1}{2\varkappa}\left(\frac{p_4}{p_0} \cdot \frac{p_0}{p_2} - 1\right)}} = \frac{\frac{a_3}{a_n}\left(\frac{p_4}{p_0} \cdot \frac{p_0}{p_3} - 1\right)}{\varkappa \sqrt{1 + \frac{\varkappa + 1}{2\varkappa}\left(\frac{p_4}{p_0} \cdot \frac{p_0}{p_3} - 1\right)}} \tag{169}$$

from which p_4/p_0 can be calculated, since the other quantities are already known. It is then possible to determine u_4 from Eq. (168) and w_{43}, w_4 and a_4 from Eqs. (64), (65) and (36), respectively.

After the front 43 has been reflected from the end of the duct, the configuration shown in Fig. 26c is obtained, where the pressure at the end of the duct has been

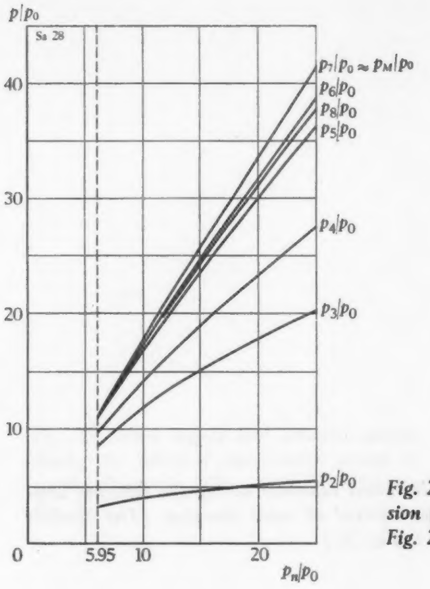

Fig. 27. Front pressures during the reflected compression period of rapid charging. (The symbols refer to Fig. 26.)

increased to p_5 due to the reflection, and a negative shock front 5 moves once again towards the boundary layer *b*. Here this shock front meets air having a higher density. As shown in Fig. 26d this results both in a reflected front 65, which returns towards the end of the duct, and in a front 6, which, superimposed on the pressure p_4, moves towards the container. These phases can be calculated in the same way as above, and Figs. 27–29 show curves for pressures and velocities during successive stages in the development which have been derived as a function of the container pressure. From the above it is apparent that the pressure at the end of the duct increases in steps with the reflections at the ends of the hot column of air between the boundary layer and the end of the duct. The pressure steps fall off, however, rapidly in size, and after the pressure p_7 has been reached as a result of the conditions shown in Fig. 26e, only an insignificant additional increase in the pressure occurs.

It is possible to determine a theoretical maximum value for the pressure in the duct on the basis of Eq. (65) by introducing $u/a_n = 0$. In other words, it is assumed that the secondary oscillations have been damped out and that consequently a constant pressure p_M prevails along the duct between the end and the negative shock front travelling towards the container. According to Eq. (65), the following expression will then apply:

$$\frac{u_2}{a_{22}} = \frac{\dfrac{p_M}{p_2} - 1}{\varkappa \sqrt{1 + \dfrac{\varkappa + 1}{2\varkappa}\left(\dfrac{p_M}{p_2} - 1\right)}} \,. \tag{170}$$

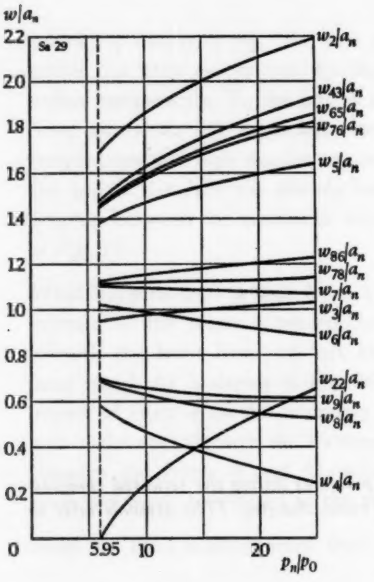

Fig. 28. Front velocities during the reflected compression period of rapid charging. (The symbols refer to Fig. 26.)

By introducing the quantities u_2/a_n, a_{22}/a_n and p_2/p_0 (Fig. 25) determined previously, it is possible to obtain from this equation the relationship between p_M/p_0 and p_n/p_0. The pressure ratio p_M/p_0 has practically the same value as p_7/p_0, as is apparent from Fig. 27.

The impact of front 6 on front 4 gives rise to two fronts travelling in opposite directions. If it is assumed that both these fronts are shock fronts, the calculation leads to a pressure p_8 after the impact which is slightly lower than p_6. This is equivalent, however, to the fact that the front travelling towards the end of the duct is a retrogressive shock front, which, as has previously been said, is a physical impossibility. From this it is possible to draw the conclusion that the front travelling towards the end is a positive expansion front. If the calculation is performed with this assumption, it will also lead to a pressure p_8 slightly lower than p_6 and a velocity of the front 8 travelling towards the container which is slightly higher than the velocity of front 4.

It is hardly necessary to describe in detail the calculation of these latter fronts, since the method to be adopted is basically the same as that for a reflection against the boundary layer *b*, with the exception that the equation for a positive expansion front must be applied for one of the fronts.

As the calculations show, it can be assumed without any great error that p_7 is the highest pressure attained at the end of the duct, and consequently the reflection phenomenon can be neglected in the boundary layer *b* when the front 76 meets this.

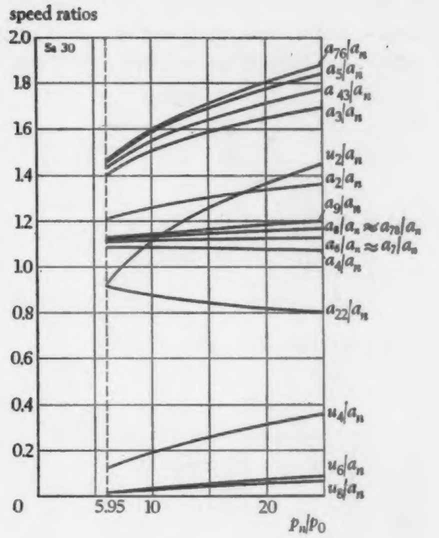

Fig. 29. Mass speeds and acoustic speeds during the reflected compression period of rapid charging. (The symbols refer to Fig. 26.)

It is assumed that the front passes the boundary layer with the pressure p_7 unaltered (Fig. 26f), but that its velocity decreases after the passage, since the air here has a lower temperature. This front is called hereafter front 7. During its continued movement towards the container, it will meet the expansion front 86 travelling in the opposite direction, which gives rise once again to a reflection. The differences in pressure of the two fronts are, however, so small, that it is hardly worth while making a precise calculation of the conditions. A sufficiently accurate result will be obtained if it is assumed that the sudden change in pressure $p_7 - p_8$ hereafter moves as a negative shock front towards the container. A calculation made on this basis shows that the front 78 (Fig. 26g) will soon catch up with front 8. If the reflection resulting from the impact is also neglected here, a new uniform front 9 will move after this towards the container. The pressure p_7 will then prevail between this front and the end of the duct along its entire length.

It is now possible to reckon upon an undisturbed propagation of the front 9 until it meets the positive expansion front $c2$ coming from the inlet of the duct. The base of front $c2$ moves with the velocity w_{22} towards the end of the duct.

The conditions during the successive transition of the expansion front into the negative shock front will now be investigated.

The pressure behind the shock front s is denoted p_s (Fig. 26i), and it is assumed at present that the mass speed after the shock compression drops to zero. The velocity of the shock front at an arbitrary instant after it has encountered the base of the expansion front and until it reaches the duct inlet is denoted w_s. The pressure p_e, the mass speed u_e and the speed of sound a_e then prevail just ahead of the shock front. From Eq. (160) it follows that

$$\frac{u_e}{a_n}=\frac{\sqrt{2(\varkappa+1)}}{(\varkappa-1)-\dfrac{2}{\varkappa-1}\cdot\dfrac{a_e}{a_n}} \tag{171}$$

and from Eq. (24) that

$$\frac{a_e}{a_n}=\left(\frac{p_e}{p_n}\right)^{\frac{\varkappa-1}{2\varkappa}} \tag{172}$$

Eqs. (65) and (66) give

$$\frac{u_e}{a_e}=\frac{\dfrac{p_s}{p_e}-1}{\varkappa\sqrt{1+\dfrac{\varkappa+1}{2\varkappa}\left(\dfrac{p_s}{p_e}-1\right)}} \tag{173}$$

and

$$\frac{w_s}{a_n}=\frac{a_e}{a_n}\sqrt{1+\frac{\varkappa+1}{2\varkappa}\left(\frac{p_s}{p_e}-1\right)}-\frac{u_e}{a_n} \tag{174}$$

By applying the above equations, we obtain

$$\frac{p_e}{p_0}=\frac{p_n}{p_0}\left[\frac{\sqrt{2(\varkappa+1)}}{2+\dfrac{\varkappa-1}{\varkappa}\cdot\dfrac{\dfrac{p_s}{p_e}-1}{\sqrt{1+\dfrac{\varkappa+1}{2\varkappa}\left(\dfrac{p_s}{p_e}-1\right)}}}\right]^{\frac{2\varkappa}{\varkappa-1}} \tag{175}$$

Curves for the last-mentioned period are given in Fig. 30. The front velocity of an arbitrary point within the expansion front moving towards the end of the duct is denoted w_e. The expression $w_e = u_e - a_e$ will then apply to this velocity. The curve for a_s has been determined on the basis of the curve for a_e applying Eq. (36). These curves show that the velocity w_s of the shock front increases slightly on its way towards the duct inlet, at the same time as the pressure p_s behind the front increases slightly too. This latter will result in a slight press front, which moves towards the end of the duct, tending to even out the pressure difference along the duct behind the shock front. Such a press front is related to a mass flow outwards. It is thus not quite correct to say that the condition for the curves in Fig. 30 is that the mass speed resulting from the shock compression is reduced to zero. If a mass speed u_s is introduced into the calculations, the velocity of the shock front and also the pressure behind it will become lower than is shown by the curves in Fig. 30. The quantities w_s and p_s will then not differ greatly from the corresponding quantities of the shock front left undisturbed by the expansion front. Sufficiently accurate results would

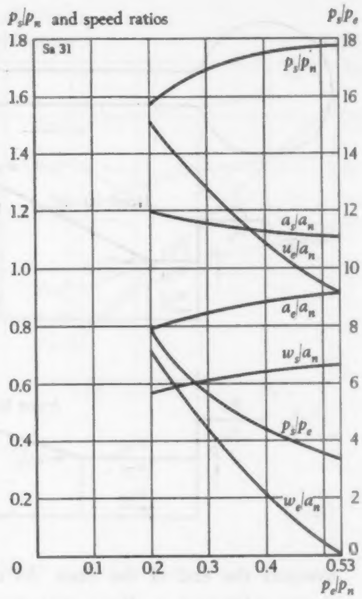

Fig. 30. Front curves for later part of the reflected compression period of rapid charging. (The symbols refer to Fig. 26. The mass speed, u_s, behind the shock front is assumed to be zero.)

probably be obtained therefore for the comparison to be made in chapter L with experimentally determined pressures and velocities, if it is assumed that the expansion front *c*2 does not exert any influence whatsoever on the propagation of the shock front towards the inlet. It may be inferred instead that front 9 will travel undisturbed with the velocity w_9 and with the pressure p_7 right up to the inlet. This will also facilitate the calculation of the associated expansion phenomenon.

III. Direct expansion period

From what has been said above it is necessary here to consider the following initial state. The pressure p_7 prevails along the entire duct and the air is in a state of rest. The air between the boundary layer *b* and the end of the duct is relatively much hotter than between the boundary layer and the container. This latter column of air comprises sections of varying temperatures, which do not differ, however, very much from one another. It is therefore possible to reckon upon with sufficient accuracy a mean acoustic speed a_M for this column. The hot column of air between the boundary layer *b* and the end of the duct has an acoustic speed a_{76}.

Immediately after the negative shock front 9 has reached the inlet, air will commence to flow from the duct to the container, since the pressure p_7 in the duct is higher than the pressure p_n in the container and since the air in both spaces is at rest. This takes place as a negative expansion front, which moves from the inlet

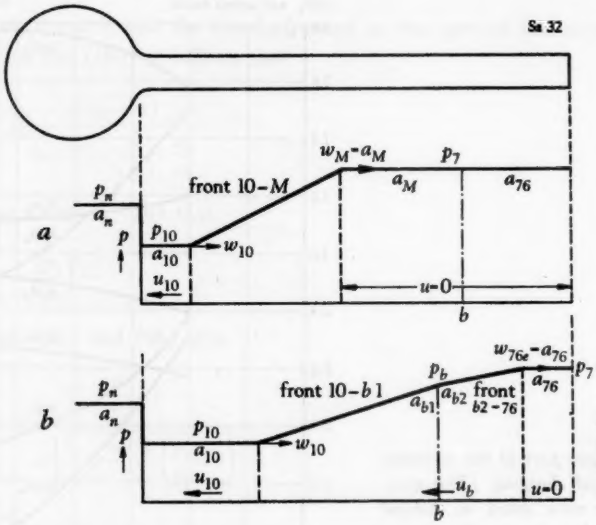
Sa 32
a
p_n
a_n
p
p_{10}
a_{10}
u_{10}
w_{10}
front 10-M
$w_M - a_M$
p_7
a_M
a_{76}
u-0
b
b
p_n
a_n
p
p_{10}
a_{10}
u_{10}
w_{10}
front 10-b 1
p_b
a_{b1}
a_{b2}
front b2-76
$w_{76e} - a_{76}$
a_{76}
p_7
u_b
u-0
b
Boundary layer (b)

Fig. 31. Calculation of fronts in conjunction with the rapid charging of a duct from a container.

towards the end of the duct. As depicted in Fig. 31a, a state of flow 10 is formed at the inlet and air flows into the container with the mass speed u_{10}. The acoustic speed at the inlet is a_{10} and the static pressure p_{10}.

From Eq. (56) it follows that

$$\frac{u_{10}}{a_{10}} = \frac{2}{\varkappa - 1}\left(\frac{a_M}{a_{10}} - 1\right) \tag{176}$$

applies to a negative expansion front 10-*M*, which moves within the range between the inlet and the boundary layer *b*.

It is assumed that the air flowing into the container comes to rest at the pressure p_n. Its acoustic speed for this state of rest is determined according to the change of state from the state *M* on the basis of the static adiabate. If this acoustic speed is denoted a_{nM}, we have

$$\frac{a_{nM}}{a_M} = \left(\frac{p_n}{p_7}\right)^{\frac{\varkappa - 1}{2\varkappa}} \tag{177}$$

Applying the equation of energy (17) gives

$$a_{nM}^2 = \frac{\varkappa - 1}{2}\, u_{10}^2 + a_{10}^2 \tag{178}$$

or

$$\left(\frac{u_{10}}{a_{10}}\right)^2 = \frac{2}{\varkappa - 1}\left[\left(\frac{a_{nM}}{a_{10}}\right)^2 - 1\right] \tag{179}$$

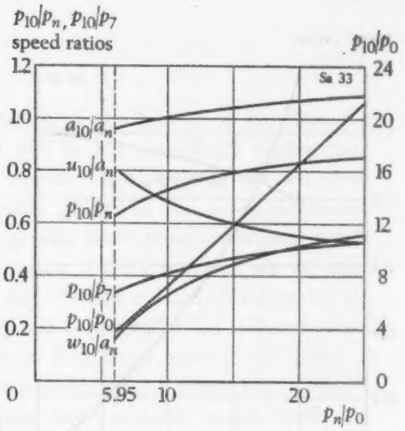

Fig. 32. Curves for the flow conditions by the duct inlet during the direct expansion period of rapid charging. (The symbols refer to Fig. 31.)

Inserting Eq. (176) after squaring in Eq. (179) gives

$$a_{10} = \frac{2}{\varkappa+1} a_M \pm \sqrt{\frac{\varkappa-1}{\varkappa+1} a_{nM}{}^2 - \left[\frac{2}{\varkappa+1} - \left(\frac{2}{\varkappa+1}\right)^2\right] a_M{}^2} \tag{180}$$

After this, u_{10} is obtained from Eq. (176) and p_{10} from

$$\frac{p_{10}}{p_7} = \left(\frac{a_{10}}{a_M}\right)^{\frac{2\varkappa}{\varkappa-1}} \tag{181}$$

The curves reproduced in Fig. 32 show how the state by the duct inlet varies with p_n/p_0. This figure also shows the velocity w_{10} with which the base of the expansion front propagates towards the end of the duct. The expression $w_{10} = a_{10} - u_{10}$ applies to this velocity.

When the top of the front 10-*M* reaches the boundary layer *b*, this starts moving towards the container, while the static pressure in the layer decreases gradually at the same time. In this way the original front 10-*M* becomes truncated and is then called front 10-*b*1. A new associated front *b*2-76, which propagates within the hot column of air from the boundary layer *b* towards the end of the duct, is formed at the same time. In order to be able to follow the front propagation, it is best to determine first the dependence between the pressure p_b and the mass speed u_b in the boundary layer (see Fig. 31b).

$$\frac{u_{10} - u_b}{a_{10}} = \frac{2}{\varkappa-1}\left(\frac{a_{b1}}{a_{10}} - 1\right) \tag{182}$$

and

$$\frac{p_{10}}{p_b} = \left(\frac{a_{10}}{a_{b1}}\right)^{\frac{2\varkappa}{\varkappa-1}} \tag{183}$$

apply to the front 10-*b*1.

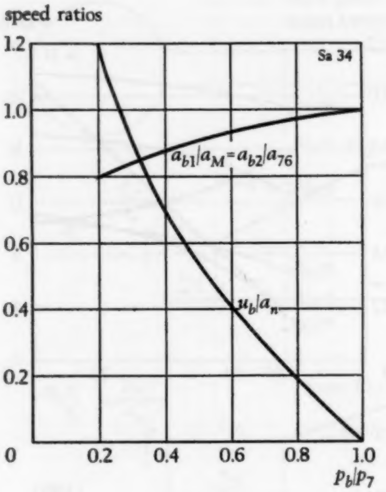

Fig. 33. Speed curves for the boundary layer during the direct expansion period of rapid charging. (The symbols refer to Fig. 31.) The curves are based on an approximate method of calculation.

These two equations together with Eqs. (176) and (181) give

$$\frac{u_b}{a_n} = \frac{2}{\varkappa - 1} \cdot \frac{a_M}{a_n} \left[1 - \left(\frac{p_b}{p_7} \right)^{\frac{\varkappa - 1}{2\varkappa}} \right] \tag{184}$$

The acoustic speed a_M is the mean value of several speeds which display rather small differences relative to one another. Each of these speeds displays also a small variation within that range for p_n/p_0 of interest in this connection. For Eq. (184) it is consequently suitable to treat a_M/a_n as a constant and, according to an estimation on the basis of Fig. 29, insert the value 1.15 for this, thus enabling Eq. (184) with $\varkappa = 1.4$ to assume the form

$$\frac{u_b}{a_n} = 5.75 \left[1 - \left(\frac{p_b}{p_7} \right)^{0.143} \right] \tag{185}$$

Eq. (185) has been graphically reproduced in Fig. 33, which also includes curves for the acoustic speeds a_{b1} and a_{b2}. These latter are obtained from the equations

$$\frac{a_{b1}}{a_M} = \left(\frac{p_b}{p_7} \right)^{\frac{\varkappa - 1}{2\varkappa}} \quad \text{and} \quad \frac{a_{b2}}{a_{76}} = \left(\frac{p_b}{p_7} \right)^{\frac{\varkappa - 1}{2\varkappa}} \tag{186}$$

It should be noted that this calculation of u_b is only approximate, since the front 10-*b*1 is not a pure expansion front. In reality, as soon as the top of the front 10-*M* has reached the boundary layer *b*, it is probable that a press front, departing from this latter and directed towards the container, will be superimposed on the front 10-*M*. A support for this hypothesis is obtained if u_b is determined as a function of p_b/p_7, assuming that front *b*2-76 is a normal expansion front. Such a calculation results in

$$\frac{u_b}{a_n} = \frac{2}{\varkappa - 1} \cdot \frac{a_{76}}{a_n} \left[1 - \left(\frac{p_b}{p_7} \right)^{\frac{\varkappa - 1}{2\varkappa}} \right] \tag{187}$$

This equation differs from Eq. (184) only in that a_{76} occurs instead of a_M. Since a_{76} is considerably higher than a_M, u_b in Eq. (187) will be correspondingly higher than in Eq. (184). As soon as the hot column of air has started to expand, this will tend to push the colder column of air, which probably results in the above-mentioned press front. It would be too tedious to discuss in greater detail these conditions, which are also complicated by the fact that the two end states of the press front are variable. The propagation of the front after front 10-*M* has reached *b* must therefore be investigated by a step-by-step method. This applies also to the reflection initiated when the top of front *b*2-76 meets the end of the duct. This latter front is not either a pure expansion front, since its end state at *b* is variable and, furthermore, a superimposed expansion front corresponding to the press front probably asserts itself.

IV. Reflected expansion period

This extends over the interval from the instant when the top of the expansion front *b*2–76 reaches the end of the duct, where it is reflected, until a change in the state of flow 10 develops at the inlet of the duct due to this reflection. During this fourth period roughly the same conditions occur as with the positive expansion front II in Fig. 18, although the picture is complicated in the present case by the presence of two air columns having different initial acoustic speeds. The problem will not be treated exhaustively, both due to its complicated nature and because the phenomenon in practice will deviate more and more from the theoretical phenomenon the more it develops, owing to the influence of damping factors. The comparison between the theoretical and the experimental results for a phenomenon in an advanced stage of development will thus be more or less illusory.

V. Example of calculation regarding the reflected compression period

Fig. 34 shows how the reflected compression period II develops according to the pressure and velocity curves calculated in Figs. 27–29, for comparison with an experimentally investigated case, treated later on, where the closing member consisted of bursting diaphragms. The duct length was 5 m and the container pressure 16 atm abs.

The conditions represented in Fig. 34a refer to the instant when the positive shock front 2 reaches the end of the duct and is reflected there. The reflected front 3 meets the boundary layer *b* in Fig. 34b and gives rise to the fronts 4 and 43. Fig. 34c depicts the instant when front 43 meets the end of the duct, and Fig. 34d the instant when front 5 resulting from the reflection meets the boundary layer. The fronts 6 and 65 are formed as a result of this impact, and Fig. 34e shows the situation when front 65 meets the end of the duct. In Fig. 34f front 6 has just reached front 4, whereas

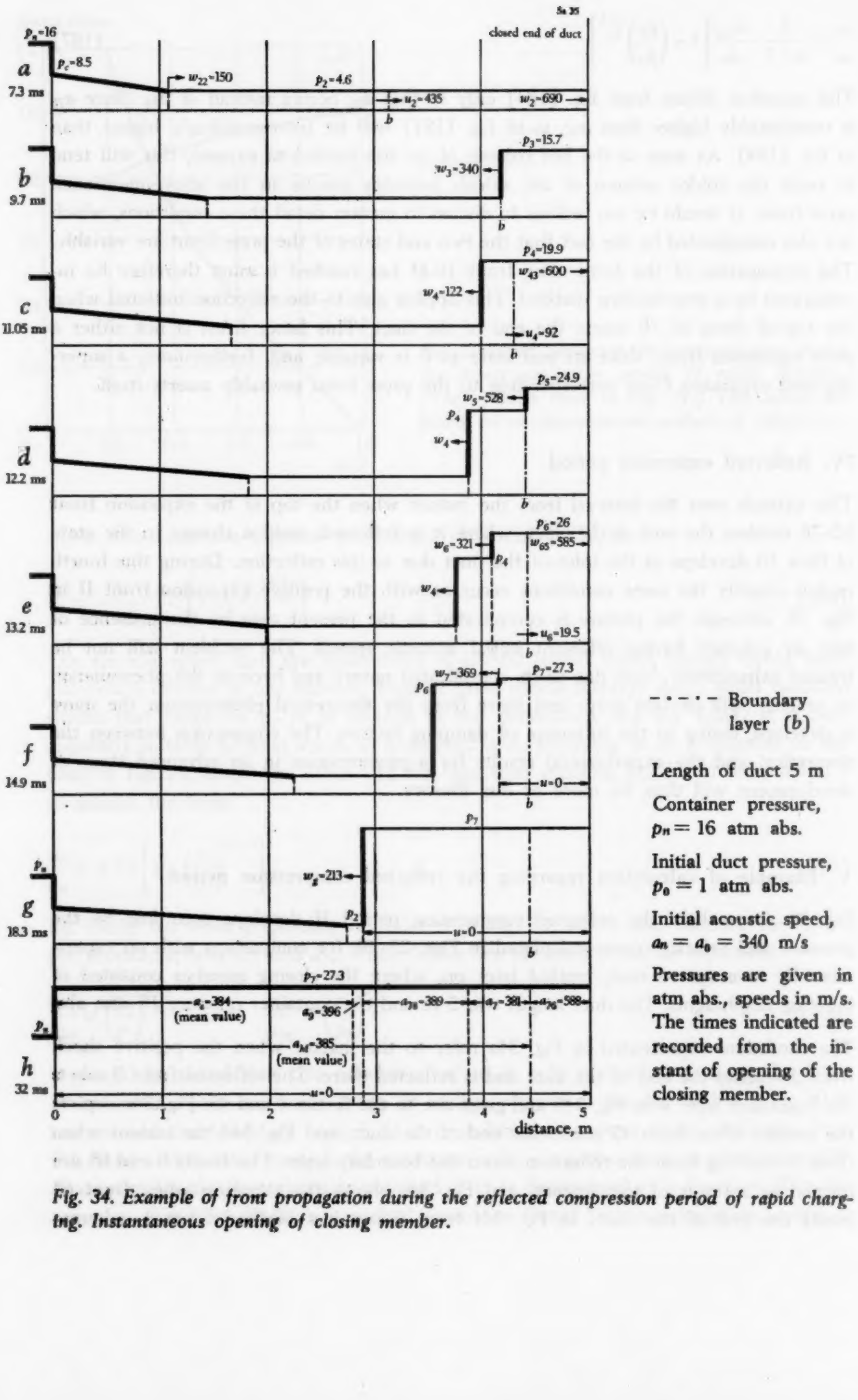
Sa 35
closed end of duct
p_n=16
a
7.3 ms
p_c=8.5
w_{22}=150
p_2=4.6
u_2=435
w_2=690
b
b
9.7 ms
p_3=15.7
w_3=340
b
c
11.05 ms
p_4=19.9
w_{43}=600
w_4=122
u_4=92
b
d
12.2 ms
p_5=24.9
w_5=528
p_4
w_4
b
e
13.2 ms
p_6=26
w_6=321
w_{65}=585
p_4
w_4
u_6=19.5
b
f
14.9 ms
w_7=369
p_7=27.3
p_6
u=0
b
p_7
p_n
g
18.3 ms
w_8=213
p_2
u=0
b
p_7=27.3
a_6=384
(mean value)
a_9=396
a_{78}=389
a_7=381
a_{76}=588
p_n
h
32 ms
a_M=385
(mean value)
u=0
0
1
2
3
4
b
5
distance, m
– · – · = Boundary layer (b)

Length of duct 5 m

Container pressure, $p_n = 16$ atm abs.

Initial duct pressure, $p_0 = 1$ atm abs.

Initial acoustic speed, $a_n = a_0 = 340$ m/s

Pressures are given in atm abs., speeds in m/s. The times indicated are recorded from the instant of opening of the closing member.

Fig. 34. Example of front propagation during the reflected compression period of rapid charging. Instantaneous opening of closing member.

front 7, resulting from the reflection of front 65 against the end of the duct, has had time to pass at this instant the boundary layer *b* (front 7 joins front 76, which latter front is not shown in the figure). Owing to the impact of front 6 on front 4, the fronts 8 and 86 (not reproduced in the figure) are formed (cf. Fig. 26), of which front 8 moves towards the container and front 86 towards the end of the duct. This latter front on its way meets front 7, which results in a front 78 travelling towards the container. Fig. 34g shows the conditions just at the instant when front 78 reaches front 8 and, as a result of this, front 9 is formed. Finally, Fig. 34h shows the situation at the instant when front 9 reaches the inlet of the duct. The pressure p_7 then prevails along the entire duct and the air is everywhere in a state of rest. The temperature and the acoustic speed are approximately the same along the entire length of the duct, with the exception of a section of about 0.5 m nearest the end of the duct, where the absolute temperature is 134 per cent and the acoustic speed 53 per cent higher than in the rest of the duct. The temperature of the first part of the duct, about 4.5 m, can be estimated to be 366 °K = 93 °C, and for the section by the end of the duct, 858 °K = 585 °C.

The velocity of the shock front 2 travelling outwards is found to be 690 m/s and the mean value of the velocities of the fronts 3, 4, 8 and 9 travelling towards the container can be estimated to be 203 m/s. The mean velocity for the propagation of the front from the inlet to the end and back again will be 313 m/s, which is practically the same value as the critical velocity u_c at the inlet (311 m/s).

J. DESCRIPTION OF EXPERIMENTAL ARRANGEMENTS

I. Apparatus arrangements

The different arrangements with which experiments have been performed are schematically illustrated in Figs. 35–41. References are given in these figures to detailed drawings showing the design of the components in question. The ducts which have been used are standard drawn steam tubes of mild steel having untreated surfaces. The inner surfaces were relatively smooth. The following table shows the data for the tubes according to the manufacturer's catalogue.

Tube	Outer diameter mm	Inner diameter mm	Wall thickness mm
3″	88.25	80.25	4.0
2″	60.0	52.5	3.75
1 ½″	48.25	41.25	3.5
1 ¼″	42.25	35.75	3.25

The tube diameters given in the figures are to be considered as approximate inner diameters.

The purpose of the experimental arrangements was to investigate the transient phenomena arising in conjunction with:

(a) Rapid discharge of tube (Fig. 35)
(b) Rapid charging of tube (Figs. 36–40) and
(c) Rapid discharge through a nozzle into the open (Fig. 41)

The conditions within each group (a)–(c) have been altered in various ways, as is apparent from the following brief survey.

a. Arrangements for rapid discharge

Arrangement 1 in Fig. 35 shows a 3″ tube with a length of 5 m, the one end wall of which consists of two diaphragms which can be made to burst. This system of diaphragms, which is included in a large proportion of the arrangements, will be

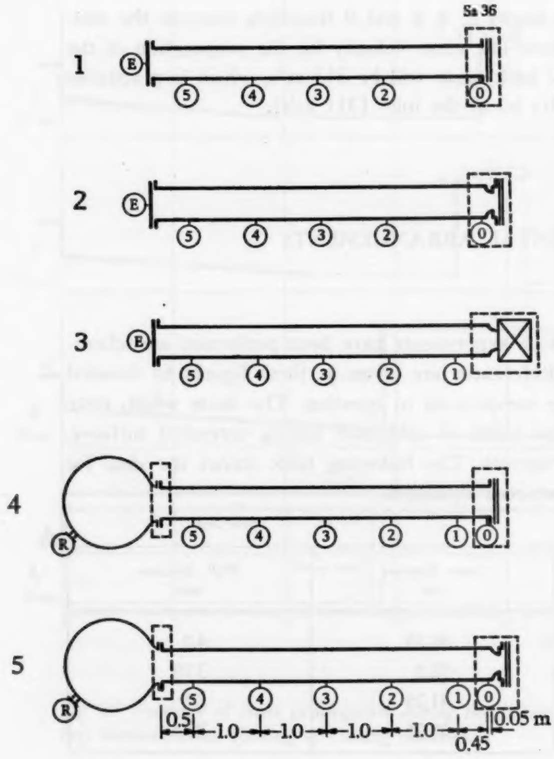

Arrangement 1: diaphragms according to Fig. 44

Arrangement 2: nozzle and diaphragms according to Fig. 45

Arrangement 3: nozzle and valve according to Fig. 46

Arrangement 4: container 0.3 m^3, container inlet according to Fig. 47, diaphragms according to Fig. 44

Arrangement 5: container 0.3 m^3, container inlet according to Fig. 47, nozzle and diaphragms according to Fig. 45

For all arrangements:
diam. 80 mm, length 5 m

E, R, 0–5 Pressure-measuring points

Fig. 35. Arrangements for rapid discharge experiments with 3″ tubes.

described in section (d) together with the operating members. The tube is from the beginning filled with air having a certain pressure, and a series of oscillations is initiated within the tube when the diaphragm end is suddenly uncovered. The propagation of the associated pressure fronts can be followed by recording the pressures in the measuring points indicated by the numbers and letters within the circles. The spacing of the points is shown for arrangement 5 in Fig. 35.

An outlet with a constricting nozzle having a minimum flow diameter of 52.5 mm has been adopted for arrangement 2.

Arrangement 3 differs from arrangement 2 in that the diaphragms have been replaced by a valve. The description of this valve, which is included in all the arrangements lacking diaphragms (with the exception, however, of arrangements 22 and 23, where a smaller valve, see Fig. 54, is used) is also given in section (d).

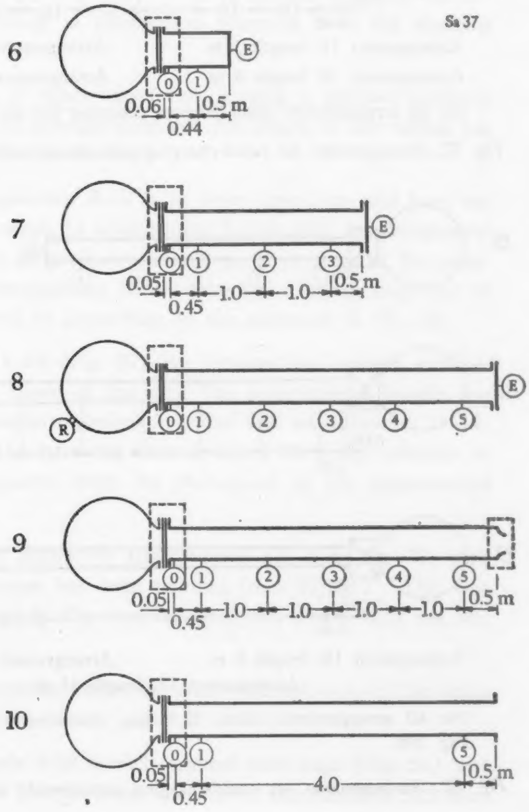

Arrangement 6: length 1 m

Arrangement 7: length 3 m

Arrangement 8: length 5 m

Arrangement 9: length 5 m, nozzle according to Fig. 49

Arrangement 10: length 5 m, full opening on outlet side

For all arrangements:
diam. 80 mm, container 0.3 m³, container inlet according to Fig. 48

Fig. 36. Arrangements for rapid-charging experiments with 3" tubes. Operation by bursting diaphragms.

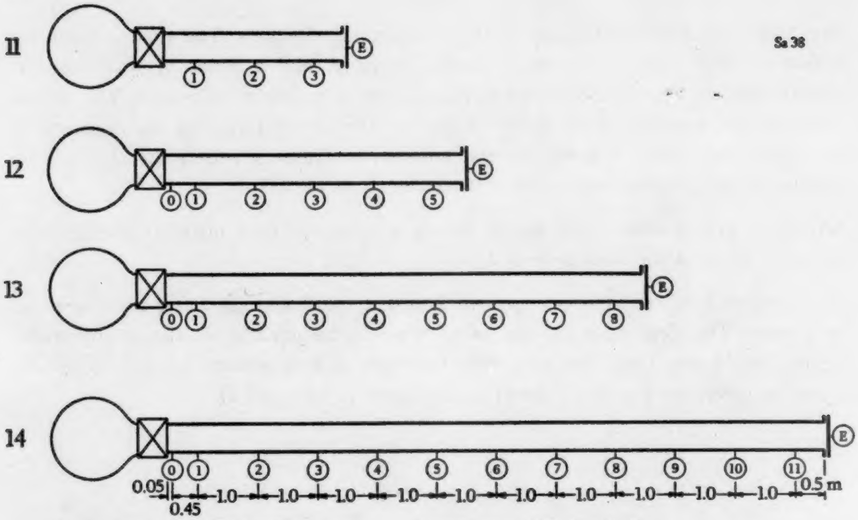
11
12
13
14
Sa 38
E
0 1 2 3 4 5 6 7 8 9 10 11
0.05
0.45
1.0
0.5 m

Arrangement 11: length 3 m
Arrangement 12: length 5 m
Arrangement 13: length 8 m
Arrangement 14: length 11 m

For all arrangements: diam. 80 mm, container 0.3 m³, inlet and valve according to Fig. 50a

Fig. 37. Arrangements for rapid-charging experiments with 3" tubes. Operation by valve.

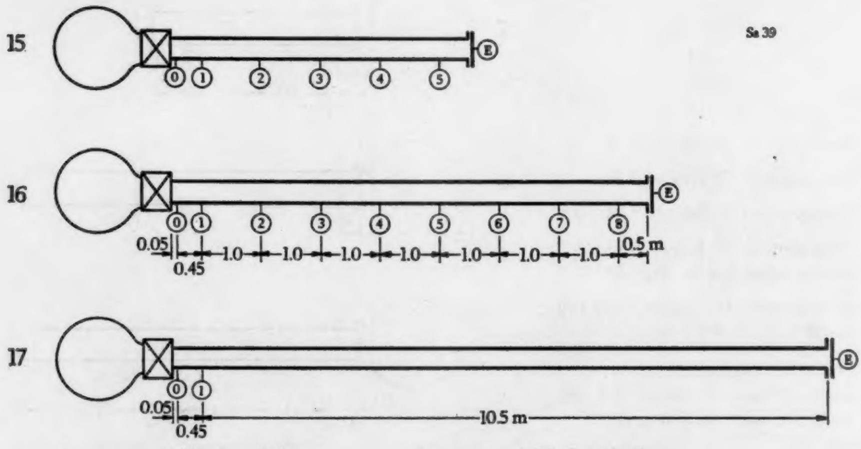
15
16
17
Sa 39
E
0 1 2 3 4 5 6 7 8
0.05
0.45
1.0
0.5 m
10.5 m

Arrangement 15: length 5 m
Arrangement 16: length 8 m
Arrangement 17: length 11 m

For all arrangements: diam. 52.5 mm, container 0.3 m³, inlet and valve according to Fig. 50b

Fig. 38. Arrangements for rapid-charging experiments with 2" tubes. Operation by valve.

The tube for arrangements 4 and 5 is connected at one end to a container with a volume of 0.3 m^3, whereas the other end can be communicated with the atmosphere by means of bursting diaphragms. In arrangement 4 the entire cross-sectional area of the tube is uncovered, whereas in arrangement 5, which has an outlet nozzle with a diameter of 52.5 mm, only 43 per cent of the cross-sectional area of the tube is uncovered. The appearance of the container is shown in Fig. 42, and the connection between the container and the tube in Fig. 47. The intermediate flange illustrated in Figs. 42 and 47 is used for all arrangements having a container. The tube for arrangements 4 and 5 thus went horizontally, that is to say, its longitudinal axis intersected the longitudinal axis of the container at a right angle.

b. *Arrangements for rapid charging*

The oscillations arising in air-blast circuit-breakers during the rapid charging of ducts are without doubt the most important and thus require particularly comprehensive investigations. This is the reason why the great majority of the experimental arrangements are intended for the study of phenomena occurring with the charging of ducts.

Fig. 36 shows arrangements having 3″ tubes where the charging is initiated suddenly by means of bursting diaphragms. In arrangements 6–8 the length of the tubing has been varied, but all of them are closed at the end.

The length of the tubing in arrangements 8–10 is in every case 5 m and here the size of the end opening has been varied. In arrangement 8 it is zero, in arrangement 9 the cross-sectional area facing the atmosphere amounts to 43 per cent of the cross-sectional area of the tube, and in arrangement 10 the tube has a full opening. Fig. 48 illustrates the diaphragm system and its connection to the container in Fig. 42.

The oscillations in arrangements 11–14 (Fig. 37) are initiated by opening a valve. All the tubes are of 3″ type and closed at the end. The experimental lengths are 3, 5, 8 and 11 m. Fig. 42 is intended to represent in actual fact arrangements 11–14. For the sake of clarity, however, the tube has been arranged vertically, whereas in reality it was horizontal, as is apparent from the photograph of the experimental equipment in Fig. 43.

Arrangements 15–17 in Fig. 38 are similar to arrangements 12–14 in Fig. 37, with the exception that the tube dimension has been reduced from 3″ to 2″. This was done to investigate whether a change in the cross-sectional area of the tube has any influence on the oscillations.

Fig. 39 shows a number of arrangements where the cross-sectional area of the ducts varies.

In arrangement 18 a diverging nozzle with a well rounded inlet edge (Fig. 51) was inserted immediately after the valve. The minimum diameter of this nozzle is 52.5 mm.

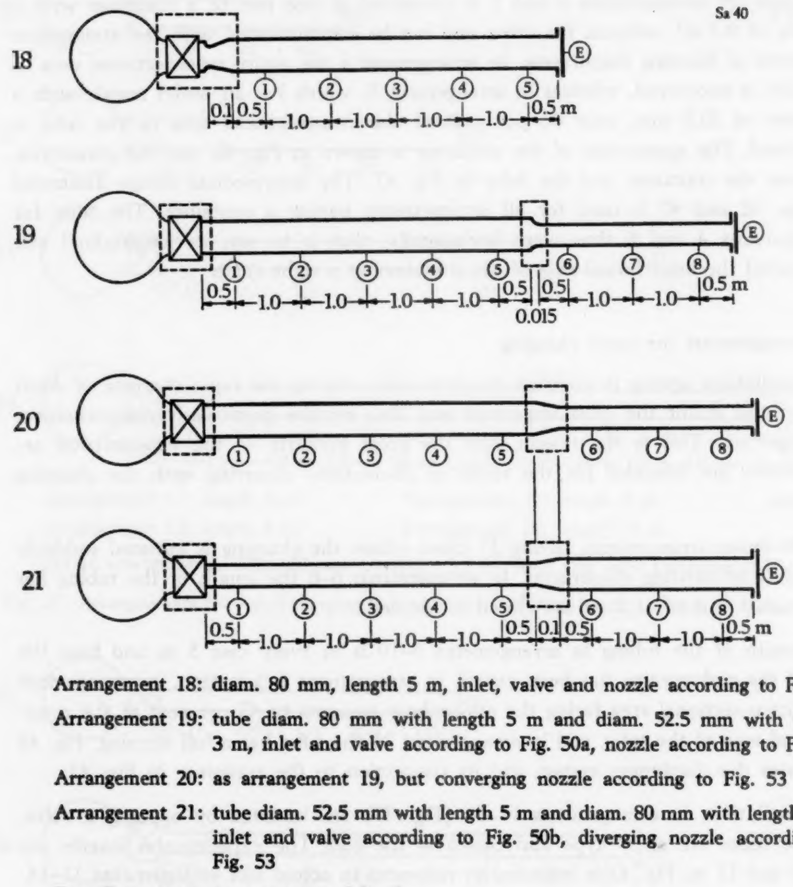
Sa 40
18
①
②
③
④
⑤
Ⓔ
0.1 0.5 1.0 1.0 1.0 1.0 0.5 m
19
⑥
⑦
⑧
0.5 1.0 1.0 1.0 1.0 0.5 0.5 1.0 1.0 0.5 m
0.015
20
21
0.5 1.0 1.0 1.0 1.0 0.5 0.1 0.5 1.0 1.0 0.5 m

Arrangement 18: diam. 80 mm, length 5 m, inlet, valve and nozzle according to Fig. 51

Arrangement 19: tube diam. 80 mm with length 5 m and diam. 52.5 mm with length 3 m, inlet and valve according to Fig. 50a, nozzle according to Fig. 52

Arrangement 20: as arrangement 19, but converging nozzle according to Fig. 53

Arrangement 21: tube diam. 52.5 mm with length 5 m and diam. 80 mm with length 3 m, inlet and valve according to Fig. 50b, diverging nozzle according to Fig. 53

For all arrangements: container 0.3 m^3

Fig. 39. Arrangements for rapid-charging experiments with non-uniform ducts. Operation by valve.

An even transition from this diameter to the tube diameter of 80 mm was obtained by means of an expanding cone. This transition extended over a length of about 100 mm, that is to say, the angle between the wall in the cone and the longitudinal axis does not exceed about 8°, which, according to generally known experience, ought to ensure that the flow does not depart from the wall.

Arrangement 19 consists of a 3" tube having a length of 5 m to which is connected a 2" tube with the length of 3 m by means of a simple nozzle (Fig. 52).

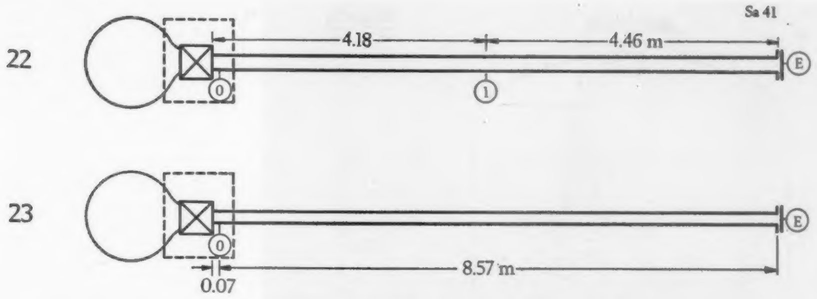

Arrangement 22: diam. 41 mm, inlet and valve according to Fig. 54a

Arrangement 23: diam. 36 mm, inlet and valve according to Fig. 54b

For both arrangements: length 8.64 m, container 0.3 m^3

Fig. 40. Arrangements for rapid-charging experiments with 1 ½" and 1 ¼" tubes.

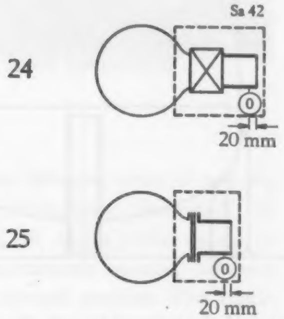

Arrangement 24: diam. 80 mm, length 75 mm, container 0.3 m^3, valve according to Fig. 55

Arrangement 25: diam. 80 mm, length 100 mm, container 0.3 m^3, diaphragms according to Fig. 56

Fig. 41. Arrangements for experiments on the free escape of air.

The same tube arrangement as in arrangement 19 is used for arrangement 20, with the exception that the transition between the tubes consists here of a converging nozzle (Fig. 53).

In arrangement 21 a 2" tube having a length of 5 m is connected to the valve, whereas a diverging nozzle at the end of this tube forms the transition to a 3" tube having a length of 3 m. The nozzle arrangement is the same as in Fig. 53, although a mirror image of this.

Fig. 40 shows two arrangements having a smaller valve (Fig. 54) and tube diameters of 1 ½" (arrangement 22) and 1 ¼" (arrangement 23) with a tube length of 8.64 m.

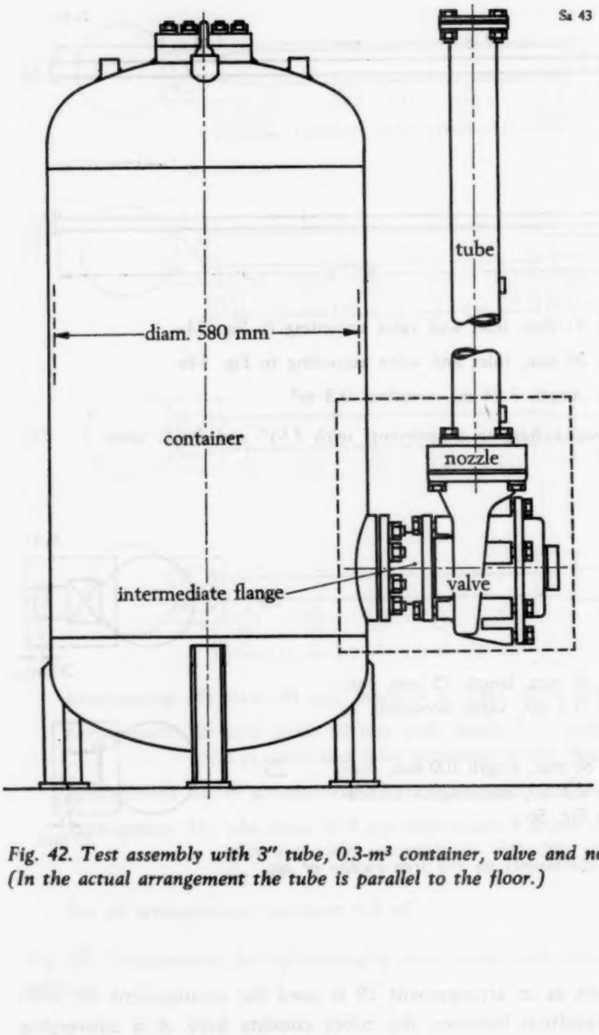

Fig. 42. Test assembly with 3" tube, 0.3-m³ container, valve and nozzle according to Fig. 50a. (In the actual arrangement the tube is parallel to the floor.)

c. *Arrangements for free escape*

The arrangements 24 and 25 in Fig. 41 comprise the container illustrated in Fig. 42 and closing member (valve shown in Fig. 55 and diaphragms in Fig. 56) and a nozzle, with an inner diameter of 80 mm, placed outside this member. These arrangements were used to determine the time dependence of the static pressure in the nozzle during the first stage of the discharge. The jet of air emanating from arrangement 24 was photographed at the same time by means of a high-speed camera.

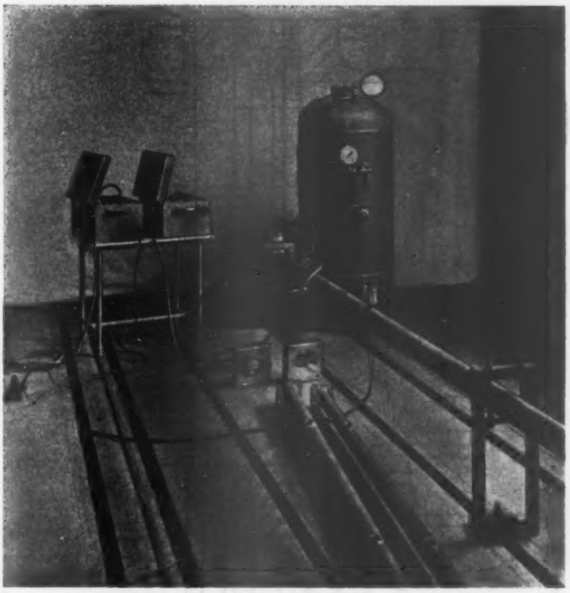

Fig. 43. View of the experimental arrangement. (Z 11779.)

d. Opening members

As is apparent from what has been mentioned above, three different types of opening member have been used, namely a system of bursting diaphragms, illustrated, for example, in Fig. 44, a valve shown in, for example, Fig. 46, and a valve shown in Fig. 54. The diaphragm system results in an almost instantaneous opening, whereas a valve requires about 0.005–0.01 s to attain the fully opened position. The initial front has thus a relatively low steepness when the valve opens. Only valves can be adopted for air-blast circuit-breakers, however, and the investigation of the oscillations resulting from an opening valve is therefore as important as the study of the phenomena resulting from bursting diaphragms. The latter, however, are better suited when making a comparison between practical and theoretical results.

The diaphragm system comprises two parallel diaphragms, Fig. 44, secured around their circumference and placed at a distance of 12 mm from one another. Between them is interposed a metal ring having a radial hole with a diameter of 3 mm, through which compressed air can be fed to the space between the diaphragms. This arrangement is clamped between bakelite rings. It has been used only for experiments with an initial pressure of 16 atm abs., which is a standard pressure for air-blast circuit-breakers, and its dimensions have been worked out with regard to this pressure. The surface exposed to the compressed air has a diameter of 92 mm and the thickness of each diaphragm, which is made from hard brass sheet, is 0.15 mm. The bursting

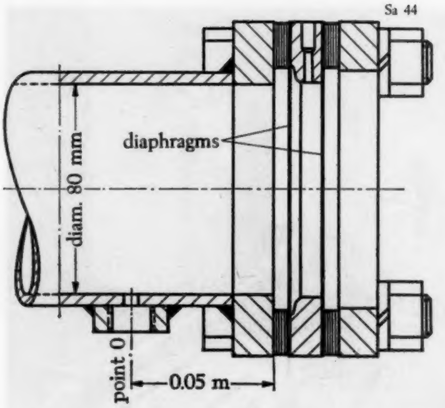

Fig. 44. Outlet with diaphragms (arrangements 1 and 4).

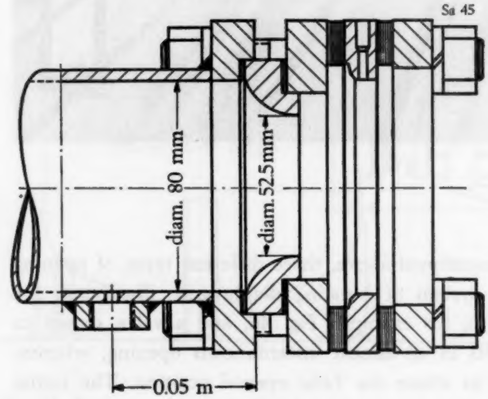

Fig. 45. Outlet with nozzle and diaphragms (arrangements 2 and 5).

pressure of a single diaphragm is about 10–12 atm and depends to a certain extent on how carefully the diaphragms are fixed. Since each diaphragm at the beginning of the experiment is only subjected to a load of half the initial pressure, there is a relatively good margin of safety that they will not burst prematurely. When bursting is to be initiated, each diaphragm in turn is subjected to the full initial pressure. The basic principle for the initiation of this is illustrated in Fig. 57.

This arrangement includes the manually operated valves *A* and *B* and the electrically operated valve C. The manometer *E* indicates the container pressure and the manometer *F* the pressure in the space *D* between the diaphragms. To start off with all the valves are closed. If the test arrangement is to be filled when making an experiment, valve *B* is opened first and then valve *A*. The container and the directly connected test tube G then start filling. At the same time, space *D* is filled via valve *B*

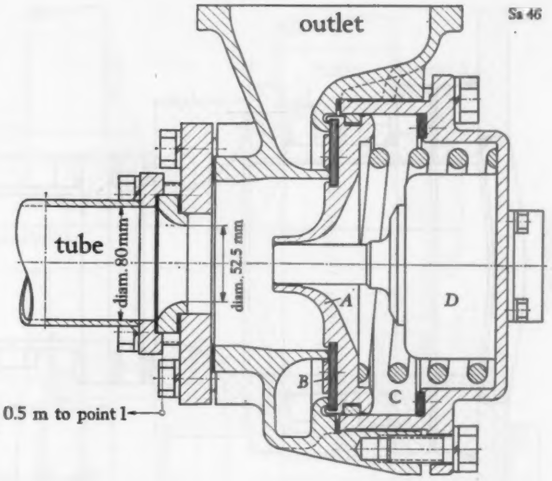
Sa 46
outlet
tube
diam. 80 mm
diam. 52.5 mm
A
B
C
D
0.5 m to point 1

A Tapered piston
B Rubber washer
C Space
D Servo-operated valve

Fig. 46. Outlet with nozzle and valve (arrangement 3).

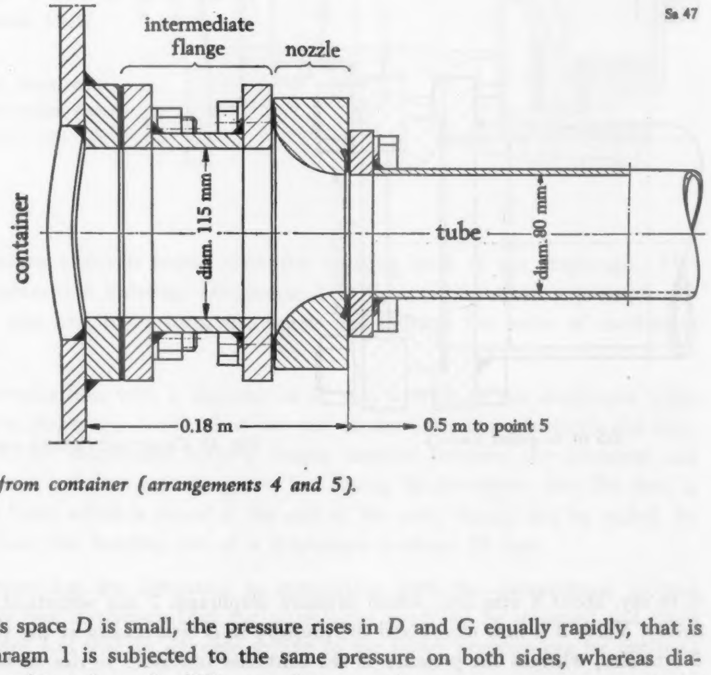
Sa 47
intermediate flange
nozzle
container
diam. 115 mm
tube
diam. 80 mm
0.18 m
0.5 m to point 5

Fig. 47. Inlet from container (arrangements 4 and 5).

and, since this space *D* is small, the pressure rises in *D* and G equally rapidly, that is to say, diaphragm 1 is subjected to the same pressure on both sides, whereas diaphragm 2 is subjected to the difference between the container pressure and the atmospheric pressure. This charging procedure is allowed to proceed until the pressure indicated by the manometers *E* and *F* has reached half the initial pressure, that

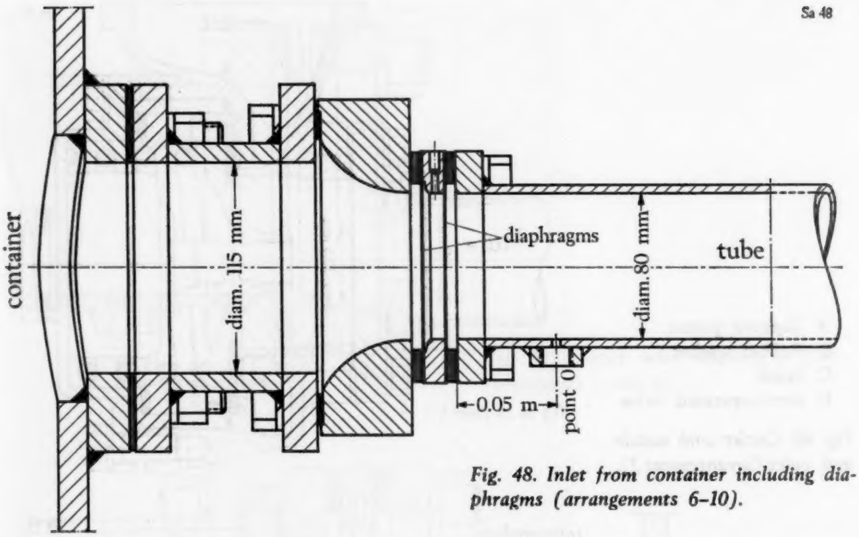
Sa 48
container
diam. 115 mm
diaphragms
diam. 80 mm
tube
0.05 m
point 0

Fig. 48. Inlet from container including diaphragms (arrangements 6–10).

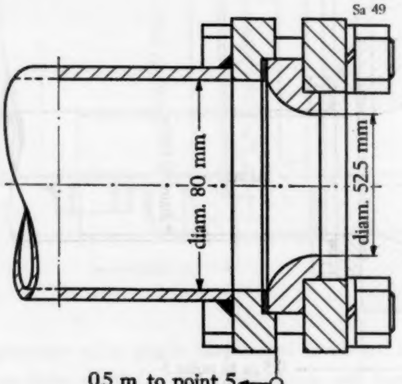
Sa 49
diam. 80 mm
diam. 52.5 mm
0.5 m to point 5

Fig. 49. Outlet with nozzle (arrangement 9).

is to say, about 8 atm abs., which pressure diaphragm 2 can withstand without difficulty. Valve *B* is now closed and the pressure in *D* will remain at the value of about 8 atm abs., whereas the pressure in the container continues to rise to the final value of 16 atm abs., when valve *A* is also closed. Both diaphragms are now subjected to a pressure difference of about 8 atm. When initiating the test, valve C is operated electrically, which causes the space *D* instantaneously to attain full pressure, that is

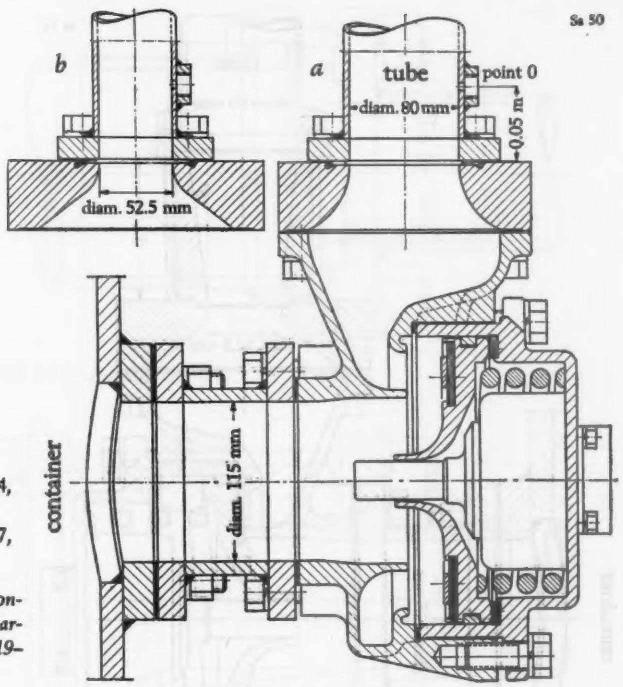

a Arrangements 11–14, 19, 20
b Arrangements 15–17, 21

Fig. 50. Inlet from container including valve (arrangements 11–17 and 19–21).

to say, a pressure which is higher than the bursting limit of the diaphragm. This results in diaphragm 2 bursting. Diaphragm 1 is then subjected to a pressure difference of 15 atm and, in its turn, also bursts and initiates the series of oscillations in the duct G.

As a rule a circular hole with a diameter of 92 mm is made in the diaphragm when it bursts. If the diaphragm is placed at the end of the tube, it is shattered and scattered about. If the diaphragms form a closing member between the container and tube, the sheet is not torn up into pieces but during its movement into the duct is formed into a lump which is found at the end of the tube, should this be sealed. At the bursting limit the bending out of a diaphragm is about 10 mm.

This arrangement has the advantage in comparison with the conventional method employing only one diaphragm that the diaphragms need not be designed and fixed with special care and that an accurate setting of the initial pressure can be obtained for each test.

Fig. 46 shows the valve used in all the test arrangements employing such a member, except arrangements 22 and 23. It has a minimum geometric flow area of about

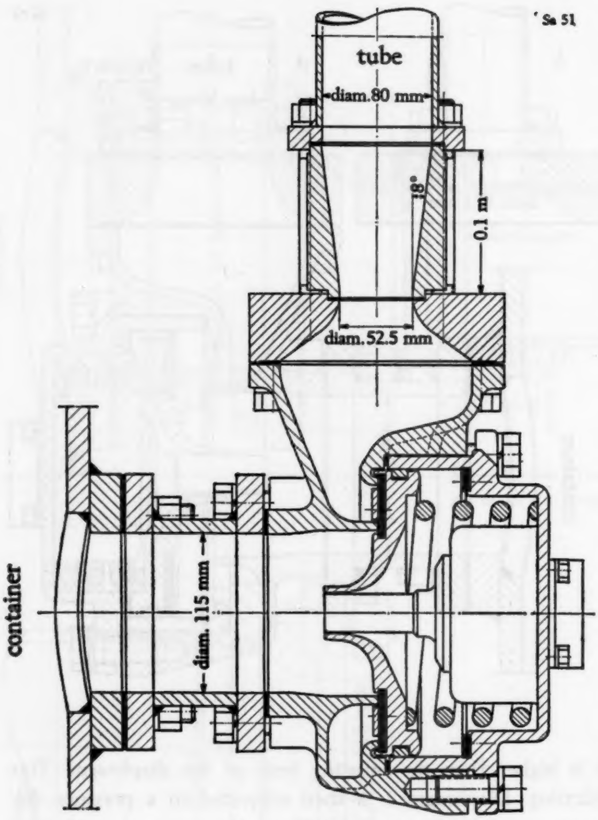

Fig. 51. Inlet from container including valve and nozzle (arrangement 18).

90 cm², that is to say, about twice the cross-sectional area of a 3″ tube, the cross-sectional area of which is about 50 cm². Experiments on the charging of a container have established that the flow coefficient of the valve for stationary flow of the order of the speed of sound is 0.80–0.85, corresponding to an effective flow area of 75 cm². Its nozzle value with regard to a simple nozzle with a well rounded inlet edge is about 80 cm², if the flow coefficient for such a nozzle is assumed to be 0.95. The effective flow area is thus about 50 per cent greater for a fully open valve than for the cross-sectional area of the largest size of test tube, namely the 3″ tube.

The closing member of the valve consists of the tapered piston *A* in which is embedded a rubber washer *B*. When the valve is closed, this washer rests against two concentric sealing edges. The surface enclosed by the inner edge forms the inlet, and the ring-shaped surface between the edges the outlet. That part of the piston surface limited by the inner edge is maintained under the container pressure when the valve

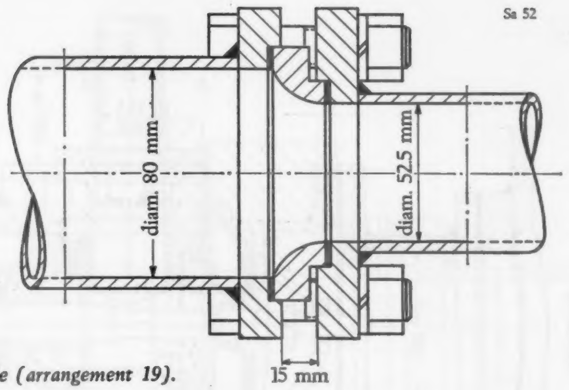

Fig. 52. Intermediate nozzle (arrangement 19).

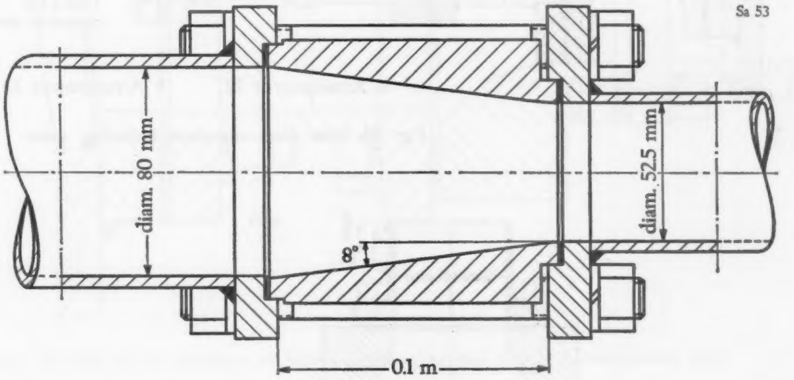

Fig. 53. Intermediate nozzle (arrangements 20 and 21).

is closed, and that part of the piston surface limited by the two edges under atmospheric pressure. On the other side of the piston the container pressure acts on the entire surface enclosed by the outer sealing edge. This means that, besides the spring pressure, a force equivalent to the above-mentioned ring surface area times the specific container pressure forces the piston against the sealing edges.

The valve is opened by means of a servo-operated valve *D* linking the space C with the atmosphere, thus causing the pressure in this space to drop rapidly to atmospheric pressure. The container pressure acting on the surface limited by the inner sealing edge then causes the piston to move against the spring pressure.

The total stroke of the piston is about 30 mm and the total time of movement has been found by measurements to have the values given in the table on page 85.

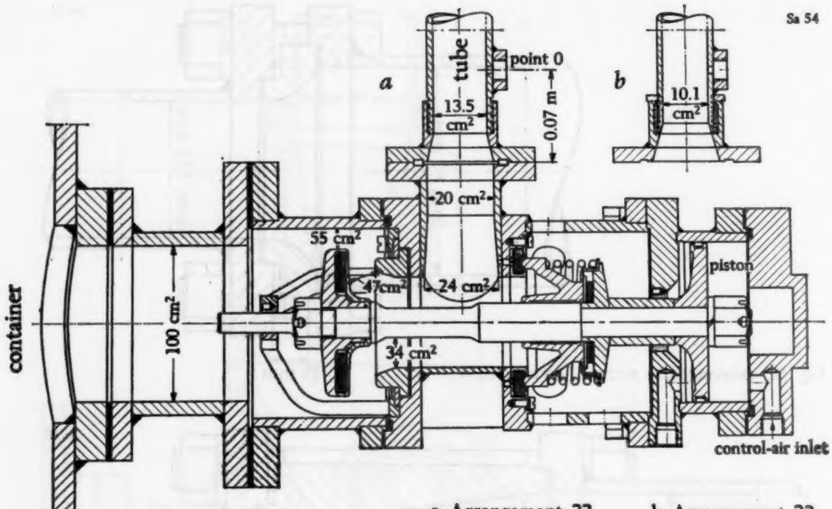
Sa 54
a
b
tube
point 0
13.5 cm²
0.07 m
10.1 cm²
20 cm²
55 cm²
47cm²
24 cm²
34 cm²
100 cm²
container
piston
control-air inlet

a Arrangement 22 b Arrangement 23

Fig. 54. Inlet from container including valve.

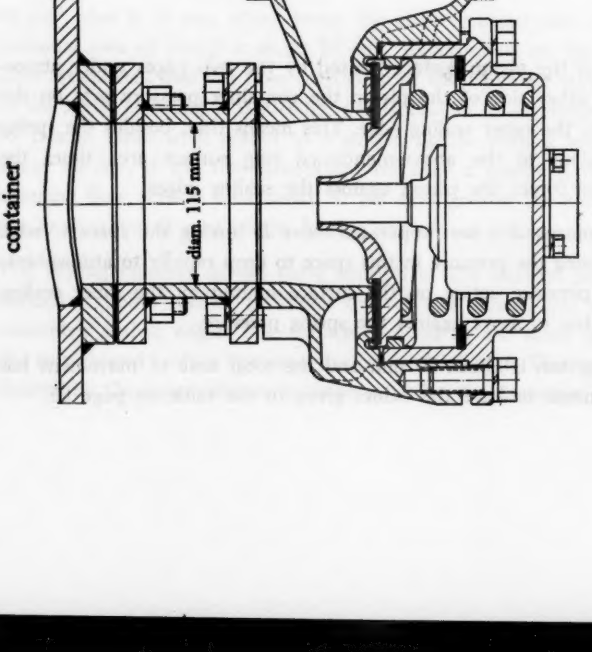
Sa 55
20 mm
diam.80 mm
diam. 115 mm
container

Fig. 55. Inlet from container including valve and nozzle (arrangement 24).

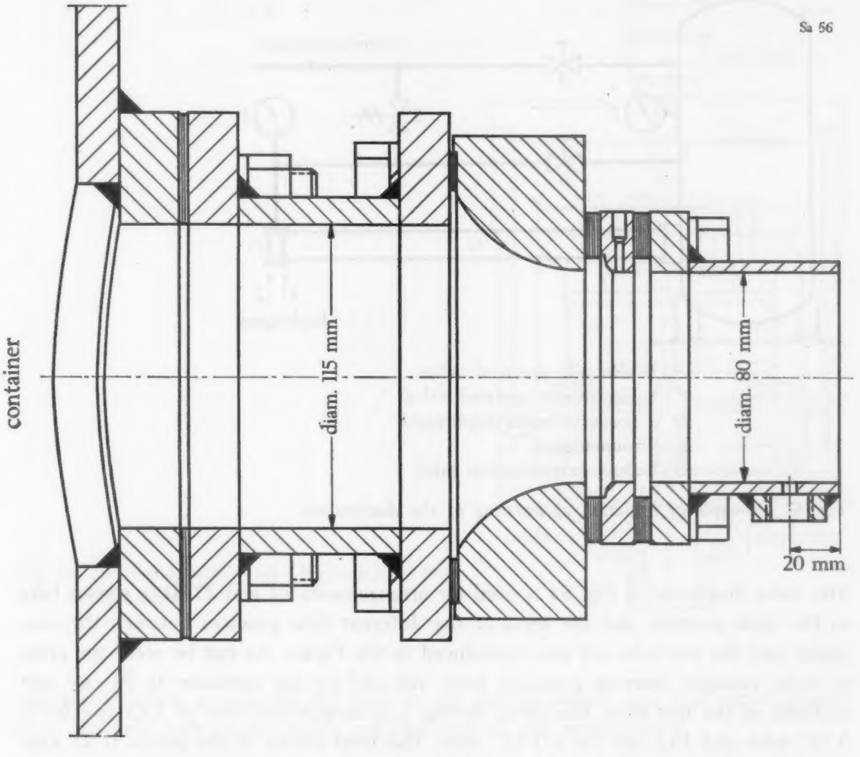

Fig. 56. Inlet from container including diaphragms and nozzle (arrangement 25).

Since in reality the valve does not open until the piston has moved 1–2 mm, due to the resilience of the sealing material and because the characteristic curve of the stroke as a function of time has proved to be almost parabolic, the effective times of movement will be only 75 to 80 per cent of the measured total times. These effective times are given in the last column of the table.

Container pressure atm abs.	Total time of movement s	Effective time of movement s
3	0.028	~ 0.022
6	0.010	~ 0.008
8	0.0095	~ 0.0075
12	0.0090	~ 0.0070
16	0.0087	~ 0.0068

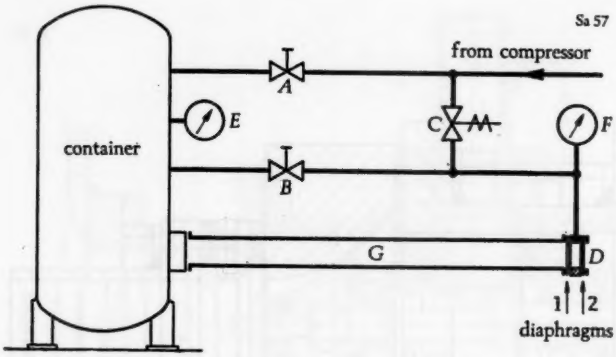

A, B	Manually operated valves
C	Electrically operated valve
D	Space between diaphragms
E, F	Manometers
G	Duct (experimental tube)

Fig. 57. Principle of initiation of bursting of the diaphragms.

The valve illustrated in Fig. 54 is used for arrangements 22 and 23. It is shown here in the open position, and the areas of the different flow passages between the container and the test tube are also reproduced in the Figure. As can be seen, the areas of these passages decrease gradually from 100 cm² by the container to 20 cm² just in front of the test tube, this latter having a cross-sectional area of 13.5 cm² for a 1 ½" tube and 10.1 cm² for a 1 ¼" tube. The total stroke of the piston is 23 mm. The movement of the piston from closed to open position takes place within 0.005 s at a pressure of 16 atm abs., and the stroke displays an almost linear dependence upon time.

II. Measuring devices

Various sensing instruments are available for measuring a rapidly varying static flow pressure. All of these, however, are not equally suited for a given test arrangement. When making tests of the nature described here, where rather pronounced mechanical shocks occur, caused both by the opening of the closing member and by the reflection of the pressure fronts, it has been found from experience at Asea that the *electromagnetic, piezo-electric* and *capacitive gauges* are practical, whereas *strain gauges* have had to be rejected after exhaustive preliminary investigations, since they displayed a pronounced sensitivity to mechanical shocks. The fact that the selection of the gauges for measuring transient pressures must be made with due care is clearly shown if, for example, these experiences are compared with the observations made by Montgomery and Ward [67]. It is stated in their paper that electromagnetic

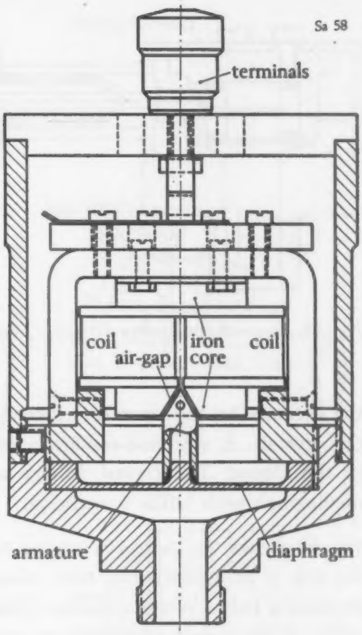

Fig. 58. Electromagnetic gauge (M-gauge) for pressure measurements.

and piezo-electric gauges did not lead to the desired results and that strain gauges were the only instruments which fulfilled here all the requirements.

Gauges of electromagnetic and piezo-electric type were used in the experiments at Asea and the designs used are described in the following.

Fig. 58 shows the *electromagnetic* gauge (M-gauge). It is built into a housing, the lower end of which can be screwed into a hollow threaded protuberance on the test tube. The air pressure actuates a diaphragm to which is attached a pointed armature forming part of the magnetic circuit of a fixed iron core, thus producing a double air-gap between the armature and the core. A winding is arranged on the core, the conductors of which are connected to terminal screws, and is fed with alternating voltage having a frequency of 10 000 c/s. When the pressure changes, the diaphragm is bent out and this brings about a change in the air-gap, resulting in a change in the inductance and consequently of the alternating current through the winding. A current proportional to the inductance is taken out via a bridge circuit, and this current actuates, after amplification and rectification, an element of an oscillograph with bifilar suspension.

The *piezo-electric* gauge (P-gauge) is illustrated in Fig. 59. In this case, two quartz crystals are actuated by the air pressure on a diaphragm. The voltage generated by

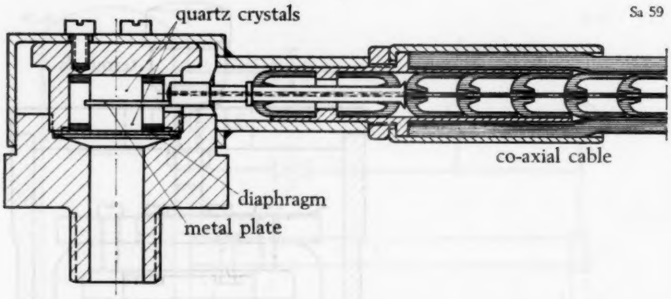

Fig. 59. Piezo-electric gauge (P-gauge) for pressure measurements.

the pressure on the crystals is taken out by means of a metal plate inserted between the crystals. A screened conductor connected to this plate can be seen to the right in the Figure. The crystal voltage actuates, after amplification, an element of an oscillograph with bifilar suspension.

Fig. 60 shows the gauges according to Figs. 58 and 59 fitted to measuring points on the side of an experimental tube, which is connected to the gauges by means of 5-mm measuring holes. When a sudden change in pressure takes place in the tube, the inlet space of the gauges causes a very small, but measurable, delay in the recording. This delay could be avoided if the measuring hole in the tube was made equally large as the hole in the gauge, that is to say, with a diameter of 10 mm. With an increasing measuring hole, however, the accuracy of measurements of the static flow pressure decreases and it was therefore considered desirable not to increase the hole diameter above 5 mm. Necessary corrections for the delay could, however, be made. As a basis for the estimation of the delay, it may be mentioned that if a shock front with a pressure of 1 atm abs. at the base and 10 atm abs. at the top passes the measuring point, the following times must elapse before the appropriate pressure is attained at the diaphragm:

	M-gauge			P-gauge		
atm abs.	5	9	10	5	9	10
ms.	0.57	1.29	1.80	0.25	0.57	0.80

These times apply to the case where the air in the tube is at rest. Flowing air will probably increase these times, since the inflow of air into the measuring hole will then be unsymmetrical.

In order to avoid burrs around the measuring hole, which would have made the measured values unreliable, the hole was drilled from the inside of the test tube

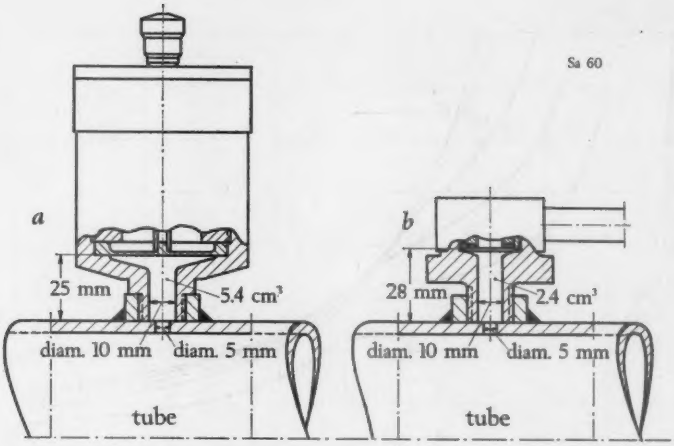
a M-gauge
b P-gauge
Sa 60
a
b
25 mm
5.4 cm³
28 mm
2.4 cm³
diam. 10 mm
diam. 5 mm
diam. 10 mm
diam. 5 mm
tube
tube

Fig. 60. Method of fitting M-gauge and P-gauge to the experimental tube.

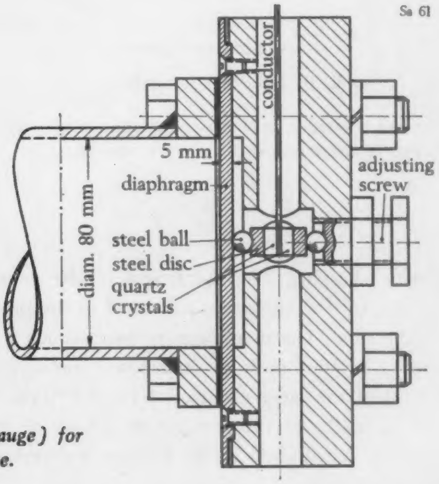
Sa 61
conductor
5 mm
diaphragm
adjusting screw
diam. 80 mm
steel ball
steel disc
quartz crystals

Fig. 61. Special piezo-electric gauge (SP-gauge) for pressure measurements at closed end of tube.

and outwards through a hole made in the opposite wall of the test tube, which was then blocked up again by welding.

When making experiments with an M- or P-gauge placed in the closed end of the tube, the inlet to the diaphragm was left unthrottled, that is to say, the inlet opening had a diameter of 10 mm. The delay in the recording due to the space in the gauge was then practically negligible.

A special piezo-electric gauge (SP-gauge), which is illustrated in Fig. 61, was made in order to study more closely the reflection phenomena at the closed end of a tube

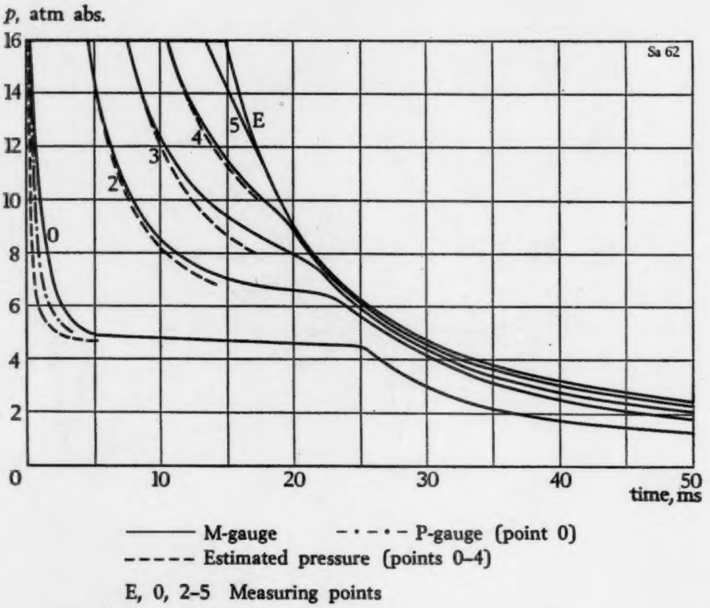

Fig. 62. Pressure as function of time when measured with M-gauge at various measuring points in arrangement 1 (p_n= 16 atm abs.).

during charging. The diaphragm of the gauge forms the end of the tube and the surface of the diaphragm subjected to the pressure is equal to the cross-sectional area of the tube. The diaphragm presses against a centrally placed column containing two quartz crystals with an interposed metal slab to enable the voltage generated by means of the piezo-electric effect to be taken out. The mechanical pressure is transmitted to the crystal surfaces by means of surface-ground steel washers to ensure a uniform distribution of the load on the crystals.

Steel balls are placed between the washer and diaphragm and the setting screw, respectively, for the purpose of concentrating in the centre the force exerted by the diaphragm. Since the crystals in this arrangement are subject to a high specific load and the piezo-electric voltage will thus also be relatively high, a fairly weak amplification can be adopted, which ensures that this arrangement will be rather insensitive to external electrical disturbances.

An oscillograph with bifilar suspension was used for recording the phenomena, the pressure-recording element having a natural frequency of about 5 500 c/s.

*

The following chapters K–M give an account of the results of the investigations using the experimental arrangements described above, as well as of certain comparisons with the theoretical derivations.

When recording pressure curves for the different measuring points along a duct, two gauges were normally utilised, of which one was retained at the same point throughout an experimental series, whereas the other one was moved from point to point during the series. The pressure curve recorded by the fixed gauge is thus to be found in all the oscillograms from the same experimental series. With the aid of this curve, it is possible to relate the pressure curves for all the measuring points with regard to time, which permits the study of the propagation of the pressure fronts along the ducts. An indicator was often used as well in conjunction with the closing member for the purpose of showing on all the oscillograms from a test series the instant when the member started to open. Such an indication serves the same purpose as a fixed gauge.

The initial temperature during the measurements was as a rule about 288 °K (about 15 °C).

K. EXPERIMENTS WITH THE RAPID DISCHARGE OF DUCTS

I. Discharge of a duct only

Arrangement 1: Operation by bursting diaphragms, full discharge opening
(Figs. 35, 44 and 47)

For these experiments a P-gauge was fixed at the point 0, while an M-gauge was moved between the other measuring points. On one occasion the pressure was measured at the point 0 by means of an M-gauge. For checking purposes the instant of bursting of the diaphragms was indicated electrically. The initial pressure in this case was $p_n = 16$ atm abs.

The curves with full-drawn lines in Fig. 62 show the pressures recorded with the M-gauge at the different measuring points. The pressures obtained with the P-gauge at the point 0 are denoted in the Figure by means of the chain-dotted line. In addition, the ideal pressures according to the calculations based on Eqs. (105) and (107) and with $w = a - u$ are indicated by means of broken lines. Since the measuring arrangement has a certain dead time, the actual pressures lie somewhere between the measured and the calculated values. In view of the flow losses occurring, the actual changes in pressure must be assumed to take place slightly more slowly than the calculated changes. As regards the point 0, where the pressure drops particularly rapidly, the space in the gauge causes a rather large delay in the pressure indication. The difference between the M-gauge and the P-gauge in this respect is clearly apparent in the relative position of the curves. According to these curves, the actual

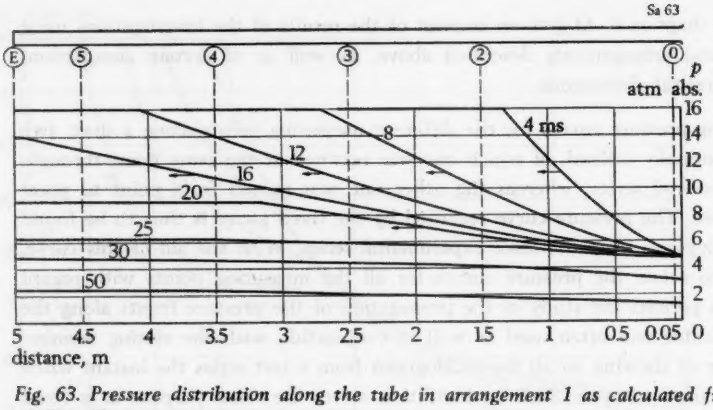

Fig. 63. Pressure distribution along the tube in arrangement 1 as calculated from the curves of Fig. 62.

pressure change at the point 0 must be considered as being rather close to the estimated change.

The pressure drops considerably more slowly at the other measuring points than at the point 0, and consequently the pressure changes measured here only with the M-gauge probably correspond rather closely to the actual pressure changes. For the pressure change at the point 0, it has been assumed that this point lies 7 cm from the end of the duct, which latter must be considered as being located in the position of the outer diaphragm.

When assessing the delay in the indication due to the space in the gauge, the state of flow in the experimental duct must be taken into account. If the pressure in the latter drops rapidly, as is the case at the point 0, while the velocity at the same time rises considerably, the air flowing past the measuring hole will hinder to an increasing extent the flowing out of air from the gauge. A calculation of the pressure in the M-gauge when its space is being evacuated from 16 atm abs., assuming that the air in the experimental duct is at rest, accords very well down to about 10 atm abs. with the difference between the values of the measured and the estimated curve. As the pressure drops still further, the actual delay increases in comparison with that determined in this manner. This must be attributed to the air velocity in the experimental duct becoming so high and the pressure difference between the gauge space and the duct becoming so small at the same time that the flowing out of air from the gauge is considerably hindered.

The delay in the oscillograph element, which constitutes only about 0.05 ms, can be neglected. The process of acceleration of the burst diaphragms can be estimated to delay the development of the stationary state of flow at the tube outlet by about 0.3 ms.

The theoretical value of the pressure arising at the mouth of the tube when the stationary state of flow is attained after the diaphragms have burst is, according to Fig. 21, equivalent to $p_1 = 0.278\ p_n$ at $F_0/F_1 = 1$, i.e., $p_1 = 0.278 \times 16 = 4.45$ atm abs. As is apparent from Fig. 62, the measurements have resulted in practically the same pressure.

On the basis of Fig. 62 and with due regard being paid to the delays in the indication, curves have been plotted in Fig. 63 for the pressure distribution along the tube at certain points of time after the diaphragms have burst. It is thus possible to follow in this figure the propagation of the wave fronts along the tube. The propagation of the negative expansion front travelling inwards is most conspicuous. Its top travels with the normal acoustic speed of 340 m/s (corresponding to about 288 °K) inwards along the tube, whereas the base remains at the opening, since the flowing out takes place here at the acoustic speed corresponding to the air temperature at the opening. When the top reaches the closed end of the tube, the front is partly reflected. The propagation of the base of the superposed positive expansion front can be followed from the knee in the curves for 16, 20 and 25 ms. The mean velocity of the base is, according to Fig. 63, about 430 m/s. Naturally, the reflection at the closed end of the tube can only be partial, since the top of the original front alone swings downwards with the base remaining at the outlet.

It is not possible to detect any further front movement from Fig. 63, but the phenomenon hereafter has the characteristic of a stable discharge with a rather uniform pressure drop in the direction of flow.

Arrangement 2: Operation by bursting diaphragms, throttled discharge opening (Figs. 35 and 45)

The minimum flow area of the nozzle is 43 per cent of the tube cross-sectional area, i.e., $F_0 = 21.7$ cm^2. The gauges were moved between the measuring points in the same manner as for arrangement 1. The initial pressure in the tube was $p_n = 16$ atm abs.

The pressure changes, which were recorded at the different measuring points with the M-gauge, but at point 0 also with the P-gauge, are reproduced in Fig. 64, while Fig. 65 shows the pressure distribution along the tube at different points of time.

When a stationary state of flow prevails in the outlet, the theoretical value of the static flow pressure within the nozzle is, according to Fig. 21, equivalent to $p_1 = 0.7\ p_n$ at $F_0/F_1 = 0.43$, i.e., $p_1 = 0.7 \times 16 = 11.2$ atm abs. The measurements have resulted in practically the same value of the pressure. The pressure at the closed end of the tube after the negative expansion front travelling inwards has been completely reflected from this end, that is to say, nearly 20 ms after the diaphragms have burst, corresponds rather well with the calculated value. The theoretical value of the pressure is, according to Fig. 21, equivalent to $p_2 = 0.49\ p_n = 0.49 \times 16 = 7.8$ atm abs.

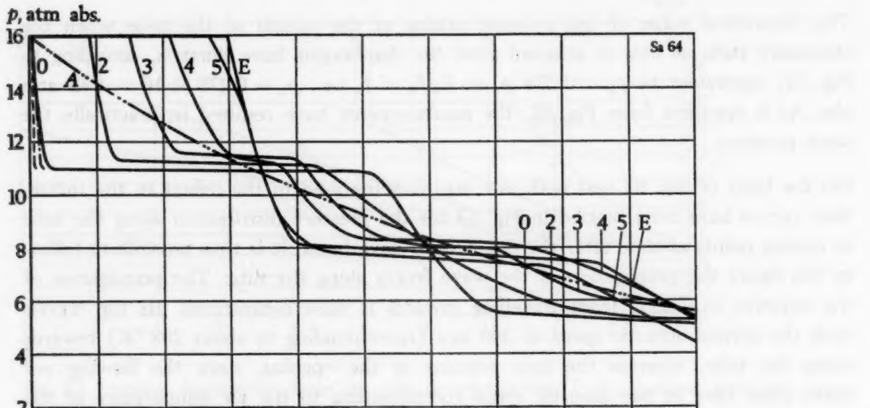

Fig. 64. Pressure as function of time when measured with M-gauge at various points in arrangement 2 ($p_n = 16$ atm abs.).

From the curves for 20 and 25 ms in Fig. 65 it is possible to derive a front velocity of the top of the positive expansion front travelling outwards of, in round figures, 500 m/s. According to Fig. 21, the theoretical value is equivalent to $w_{11} = 1.2\ a_n = 1.2 \times 340 =$ approx. 410 m/s. The rather marked difference is plainly due to the increase in temperature of the air resulting from frictional heat.

The curves for 35 and 40 ms point to the second negative expansion front, travelling inwards, which has resulted from the reflection of the positive front against the opening. The pressure around the measuring point 5 displays later on unexpectedly low values in comparison with the pressures at point 4 and at the closed end of the tube. The irregularities can hardly be attributed to inaccuracies in the measurements. It is possible that some form of local oscillations occur in conjunction with reflection of the front at the end of the tube.

For sake of comparison, a curve in Fig. 64 designated *A* has been plotted, which shows how the pressure drops with time, if the container is not tubular as it is in this case, but has a concentrated volume, being designed, for example, as a sphere with the nozzle placed direct in the container wall. This curve has been estimated. Measurements which have been made for similar cases have shown that as a rule

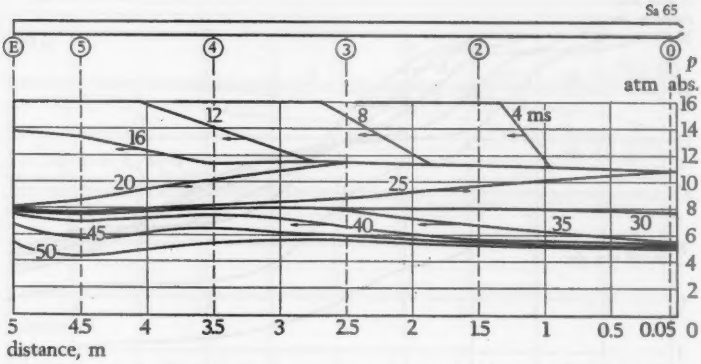

Fig. 65. Pressure distribution along the tube in arrangement 2 calculated from the curves of Fig. 64.

it takes about 5 per cent less time than calculated to come down to a certain pressure. It is assumed that the reason for this is that the compressed air available often contained substantial amounts of water vapour, which, on being cooled down in the nozzle, became condensed and flowed through this in a fluid or solid state that is to say, with a greatly reduced volume. The nozzle has consequently been able to allow a correspondingly larger volume of dry air per unit of time to flow through it, which has resulted in a more rapid drop in the pressure of the container. The air used also in the oscillation tests described here contained substantial amounts of water vapour, and consequently a comparison should be made with a curve lying slightly below the curve *A* shown in the Figure. Such a curve will almost constitute a mean curve for the pressure changes at the points 0 – E. From the above it is possible to draw the conclusion that the discharge time for a long tube will be very nearly the same as that for a container of concentrated volume.

Arrangement 3: Operation by valve, throttled discharge opening (Figs. 35 and 46)

As previously, the minimum flow area of the nozzle was 21.7 cm^2, but only M-gauges were used for this experimental series. It can be assumed that, with the relatively slow pressure changes occurring here, these gauges have recorded the values without any time delay. Electrical indication of the opening time of the piston in the valve was employed for the purpose of relating the pressure changes to one another with regard to time. The pressure changes measured are reproduced in Fig. 66, while Fig. 67 shows the pressure distribution along the tube at different points of time. The initial pressure in the tube was $p_n = 16$ atm abs. The pressures at point E, i.e., at the closed end of the tube, were also recorded at the initial pressures of 12 and 8 atm abs. Corresponding curves are plotted in Fig. 66.

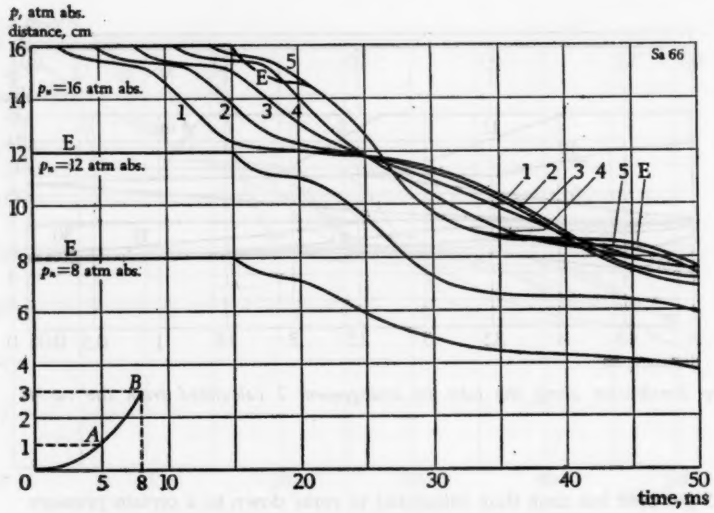

0*AB* Distance-time curve of valve piston ($p_n = 16$ atm abs.)
A Valve opening equal to nozzle area
B Valve fully open
E, 1–5 Measuring points

Fig. 66. Pressure as function of time when measured with M-gauge at various points in arrangement 3 ($p_n = 8$, 12 and 16 atm abs.).

The pressure changes with this arrangement differ materially from those in the previous arrangement with nozzle and bursting diaphragms. The fronts, particularly in the beginning, are considerably less steep, which is largely due to the fact that it takes a certain amount of time to initiate the movement of the valve piston. About 5 ms are required to attain a geometric flow area in the valve equivalent to the nozzle flow area of 21.7 cm^2. The stroke of the piston is then about 1 cm. A stationary state of flow has, however, not yet been attained in the nozzle, since a state of flow resistance prevails in the valve. It is not until the piston has reached its end position that the velocity in the nozzle increases to approximately the critical value. It can be estimated that the end position is reached after a delay of about 8 ms from the commencement of the opening of the valve. The above times refer to an effective time of movement, i.e., the times are calculated from the instant that the sealing material has sprung out when the piston lightens and a flow opening thus commences to appear in the valve. The effective time of movement at 16 atm abs. has been given as 6.8 ms in the table on page 85. In the case in question, it will be slightly longer, since the nozzle limits the flow of air acting on the valve piston. The time was not measured for this experimental series, but it can be assumed in all probability to be about 8 ms. When the valve is fully open, its geometrical flow area is about 90 cm^2, i.e., about 4 times that of the nozzle.

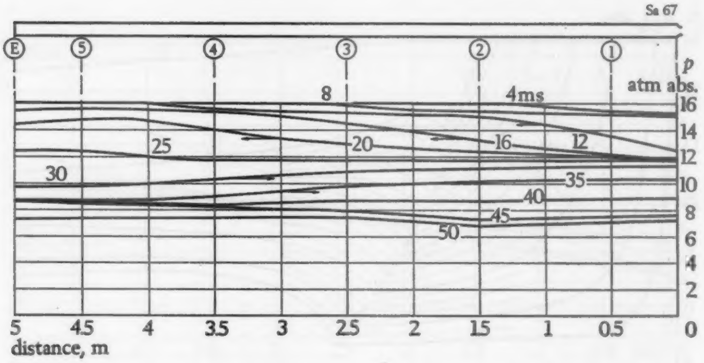

Fig. 67. Pressure distribution along the tube in arrangement 3 as calculated from the curves of Fig. 66.

The static flow pressure ahead of the nozzle is, according to Fig. 67, about 11.7 atm abs., after the first negative expansion front has been fully developed and a stationary state of flow has consequently been attained in the nozzle. This value lies slightly higher, namely 0.5 atm, than the theoretical value $p_1 = 11.2$ atm abs. When using arrangement 2 with bursting diaphragms, the corresponding value was about 11 atm abs. The result seems to indicate that the valve, also when fully open, causes a slight flow resistance. In other words, the velocity in the nozzle does not attain the full critical value, but, on the other hand, the pressure does not drop right down to the critical value. The fact that the pressure at the closed end of the tube after the reflection drops only to about 8.7 atm abs., whereas the theoretical value is 7.8 atm abs., i.e., almost 1 atm lower, points in the same direction.

During the first part of the movement of the piston after the valve has started to open, the flow area does not increase in proportion to the piston travel owing to the appearance of the metal washer which retain the rubber gasket (cf. Fig. 46). A circular slot of about 8.5 cm² is first uncovered, this remaining constant until the piston has travelled about 5 mm, after which the flow area increases rapidly. This circumstance is clearly reflected in the pressure changes. According to Fig. 66 the pressure first drops slowly at the measuring points and tends to become stabilised, but then changes over to a relatively rapidly falling curve as a result of the limiting effect of the circular slot ceasing. The stabilising pressure exhibited by the curves corresponds rather well to the pressure which can be determined on the basis of the areas of the slot and nozzle.

The curve for the measuring point E at the closed end of the tube clearly indicates the reflection of this first pressure-reducing front. The reduction in pressure after the reflection is approximately double, which it should also be in theory.

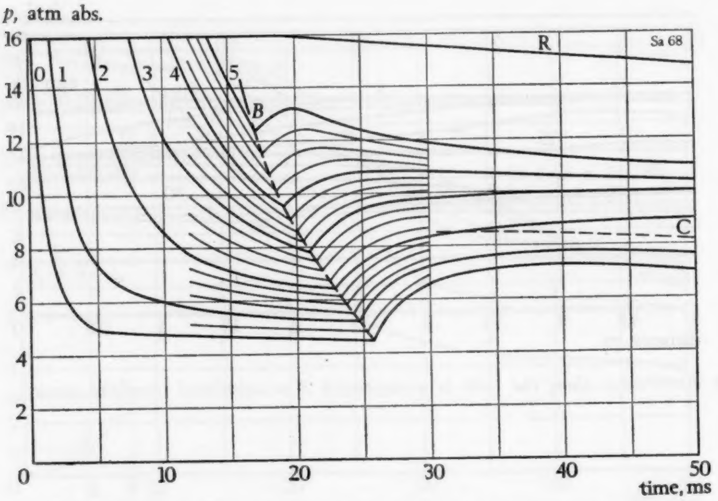

B Time, when base of press front reaches the measuring points
C Critical pressure corresponding to container pressure

R, 0–5 Measuring points

Fig. 68. Pressure as function of time when measured with M-gauge at various points in arrangement 4 ($p_n = 16$ atm abs.).

II. Discharge of a duct connected to a container

Arrangement 4: Operation by bursting diaphragms, full discharge opening (Figs. 35, 44 and 47)

The pressure changes shown in Fig. 68 were recorded with an M-gauge. At first, the pressure drops at the different measuring points in the same way as in Fig. 62 for the discharge of a duct alone, since the addition of the container does not in fact influence the first negative expansion front travelling inwards. It is only after this has started being reflected from the container that the changes in pressure differ from those reproduced in Fig. 62. The positive press front coming from the container starts becoming noticeable at the different measuring points in the way shown by the broken curve *B*, which denotes the time when the base of the press front reaches the measuring points. The pressure curves plotted for the points situated between the measuring points have been interpolated and are intended to facilitate the plotting of the pressure fronts in Fig. 69. As is apparent in this latter Figure, the conditions have become stabilised after about 40 ms, i.e., the oscillations have then ceased and a flowing outwards having a stationary characteristic prevails thereafter. According

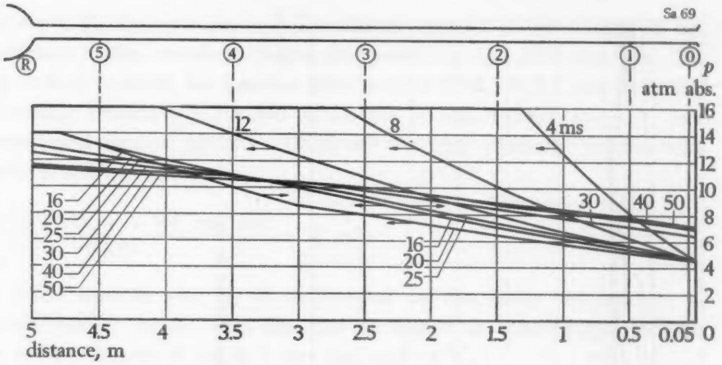

Fig. 69. Pressure distribution along the tube in arrangement 4 as calculated from the curves of Fig. 68.

to curve *B* in Fig. 68, the mean velocity of the base of the positive press front is about 500 m/s. The corresponding theoretical velocity is, according to Fig. 23b, $w_{11} = 1.667\, a_n = 1.667 \times 340 = 567$ m/s. The difference in these two values is mainly due to the fact that in the theoretical derivation it is assumed that the state ahead of the front base is always constant and equal to the state at the outlet of the tube, whereas in practice it varies. The mass velocity in the front base is thus low in that part of the tube nearest the container and increases towards the outlet, since the base of the first negative expansion front travelling inwards remains at the outlet and this front therefore only swings down inwards into the tube (see Fig. 69).

The pressure distribution within the tube, for example, after 50 ms, when a stationary state of flow must be assumed, is obviously considerably influenced by friction. Thus, the pressure drop at 50 ms is 4 atm between the points 5 and 0, i.e., over a distance of 4.5 m. In the case of loss-free flow, the pressure at the outlet of the tube would follow the curve C in Fig. 68, which curve represents the critical pressure corresponding to the measured container pressure according to curve R. The measuring point R is located at the top of the container in Fig. 42 and the distance between it and point 5 is 1.65 m. The pressure in the other parts of the tube for loss-free flow is only insignificantly higher than the critical pressure, this being caused by the pressure drop due to the limited volume of the container. The fact that the pressure at point 0 lies below the critical pressure in curve C seems to indicate that the air has become heated due to friction and that its discharge velocity has consequently increased. This in its turn results in the volume of air flowing out per second diminishing, since the drop in density, which takes place in direct inverse proportion to the temperature rise, exerts a greater reducing influence on the discharge volume than the rise in velocity has in the increasing direction, because the velocity only rises in proportion to the square root of the temperature.

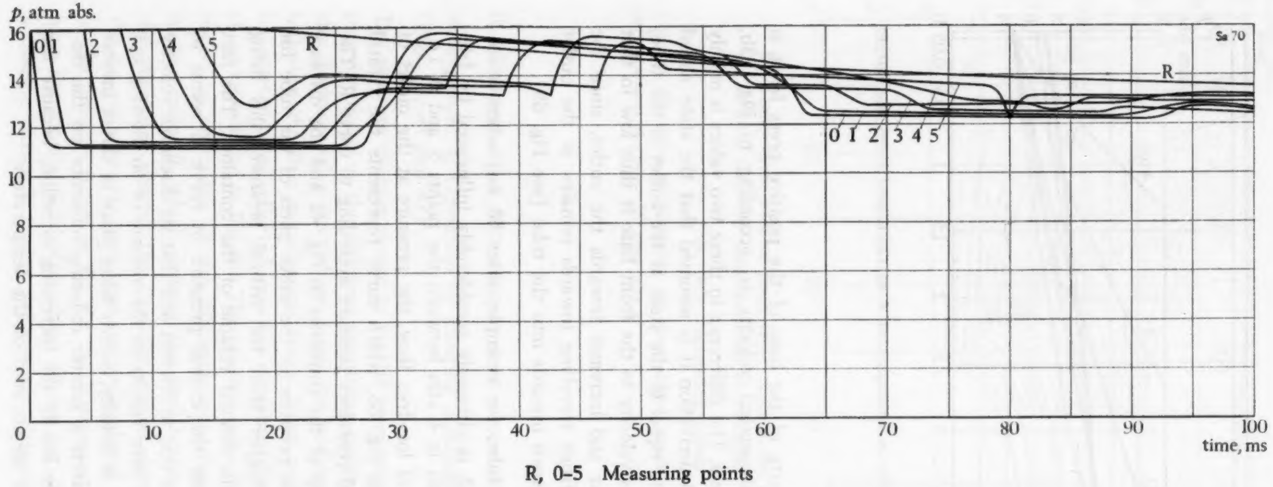

Fig. 70. Pressure as function of time when measured with M-gauge at various points in arrangement 5 ($p_n = 16$ atm abs.).

According to curve R, the pressure in the container drops 1.4 atm within 35 ms. The mean pressure in the container during this period is thus 15.3 atm abs. The corresponding critical pressure for loss-free flow is 0.53 × 15.3 = 8.1 atm abs., and the critical discharge velocity 0.913 × 340 = 310 m/s (cf. Eq. (114)). For a 3" tube with a cross-sectional area of 50 $\mathrm{cm}^2 = 0.005\ \mathrm{m}^2$ the ideal discharge volume with these assumptions will be

$$Q = \frac{310\ \mathrm{m/s} \times 0.005\ \mathrm{m}^2 \times 8.1\ \mathrm{atm\ abs.}}{0.833} = 15\ \mathrm{m}^3/\mathrm{s}$$

Dividing by 0.833 signifies that Q is determined at the initial temperature of 15°C, and multiplication by 8.1 atm abs. that Q applies at atmospheric pressure, i.e., Q refers to free volume of air of 1 atm abs. and 15 °C.

The actual mean value for Q can be determined on the basis of the container volume and the pressure drop according to the following expression:

$$Q = \frac{0.73 \times 0.3\ \mathrm{m}^3 \times 1.4\ \mathrm{atm\ abs.}}{0.035\ \mathrm{s}} = 8.8\ \mathrm{m}^3/\mathrm{s}$$

Multiplying by the coefficient 0.73 signifies that the adiabatic cooling of the container air during the propagation has been taken into consideration. In other words, the latter Q-value also refers to free air of 1 atm abs. and 15 °C [92].

This comparison between the ideal and the measured value for Q indicates that the friction at these high flow velocities considerably limits the volume of air per unit of time flowing through the tube.

Arrangement 5: Operation by bursting diaphragms, throttled discharge opening (Figs. 35, 45 and 47)

Fig. 70 shows the pressure curves, which have been determined by means of an M-gauge at the different measuring points. These curves coincide in their first part with those plotted in Fig. 64 for the pressure changes experienced with a tube alone, i.e., when the negative expansion front caused by the bursting diaphragms is travelling towards the container. A pronounced difference then takes place in comparison with the pressure changes recorded in Fig. 64 in that the pressure along the measuring points increases again, which indicates that a positive press front has arisen as a result of the negative expansion front being reflected against the container. That this will be so is also apparent from the theoretical study. The appearance of the press front 20 and 25 ms after the diaphragms have burst is shown in the diagram in Fig. 71 for the pressure distribution along the tube at different intervals. When this front arrives at the outlet, it is reflected into a negative press front, which, in Fig. 71, can be followed through the points of time 30, 35, 40 and 45 ms. The measurements confirm that the leading part of this negative press front during its propagation towards the container is converted into a shock front. This conversion probably commences when the base of the negative press front has reached 1–2 m from the outlet. Because of the inertia of the measuring arrangement, the shock front will not appear in Figs. 70 and 71 as sudden changes in pressure. In Fig. 70, for example, it can be deduced nevertheless from the pressure changes within the range 30–50 ms that a shock front must be formed, since the front steepness is already so pronounced from the start, e.g., at point 1, that it must result in the formation of a shock front after a rather short distance.

The theoretical values of the pressures are, according to Fig. 23a, for $F/_0F_1 = 0.43$ as follows:

at the outlet, behind the negative expansion front, $p_1/p_n = 0.70$
at the inlet, behind the positive press front, $p_2/p_n = 0.89$
at the outlet, behind the negative press front, $p_3/p_n = 1.08$

The theoretical pressures will be at $p_n = 16$ atm abs.: $p_1 = 11.2$ atm abs.; $p_2 = 14.2$ atm abs.; $p_3 = 17.3$ atm abs. Measurements show for point 0 the same pressure p_1 as the estimated value. Within the tube the pressure p_1 rises slightly from point to point, which must be attributed to friction. The pressure p_2 behind the positive press front has been found at point 5 by measurement to be 14.1 atm abs., which is practically the same value as that calculated. A certain attenuation is experienced during the propagation of the front towards the outlet, and the pressure p_2 displays, relative to its propagation throughout the tube, a drop of about 1 atm. As a result of this and also of the container pressure dropping, the pressure p_3 behind the negative press front does not attain the theoretical value 17.3 atm abs., but remains slightly below the original container pressure of 16 atm abs.

Figs. 70 and 71 permit certain comparisons to be made between the measured and the estimated front velocities. As is natural, the top of the first negative expansion front travelling inwards moves with the normal acoustic speed of about 340 m/s, since the air here is at rest and the conditions are thus not influenced by friction from the tube. The base velocity of this front is, according to Fig. 71, about 225 m/s, whereas the theoretical value according to Fig. 23b is $w_1 = 0.7a_n = 0.7 \times 340 = 238$ m/s. This base velocity refers to the mean velocity for a tube length of 3.6 m reckoned from the outlet nozzle. The velocity is at its maximum nearest the nozzle and decreases along the tube. During the first part of the propagation, that is to say, along the part nearest the nozzle, the base velocity is practically the same as the theoretical value, whereas in the vicinity of the inlet from the container it drops to almost 200 m/s. The base velocity w_1 constitutes the difference between the acoustic speed a_1 and the mass speed u_1 directed towards the nozzle. Since the temperature T_1 at the base is higher than the estimated value due to the influence of friction, a_1 is also higher than the theoretical value. From this it follows that the increase in u_1, reckoned as a percentage, is considerably greater than for w_1 and a_1, because w_1 in the equation $w_1 = a_1 - u_1$ decreases and a_1 increases in comparison with the theoretical values. If the pressure variations are studied while the front is

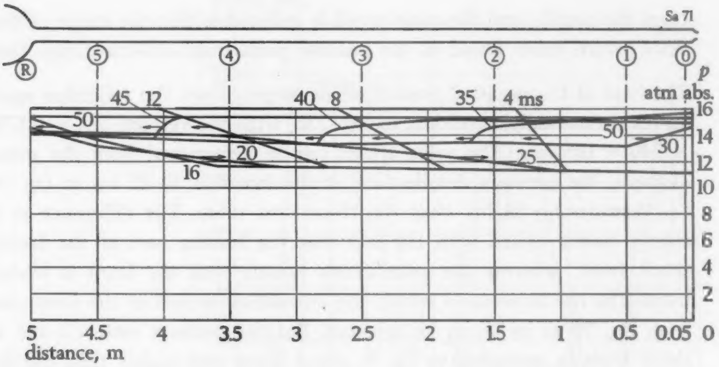

Fig. 71. Pressure distribution along the tube in arrangement 5 as calculated from the curves of Fig. 70.

travelling inwards along the tube, it is obvious that T_1, and consequently a_1 in the base, must increase during the propagation, since the conversion of static energy into kinetic energy takes place along a continuously increasing length of tube, i.e., the front range increases with the propagation, which means that the friction will exert an increasing influence. The measurements in fact show that w_1 in the front base decreases at the same time with the propagation. Since $u_1 = a_1 - w_1$, it can be inferred that u_1 increases rather considerably during the propagation. This applies to the velocity in the front base itself. A further increase in u_1 clearly takes place along the distance between the base and the outlet opening.

This relatively large increase in u_1, which apparently can be derived from the measurements for the negative expansion front, is to a certain extent at variance with the results which it has been possible to derive from the movement of the front reflected from the container, i.e., the positive press front. According to the pressure distribution curves in Fig. 71 for 20 and 25 ms, the base of this latter front moves towards the outlet with an approximate velocity of 425 m/s. The theoretical value is, according to Fig. 23b, for $F_0/F_1 = 0.43$: $w_{11} = 1.2\,a_n = 1.2 \times 340 = 408$ m/s. The measured value thus lies only about 5 per cent higher than the theoretical one. This increase can probably be attributed largely to the rise alone of the acoustic speed a_1. In such a case, the mass speed u_1 will not then differ essentially from the theoretical value, whereas the investigation of the previous front seems to indicate that u_1 is considerably higher. The likely explanation of this problem is perhaps to be found in the reducing influence of the nozzle on the air flowing out. The velocity u_1 is high just behind the negative expansion front travelling inwards and slightly higher than the value corresponding to the flow capacity of the nozzle. This acts as if a weak negative press front were moving behind the expansion front into the tube from the nozzle, and the mass speed is reduced within the range of this front to the value which exists ahead of the positive press front reflected from the container.

The base of the negative press front developing from the reflection against the nozzle moves theoretically, according to Fig. 23b, with the velocity $w_{22} = 0.575\, a_n = 0.575 \times \times 340 = 195$ m/s. The value which can be determined from the measurements, for example, the pressure distributions at the intervals 30–45 ms in Fig. 71, is 237 m/s, i.e., considerably higher than the theoretical value. The difference in the velocity is clearly closely linked with the fact that the leading part of the front consists of a shock front, whereas the calculations assume that the front is exclusively a press front. The rise in pressure within the discontinuous part of the front can be estimated from Fig. 70 to be about 10 per cent. For the pressure ratio 1.1 the velocity of the shock front is, according to Fig. 8, about 5 per cent higher than the base velocity of a continuous front. In the case in question a theoretical base velocity of about 1.05 × 195 = approx. 205 m/s can then be estimated. The measured velocity is, however, still about 30 m/s higher, which can probably be attributed to the increases in temperature of the air caused by friction.

L. EXPERIMENTS WITH THE RAPID CHARGING OF DUCTS

1. Operation by bursting diaphragms, 3″ tubes

Arrangements 6–8: Tube closed at exterior end
(Figs. 36 and 48)

An experimental series was performed with tubes of three different lengths, namely 1, 3 and 5 m, under otherwise identical conditions. The tube diameter was thus in every case 3″ and the initial pressure in the container 16 atm abs. Figs. 72, 74 and 76 show the pressure changes at different measuring points for a tube length of 1, 3 and 5 m, respectively. The pressures have been recorded by means of P-gauges. Fig. 77 shows the pressure changes in the 5-m tube recorded by means of M-gauges, whereas Fig. 78 shows the pressures at the end of the 5-m tube recorded by means of the SP-gauge illustrated in Fig. 61. The main features of the pressure changes can be best studied on the basis of the curves for the 5-m tube, which display a more uniform development with a greater attenuation of the superposed oscillations than the curves for the shorter tubes. The measured results from the 5-m tube will therefore be treated first of all.

The following observation should be made concerning the pressures measured. If the pressure curve recorded with the P-gauge for point E (the end of the tube) in Fig. 76 is compared with, for example, curve *b* in Fig. 78, which applies for exactly the same conditions, excepting that it has been recorded with an SP-gauge, it will be found that the pressures in Fig. 78 are by no means insignificantly higher than in Fig. 76. Since there is nothing to indicate that the actual pressures should differ

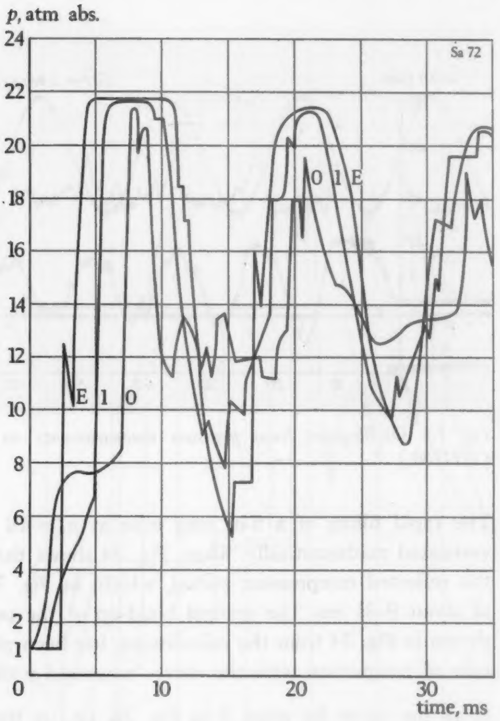

E, 0, 1 Measuring points

Fig. 72. Pressure as function of time when measured with P-gauge at various points in arrangement 6 (p_n = 16 atm abs.).

significantly from one another in both these cases, it can be reasonably suspected that there is some shortcoming in the recording of the pressures. An investigation has shown that the reason for this can probably be attributed to the amplifier of the P-gauge, which with the circuit used and at the high maximum pressures obtained when operating with bursting diaphragms has operated in the vicinity of its limiting capacity. This has consequently resulted in the pressure indication becoming unreliable. On one occasion it was found that the limiting pressure of the amplifier lies at about 24 atm abs., but this pressure appears to have varied for different tests. Thus, pressures exceeding 26 atm abs. (Fig. 74) were recorded on the 3-m tube with the same measuring arrangement. Measurements performed with the M-gauge on the 5-m tube (Fig. 77) have also resulted in a maximum pressure of about 26 atm abs. These measurements have given values which lie close to those obtained with the SP-gauge, which latter must be considered as being rather reliable because of the relatively low amplification in conjunction with the large diaphragm of the gauge. It thus appears rather certain that the maximum pressures in Fig. 76 in fact have been higher than is apparent from the curves. This is of no importance, however, for determining front velocities, but must naturally be taken into consideration when investigating the pressures and making a comparison with their theoretical values.

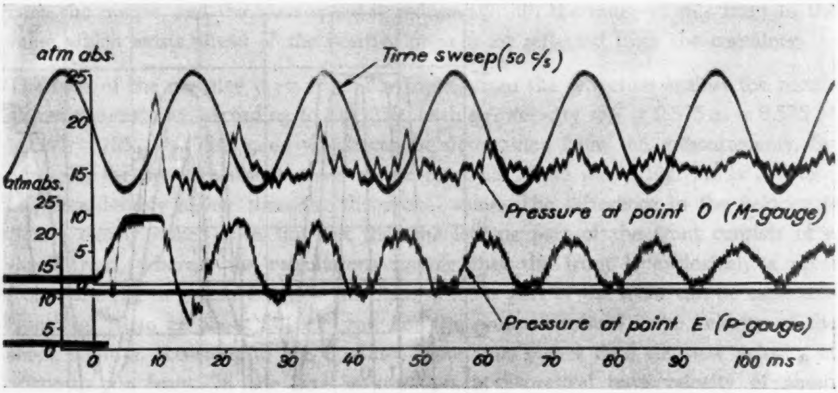

Fig. 73. Oscillogram from pressure measurements on arrangement 6 ($p_n = 16$ atm abs.). (Z 11780.)

The rapid filling of a 5-m long tube at $p_n = 16$ atm abs. has previously been investigated mathematically. Thus, Fig. 34 shows the different pressure changes during the reflected compression period, which, in Fig. 76, extends over the time interval of about 9–31 ms. The gradual build-up of the pressure at the end of the tube, as shown in Fig. 34 from the calculations, has been plotted in Fig. 78 (curve *d*) for the sake of comparison with the curves measured with the SP-gauge at point E.

From the curve for point 0 in Fig. 76, i.e., at the inlet of the tube from the container, it can be seen that the pressure rises here within about 2 ms to the static flow pressure of about 9 atm abs. The same pressure has been obtained when measuring with the M-gauge (Fig. 77), although the time for the pressure rise in this case is nearly 3 ms. According to the table on page 88, if the feeding air is stationary, it takes 1.8 ms with the M-gauge and 0.8 ms with the P-gauge for the space in the respective gauges to be filled to the pressure of 10 atm abs. The times for filling to the pressure of 9 atm abs. will be practically the same. If these times are increased by 0.35 ms to allow for the bursting of the diaphragms and the delay in the oscillograph element, values of 2.15 ms and 1.15 ms, respectively, will be obtained. These times apply, however, to air at rest. In the cases in question, air flows past the inlet hole of the gauge on a level with the hole and must consequently be deflected by 90° in order to enter the gauge space. Consequently, the volume of air flowing through the measuring hole per unit of time will be reduced, and the pressure in the gauge rises more slowly than for stationary air, which probably explains why slightly longer times have been obtained for the pressure rise with the experiments than with the calculations. A more rapid recording speed has been achieved when measuring the reflected shock front. This is natural, since the filling of the gauge space for measuring this front takes place with air which is practically at rest.

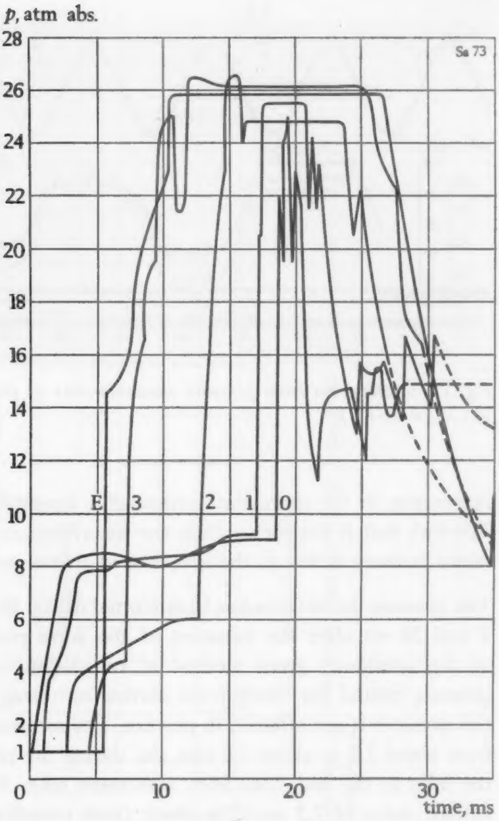

E, 0–3 Measuring points

Fig. 74. Pressure as function of time when measured with P-gauge at various points in arrangement 7 ($p_n = 16$ atm abs.).

The pressure distributions along the 5-m tube have been plotted for every 2 ms in Fig. 80 on the basis of the curves in Fig. 76, thus enabling the propagation of the pressure fronts to be followed. The measuring points are not located sufficiently close to one another to enable a complete picture of the propagation of the higher pressures to be obtained, and consequently the pressure curves in Fig. 80 have only been partly drawn in the range exceeding about 20 atm abs. During the first movement of the front outwards and backwards the static pressure at the inlet remains more or less constant at the value of 9 atm abs., which is about 0.56 times the original container pressure of 16 atm abs. The theoretical value is 0.53 × 16 atm abs. = 8.5 atm abs. After 31 ms, when the negative shock front has returned to the container, the pressure in this has dropped to 14.3 atm abs. (cf. curve R in Fig. 76). The static flow pressure at the inlet of the tube after this time is 9/14.3 = 0.63 times the container pressure. It thus does not drop, as might have been expected, in proportion to the container pressure, but displays a relatively speaking rising, supercritical value. The value of 0.56 times the container pressure is roughly that value obtained

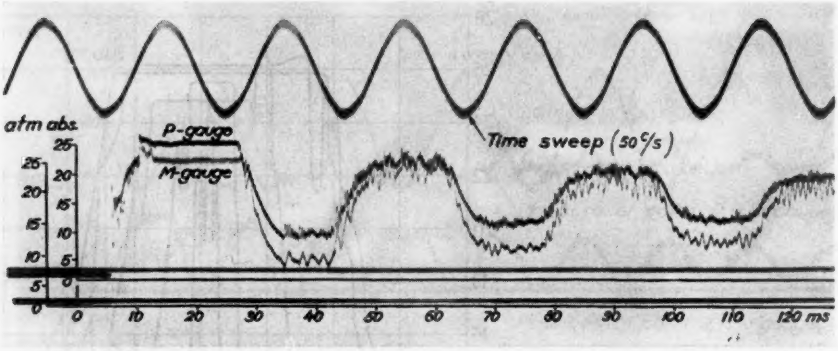

Fig. 75. Oscillogram from pressure measurements at point E in arrangement 7 ($p_n = 16$ atm abs.). (Z 11781.)

in practice in the narrowest section of a simple nozzle fed from a large container. The fact that it lies higher than the theoretical, critical value of 0.53 times the container pressure is due to the influence of friction in the nozzle.

The pressure distribution has been plotted in Fig. 80 in the form of chain-dotted curves 2 and 20 ms after the initiation of the wave phenomenon, as it will be according to the previously given method of calculation (cf. also Fig. 34). The theoretical pressure behind the shock front moving outwards is 4.6 atm abs. Owing to friction this pressure is not attained in practice. The measurements show that it rises gradually from about 2.5 to about 3.5 atm abs. during the propagation of the shock front from the inlet to the end. This front movement takes 8.8 ms in comparison with the calculated value of 7.3 ms. The shock front travelling outwards is naturally in reality vertical and not sloping as shown in Fig. 80. The inclination is due to the delay in the recording of the pressures. The pressure distribution from 2 to 30 ms shows how the negative expansion front travelling outwards develops from the inlet. As can be seen, the pressures within this front are slightly higher than the estimated values, but the propagation of the front corresponds otherwise rather well with what can be derived theoretically. The higher pressures can apparently be attributed to friction in the tube, which has a damming-up effect. The propagation of the compression front reflected from the end of the tube is represented by the pressure distributions for the interval 10–30 ms. The leading part of this front is a negative shock front. This is joined by a front which has more or less the characteristics of a negative press front and which during its propagation towards the inlet of the tube is converted into a shock front. After 30 ms the reflected front constitutes practically speaking a pure shock front.

The rather complicated picture of superposed fronts which, according to the theory, arise due to repeated reflections against the boundary layer between the original air

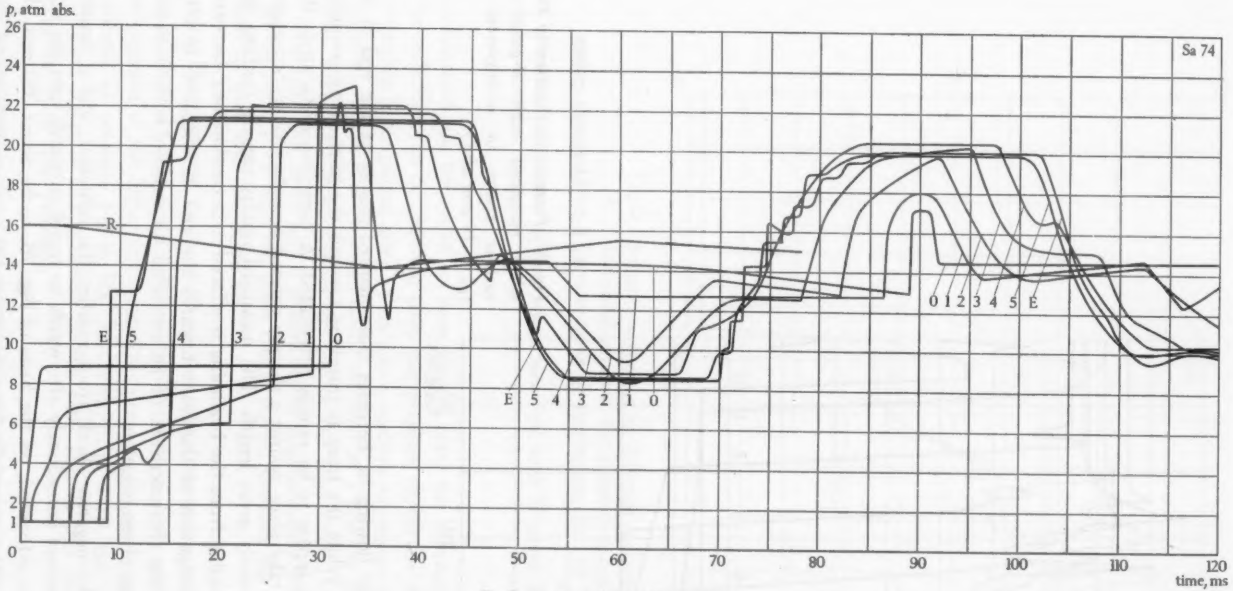

E, R, 0–5 Measuring points

Fig. 76. Pressure as a function of time when measured with P-gauge at various points in arrangement 8 ($p_n = 16$ atm abs.).

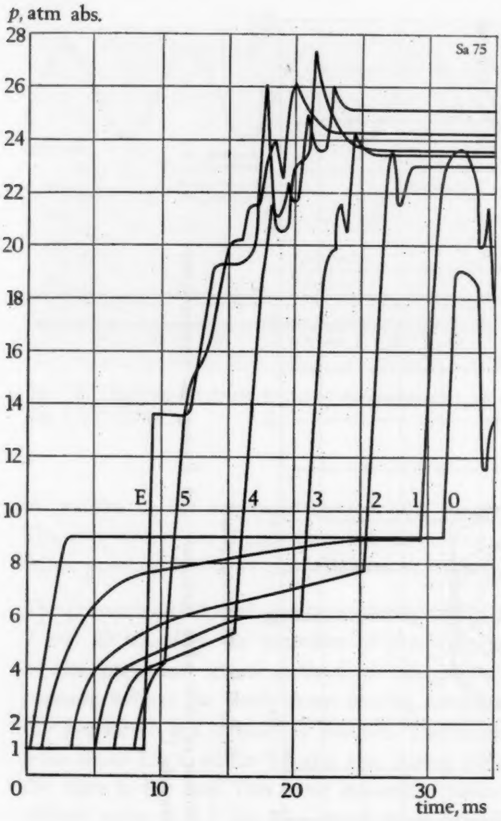

E, 0–5 Measuring points

Fig. 77. Pressure as function of time when measured with M-gauge at various points in arrangement 8 (p_n = 16 atm abs.).

in the tube and the air flowing in, becomes more marked mainly at the end of the tube during the tests. While the front is travelling towards the inlet, these secondary oscillatory phenomena appear to be rapidly attenuated. A contributory factor is that the reflections do not take place against a sharply defined boundary layer, but against an air column of relatively great length. The measured results namely confirm that the boundary layer existing from the beginning is effaced to a continuously increasing degree during the propagation of the front towards the end of the duct. In other words, it has finally the characteristics of an extended air column with decreasing density in the direction of propagation.

After about 31 ms the negative shock front reaches the container, and a negative expansion front commences immediately afterwards to travel outwards into the tube. Its top velocity can be calculated, on the basis of Fig. 76, to be about 380 m/s, that is to say, it does not differ essentially from the estimated mean acoustic speed given in Fig. 34h. The reflection of the negative expansion front against the end of the

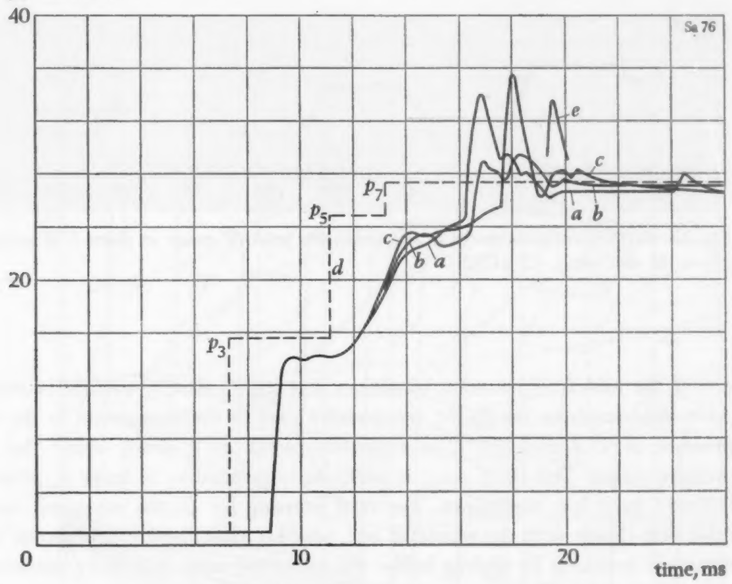

a–c Pressure according to different measurements
d Estimated pressure for frictionless conditions
e Pressure peak of oscillogram, Fig. 79

Fig. 78. Pressure as function of time when measured with SP-gauge at point E in arrangement 8 (p_n = 16 atm abs.).

tube commences just before 46 ms have elapsed after the bursting of the diaphragms, and the reflection can be followed from the pressure curves for 46–54 ms in Fig. 80. The reflection is completed after 54 ms and a positive expansion front moves towards the container, where it is reflected 60–62 ms later in a positive press front travelling outwards. This latter front reaches the end of the tube after 70 ms and then starts to be reflected. This reflection is completed at approximately 80 ms and the front, now in the form of a negative press front, travels towards the container, reaching this with its base after about 88 ms.

The static flow pressure at the inlet of the tube (measuring point 0) according to Fig. 76 is about 14 atm abs. for the stationary state of flow prevailing there during the propagation of the expansion front. This pressure has previously been determined theoretically as pressure p_{10} in Fig. 31. With $p_n/p_0 = 16$, the curve for p_{10}/p_0 in Fig. 32 gives $p_{10}/p_0 = 12.8$. Friction in the tube also in this case appears to have increased the static flow pressure.

The above-mentioned reflections against the boundary layer appear most clearly in the curves in Fig. 78, where the broken line d denotes the estimated pressures at the

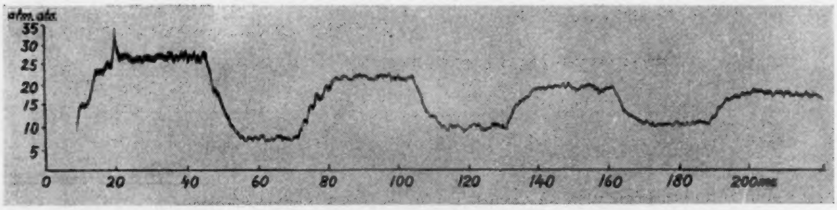

Fig. 79. Oscillogram from pressure measurements with SP-gauge at point E in arrangement 8 (p_n = 16 atm abs.). (Z 11782.)

end of the tube for frictionless conditions and with a sharply defined boundary layer. As is apparent from the figure, the pressure rises in three stages up to the maximum pressure of 27.3 atm abs. The measured curves *a* – *c* clearly show the first two pressure stages. The third stage is particularly noticeable in curve *b*, although it is followed by a few oscillations. The final pressure for all the measured curves coincides very closely with the estimated one, whereas after the first and second stages the measured pressures lie slightly below the estimated ones. The three measured curves coincide first of all, but spread out during the second pressure stage. When the oscillations have been attenuated after the third pressure stage, the measured curves coincide once again almost completely. The slope of the measured curves during the second pressure step, i.e., between about 14 and 23 atm abs., seems to indicate that the boundary layer in the tube is no longer limited to one plane but extends along the tube, since the curves show that the front reflected from the boundary layer is not a shock front but a front having the characteristics of a press front. This front has clearly developed as a result of the shock front reflected from the end of the tube being reflected gradually inwards into the limiting air column. The curves *a* and *c* display during the third pressure stage brief pressure shocks of up to 35 atm abs. It is not quite clear whether these pressure peaks are derived from the collision of the crumpled-up diaphragms with the diaphragm of the pressure-measuring device or whether they are caused by self-ignition of finely distributed oil accompanying the air from the compressor plant. The fact that such ignition really did occur during the experiments is beyond doubt, for in several cases both smoke and the smell of burnt oil were observed when the tube was opened after the experiments.

When comparing the pressure curves for the 1, 3, and 5, m tubes, it is found that the pressure changes possess the same main characteristics for these three tube lengths. They differ nevertheless from one another in certain respects. It is thus interesting to note that in the 1-m tube (Fig. 72) the second press front travelling outwards is reflected from the tube end as a pronounced shock front in the same way as the first press front travelling outwards. The third front of the same nature has, on the other hand, a clearly continuous characteristic also after the reflection. With the

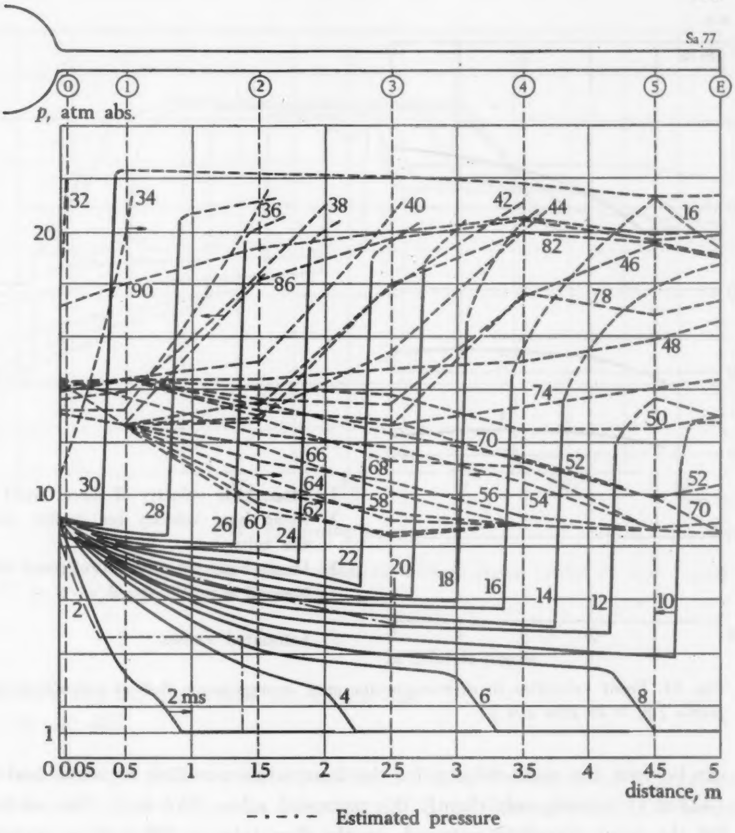

Fig. 80. Pressure distribution along the tube in arrangement 8 as calculated from the curves of Fig. 76.

3-m tube it is possible to detect from the oscillogram in Fig. 75 a build-up of the pressure at the end of the tube in several stages during the reflection against the end of the second press front travelling outwards. This is also the case with the 5-m tube, as the curves in Fig. 76 show, although the number of pressure stages has increased here. It appears as if a strongly delineated boundary layer has been formed near the end of the tube in conjunction with the second compression front travelling outwards.

Fig. 81 shows the mean front velocities which it has been possible to determine on the basis of the experimental results with 1, 3, and 5, m tubes. The values indicated by the circles denote those obtained for the 5-m tube according to the theory. As

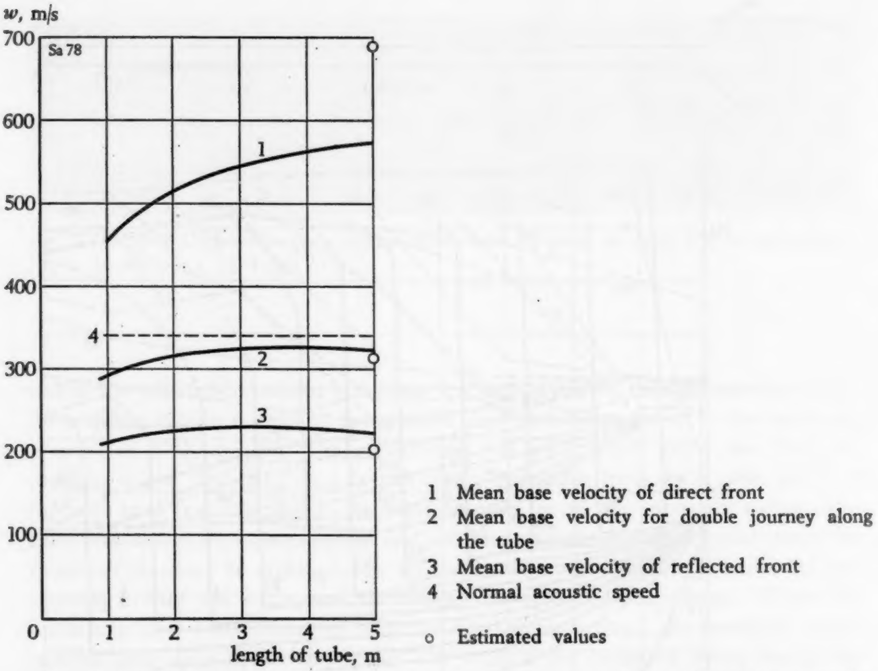

Fig. 81. Front velocities in diaphragm-operated arrangements 6–8 as calculated from oscillograms ($p_n = 16$ atm abs.).

can be seen, the mean velocity for the front when travelling forwards and back again (322 m/s) exceeds only slightly the estimated value (313 m/s). The measured value for the front travelling outwards in the 5-m tube is 570 m/s as opposed to the estimated value of 690 m/s, and the measured value for the reflected front 225 m/s as opposed to the estimated value of 203 m/s. These results appear quite natural when taking into consideration friction in the tube. The flow velocity behind the front travelling outwards is high, which results in large friction losses, that is to say, heating up of the air at the expense of its static and dynamic energy contents. As can be seen from Fig. 80, the pressure is reduced within the shock front, which from the theory should have the value of 4.6 atm abs. If the mean value of the velocity of the outgoing shock front is taken to be 570 m/s and if an initial acoustic speed of 340 m/s is assumed, i.e., the speed ratio 1.67, this will correspond according to the curves in Fig. 8 to a ratio between the pressures ahead of and behind the shock front of 3.1. This value agrees well with the mean value which can be derived from the curves in Fig. 80. After being reflected against the closed end of the tube, the negative shock front travels in air having a higher temperature than according to the theory, which may explain why its velocity is slightly higher than the theoretical value.

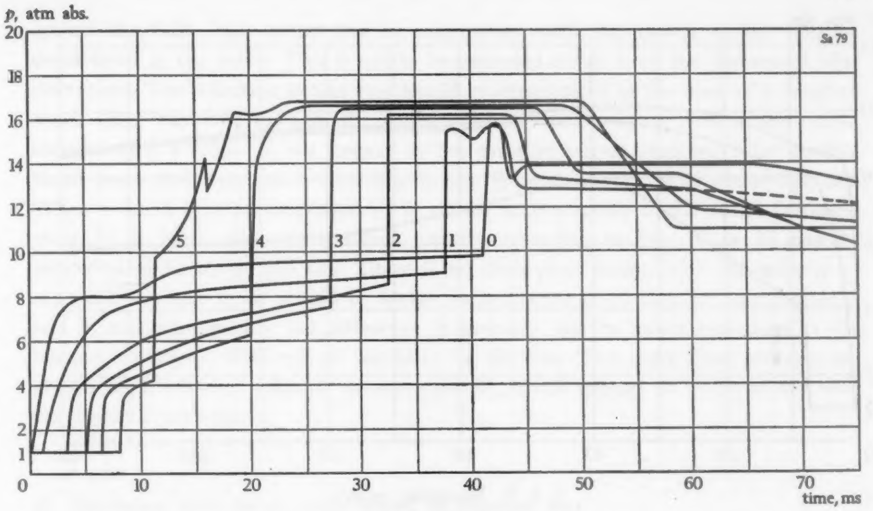

0–5 Measuring points

Fig. 82. Pressure as function of time when measured with M-gauge (point 0) and P-gauge (points 1–5) in arrangement 9 ($p_n = 16$ atm abs.).

Arrangements 9 and 10: Tube open at exterior end
(Figs. 36, 48 and 49)

The difference between these two arrangements is that in the one case the tube has a nozzle at the outer end with a min. diameter of 52.5 mm (arrangement 9), whereas in the other case the tube opens out direct into the atmosphere (arrangement 10).

Pressure curves from measurements on arrangement 9 are reproduced in Fig. 82. A partial reflection takes place here against the nozzle, when the outgoing shock front reaches the end of the tube. After the reflection, the pressures cannot attain such high values as for a closed tube. In addition, the velocity of the reflected front becomes lower, since the air behind the front does not remain at rest, but moves with a certain speed towards the outlet. The conditions can be determined on the basis of Eqs. (36), (65) and (104), if the initial stage is ignored when the boundary layer is still in the tube. It will then be found that the velocity of the front reflected from the nozzle will be 120 m/s for a container pressure of 16 atm abs. and a nozzle area of 0.43 times the tube area. The initial state ahead of this front can be found, for example, from Fig. 34 and is:

static pressure = 4.6 atm abs.
mass speed towards the front = 435 m/s
acoustic speed = 285 m/s

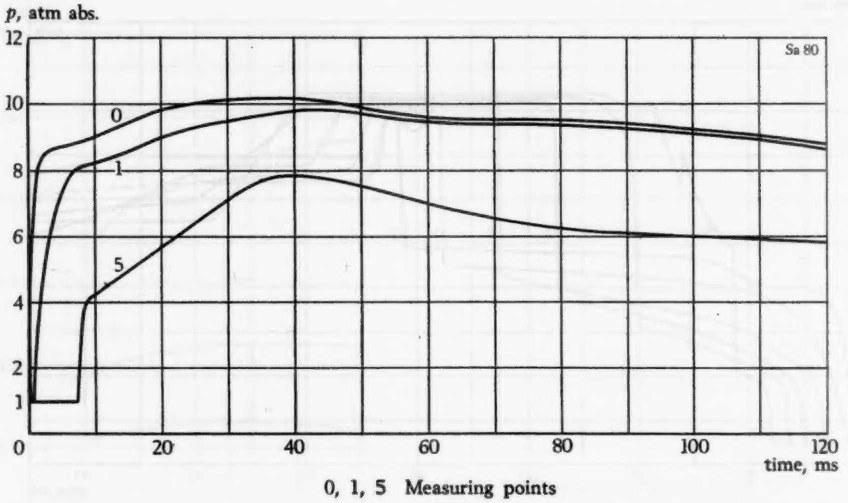

Fig. 83. Pressure as function of time when measured with P-gauge at various points in arrangement 10 (p_n = 16 atm abs.).

The calculations give the following values for the state behind the front:

static pressure = 19.5 atm abs.
mass speed towards the nozzle = 95.5 m/s
acoustic speed = 367 m/s

The values determined previously for the tube closed at the end will now be given for the sake of comparison:

static pressure behind the front = 27.3 atm abs.
front velocity = 213 m/s

Fig. 82 shows that the mean velocity of the reflected shock front will be 148 m/s, i.e., rather higher than the estimated value of 120 m/s, which can probably be attributed mainly to the fact that the air ahead of the front has a higher temperature due to friction than that assumed in the calculations. The pressure measured behind the front has, on the average, an approximate value of 16.5 atm abs. as opposed to 19.5 atm abs. The top velocity of the outgoing expansion front following on after the negative shock front has arrived at the container is, according to Fig. 82, about 560 m/s. In the case of frictionless conditions, this velocity would have a theoretical value of 95.5 + 367 = 462.5 m/s, i.e., the sum of the mass speed and the acoustic speed behind the negative shock front. In reality it is thus about 20 per cent higher, which can be attributed to the increase in temperature of the air due to friction.

Pressure curves from corresponding measurements on arrangement 10 are reproduced in Fig. 83. It is not possible to detect in the pressure curves any influence of reflection against the fully open outlet end in conjunction with the arrival of the positive shock front at the outlet. This is not to be expected either from the theoretical considerations. The reflection in this case would be experienced in the form of a negative shock front travelling towards the container, but rapid pressure rises which would indicate such a front do not appear in the pressure curves recorded. The positive shock front moves outwards according to Fig. 83 with a velocity of about 600 m/s. When a closed tube (arrangement 8) or a tube with a nozzle in the outlet (arrangement 9) is filled, the corresponding velocity according to Fig. 76 or 82 can be estimated to be about 560 m/s. There is no theoretical reason why the velocity of the positive shock front should be higher in arrangement 10 than in arrangement 8 and 9, and consequently the difference is probably due to minor variations in the friction conditions, different air humidity, or the like. The static flow pressure too attains slightly higher values in arrangement 10, which appears to be associated with the higher front velocity.

II. Operation with valve, tube closed at exterior end

Arrangements 11–14: 3" tubes
(Figs. 37 and 50a)

As is apparent from Fig. 37, these four arrangements differ from one another only in their tube length, which is 3, 5, 8 and 11 m, respectively. The pressure curves for arrangements 11 and 12 have been recorded at four different initial pressures in the container, namely 6, 8, 12 and 16 atm abs. The curves for arrangements 13 and 14 were recorded at the initial pressures of 8, 12 and 16 atm abs. For reasons of space, a suitable selection has had to be made when plotting the pressure changes. Thus, Fig. 84 shows the pressures at all the measuring points in the 3-m tube at the initial pressures of 6 and 16 atm abs., and Fig. 85 all the pressures for the 5-m tube at an initial pressure of 16 atm abs. Fig. 87 shows the pressures at the end of the tube of all the arrangements and at all the initial pressures employed. In every case the pressures have been recorded by means of M-gauges.

In order to get an idea of how the conditions vary when opening a valve in comparison with opening by means of bursting diaphragms, Figs. 77 and 85 can be suitably studied. These both refer to a tube of 5 m, an initial pressure of 16 atm abs. and measurement with an M-gauge. Fig. 77 concerns opening by means of bursting diaphragms and Fig. 85 opening by means of a valve. When a valve opens, 13.4 ms elapse before the base of the outgoing front reaches the end of the tube as opposed to 8.8 ms for opening with bursting diaphragms. This is associated with the fact that in the latter case a shock front is formed almost immediately after the diaphragms have burst and such a front travels with a considerable supersonic velocity. Its mean velocity amounts to about 570 m/s for a travelling time of 8.8 ms along a tube of 5 m, i.e., 1.67 times the normal acoustic speed of 340 m/s. This is equivalent, in

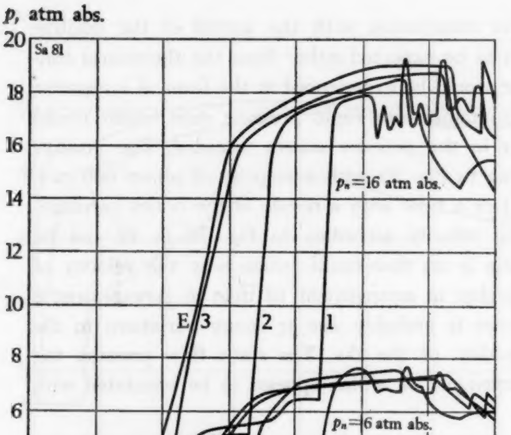

E, 1–3 Measuring points

Fig. 84. Pressure as function of time when measured with M-gauge at various points in arrangement 11 (p_n = 6 and 16 atm abs.).

Fig. 8, to a pressure within the front of about 3.1 atm abs., which corresponds approximately to the mean pressure in Fig. 77. When a valve opens, a relatively well extended press front is formed, which is joined by a negative expansion front with its top at the inlet. The top of the press front, which coincides with the base of the expansion front, can, according to Fig. 85, have a static pressure of about 3.5 atm abs. when approaching the closed end of the tube. This is roughly the same pressure as that shown in Fig. 80 at the top of the positive shock front on the arrangement with bursting diaphragms. The following table contains a comparison of the measured results in Fig. 85 and the calculated results in Fig. 8 concerning the front velocity of the positive press front at different pressures and for a tube length between measuring points 0 and 5 of 4.45 m.

Static pressure p atm abs.	Travelling time between points 0 and 5 ms	Front velocity w m/s	Relative front velocity $w/340$	According to Fig. 8:	
				Pressure at $w/340$ atm abs.	Relative front velocity at pressure p
1.0	11.7	380	1.12	1.1	1.0
1.5	9.6	463	1.36	1.5	1.36
2.0	8.0	557	1.63	2.0	1.63
2.5	6.8	655	1.92	2.7	1.85
3.0	6.0	743	2.18	3.5	2.0
3.5	5.6	795	2.34	4.1	2.17

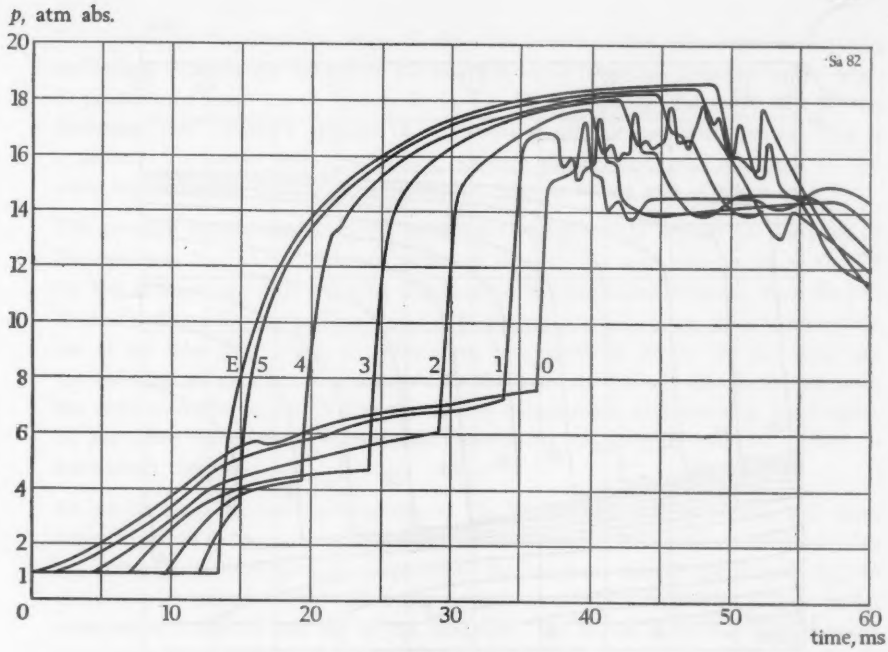

E, 0–5 Measuring points

Fig. 85. Pressure as function of time when measured with M-gauge at various points in arrangement 12 (p_n= 16 atm abs.).

As is apparent, there is full agreement between theory and measurements at the pressures 1.5 and 2.0 atm abs., whereas the measured velocity of the following parts of the front is slightly higher and the corresponding pressure slightly lower than according to the calculations for loss-free conditions. The differences point direct to the influence of friction, which causes a drop in the pressure and heating of the air, leading consequently to an increase in its acoustic speed. If this increase alone is the reason for the higher front velocity, or if an increase in the mass speed occurs as well, cannot be determined direct on the basis of the measured results. As can be seen from the table, the front velocity at $p = 1$ atm abs. is higher than the normal acoustic speed, namely 380 m/s as opposed to 340 m/s. This indicates that the front is converted to a certain extent into a shock front in its leading part during the propagation, because a pure press front would have a front velocity at the base exactly equal to the acoustic speed of the air lying ahead, since this is at rest. A front velocity of 380 m/s occurs with a shock front having a top pressure of about 1.1 atm abs., which is only about 10 per cent higher than atmospheric pressure and thus is not very easy to distinguish in the oscillograms.

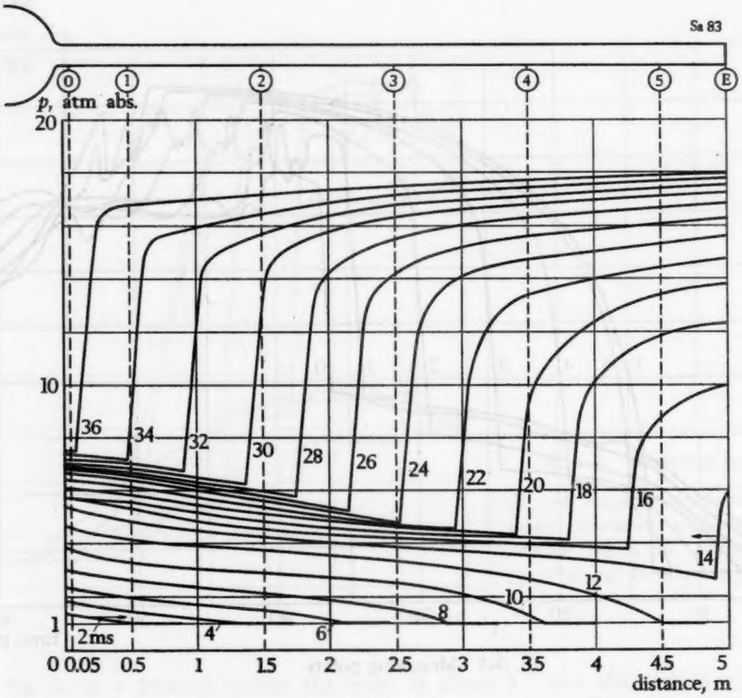

Fig. 86. Pressure distribution along the tube in arrangement 12 as calculated from the curves of Fig. 85.

The front velocity at pressures exceeding 3.5 atm abs. displays, on the other hand, falling values, from which it can be concluded that the expansion front takes over at approximately this pressure. The front velocity is, for instance (Fig. 85), 627 m/s at 4 atm abs., 234 m/s at 5 atm abs., and 161 m/s at 6 atm abs. Relative to the front point 3.5 atm abs., point 4 atm abs. moves within the expansion front towards the container with the velocity 168 m/s, point 5 atm abs. with 561 m/s and point 6 atm abs. with 634 m/s. The relative front velocity within the negative expansion front should rise theoretically only to the critical flow velocity of 311 m/s at the inlet of the tube. The high values obtained with the measurements are probably due to the fact that the air when flowing through the valve arrangement is heated up considerably due to friction.

A negative shock front is formed after the reflection against the end of the tube, and this front does not attain such high top pressures as for opening with bursting diaphragms (cf. Fig. 77). Its mean velocity during the propagation towards the container is, however, very close to that for opening with bursting diaphragms.

As a result of the irregular shape of the duct ahead of the tube inlet, superposed oscillations occur in the flow after the negative shock front has returned to the inlet. A pronounced wave top is noticeable in Fig. 85 and during the movement of the discharge front outwards appears in succession at all the measuring points. This is a matter of a partial reflection of the negative shock front, and the front of the wave top maintains its shock characteristics right up to the end of the tube.

The pressure distribution along the tube has been plotted in Fig. 86 on the basis of the curves in Fig. 85 for different points of time in the same manner as in Fig. 80 for the arrangement with bursting diaphragms. A comparison between Figs. 80 and 86 clearly shows the higher flow losses with the valve arrangement, since the pressure rise at the tube inlet (point 0) takes place here relatively slowly. By the time that the reflected shock front has returned to the inlet after about 36 ms the pressure has risen gradually up to 7.5 atm abs. In the arrangement with bursting diaphragms, on the other hand, the pressure rises immediately to about 9 atm abs., which is maintained thereafter.

As can be seen, the wave propagation in Fig. 86 forwards and backwards also takes longer time, and the maximum pressures lie considerably below those obtained with the arrangement with bursting diaphragms. As has been already mentioned, Fig. 84 concerns measurements made on a test arrangement with a tube 3 m long at initial pressures of 6 and 16 atm abs. in the container. The curves show that the first outgoing press front with an initial pressure of 6 atm abs. is a pure press front without any shock front forming on its leading part. Its base moves namely with the normal acoustic speed of about 340 m/s. The conditions are quite different for an initial pressure of 16 atm abs., where the formation of a shock front clearly takes place while the front travels towards the end of the tube. The mean velocity of the front base is about 380 m/s with the initial pressure of 16 atm abs. The conditions can be seen most clearly in the pressure curves for point E (end of the tube), which show that the outgoing front with the initial pressure of 6 atm abs. is still a press front after the reflection, whereas the outgoing front with the initial pressure of 16 atm abs. has been reflected in its leading part as a shock front with a top pressure of about 3 atm abs.

The press front with the initial pressure of 6 atm abs. arriving at the end of the tube, remains a press front also after the reflection. From the pressure curves in Fig. 84 it can be found that before the reflection this press front has a static top pressure near the end of the tube of about 2.8 atm abs. and after the reflection a top pressure of about 6.8 atm abs. The ratio between these pressures is very nearly the same as according to the estimated curves in Fig. 17 for reflection against a rigid wall. The ratio between the pressures before and after the reflection at the end of the tube for the initial pressure of 16 atm abs. is also very close to the estimated value shown in Fig. 17.

The pressure changes at the end of the tube for all tube lengths and for all initial

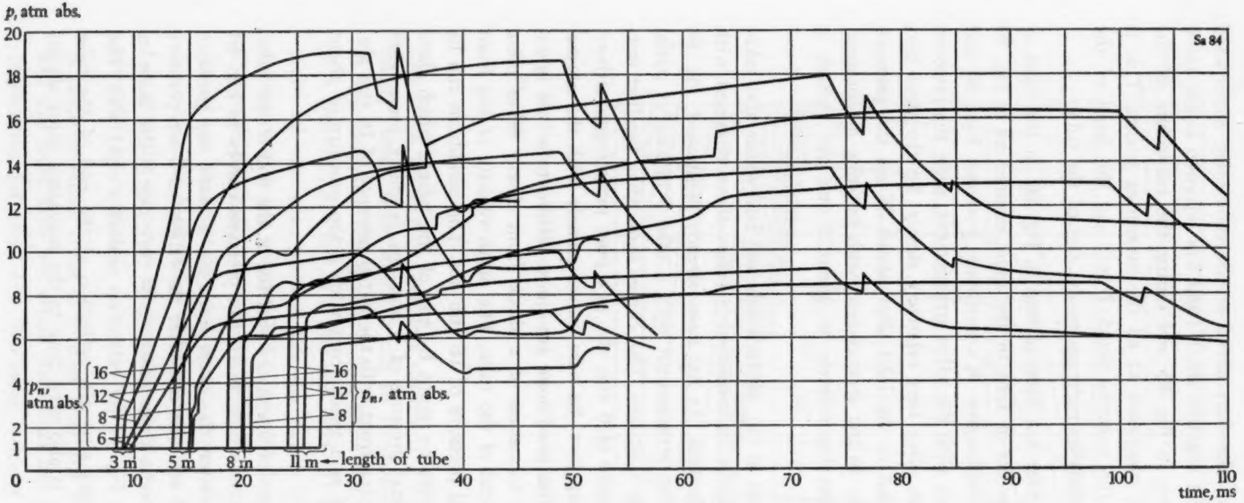

Fig. 87. Pressure as function of time when measured with M-gauge at point E in arrangements 11–14 ($p_n = 6, 8, 12$ and 16 atm abs.).

pressures are reproduced in Fig. 87. It can be seen from these curves that the outgoing front, i.e., the positive press front resulting from the opening of the valve, only arrives at the end of the tube as a pure press front in the 3-m tube and at the lowest initial pressures of 6 and 8 atm abs. In all the other cases, the tube length is so great or the pressure so high that the leading part of the press front starts being converted into a shock front while travelling towards the end of the tube. This is apparent from the sudden increase in pressure at the beginning of the curves. The pressure rises just after the reflection of the shock front, as can be seen, both with the initial pressure and with the tube length. Another factor apparent from the curves is that the maximum pressure obtained with the same initial pressure decreases with increasing tube length, this being due to the increasing losses. The superposed shock front which occurs in every case at the beginning of the discharge front is caused, as mentioned above, by the design of the valve and its connection to the tube, which leads to a partial reflection of the negative shock front travelling towards the container.

Fig. 88 shows the mean velocities of the fronts which can be determined on the basis of the measurements.

Arrangements 15–17: 2″ tubes
(Figs. 38 and 50b)

No attempt has been made to plot pressure curves for these arrangements on the basis of the oscillograms, since the curves show in the main the same characteristics as those for 3″ tubes. It is true that the smaller tube diameter influences to a certain extent the propagation velocity of the fronts. The tube diameter exerts, however, a more pronounced influence on the pressure conditions within the front. A comparison between the velocities and pressures for the 3″ and 2″ tubes is given in Figs. 88 and 89. The front velocities in Fig. 88 are shown as a function of the tube length and for different initial pressures in the container. The velocity of the outgoing front increases both with the pressure and with the tube length. As a rule, it is slightly lower for the 2″ tubes. The velocity of the reflected front decreases slightly with increasing pressure. The velocity curve has a relatively flat maximum for a tube length of about 8 m. The velocity of the outgoing front is considerably lower than for the arrangements with bursting diaphragms (cf. Fig. 81).

A comparison has been made in Fig. 89 between the pressure changes at the instant when the reflected shock front reaches the measuring point 0. Here, p_1 denotes the value to which the container pressure has dropped at this instant. The pressure p_2 ahead of the front is, as can be seen from the curves for p_2/p_1, substantially higher for the 2″ tubes than for the 3″ tubes. This implies that the valve arrangement has a throttling effect. This effect will naturally be more pronounced, the greater the area of the tube which is connected to the valve. As far as the pressure behind the

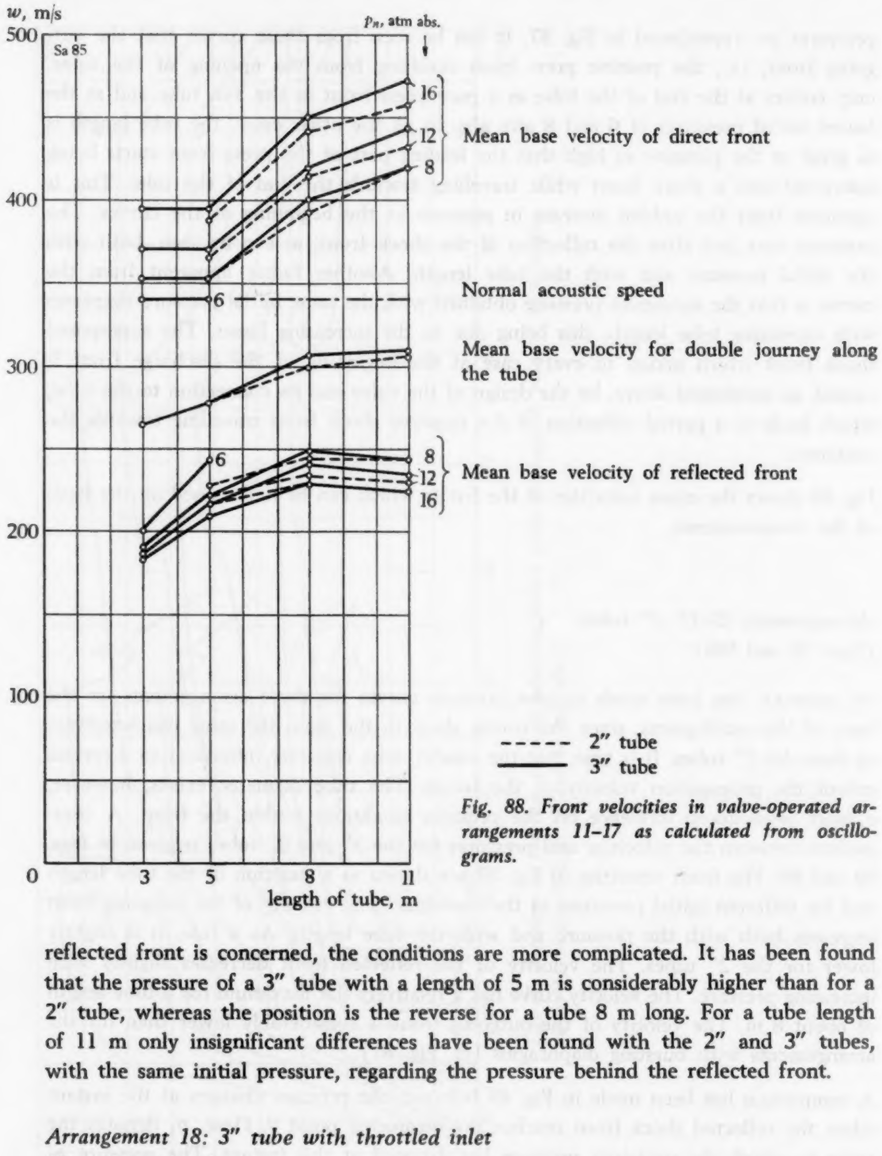

Fig. 88. Front velocities in valve-operated arrangements 11–17 as calculated from oscillograms.

reflected front is concerned, the conditions are more complicated. It has been found that the pressure of a 3" tube with a length of 5 m is considerably higher than for a 2" tube, whereas the position is the reverse for a tube 8 m long. For a tube length of 11 m only insignificant differences have been found with the 2" and 3" tubes, with the same initial pressure, regarding the pressure behind the reflected front.

Arrangement 18: 3" tube with throttled inlet
(Figs. 39 and 51)

A 2" diverging nozzle forms here the inflow opening from the valve to the 5-m long 3" tube. The pressure changes at the different measuring points and at an initial pressure of 16 atm abs. in the container are shown in Fig. 90. The pressure distribu-

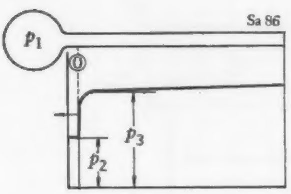

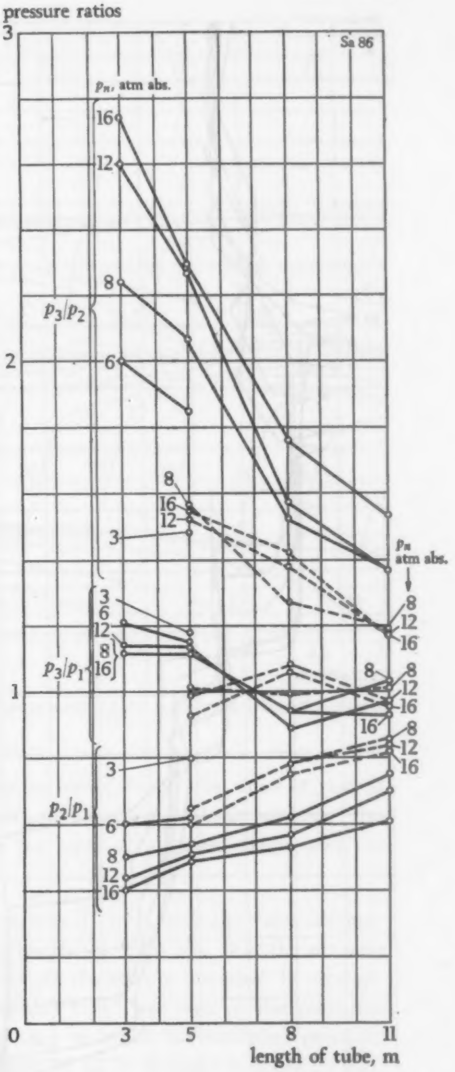

----- 2″ tube
——— 3″ tube

Fig. 89. Pressure ratios of reflected fronts at point 0 in valve-operated arrangements 11–17 as calculated from oscillograms.

tion along the tube at intervals of 2 ms has been plotted in Fig. 91 on the basis of these pressures. It is apparent from the curves that the diverging nozzle brings about a flow with supersonic speed in the beginning of the tube. Except for the initial stage, the pressure at point 1 remains all the time at the relatively low value of about 2 atm abs. until the reflected front has returned to the measuring point. A transition to a flow with lower velocity takes place along the stretch between points 1 and 2. This can be attributed to the circumstance that the static flow pres-

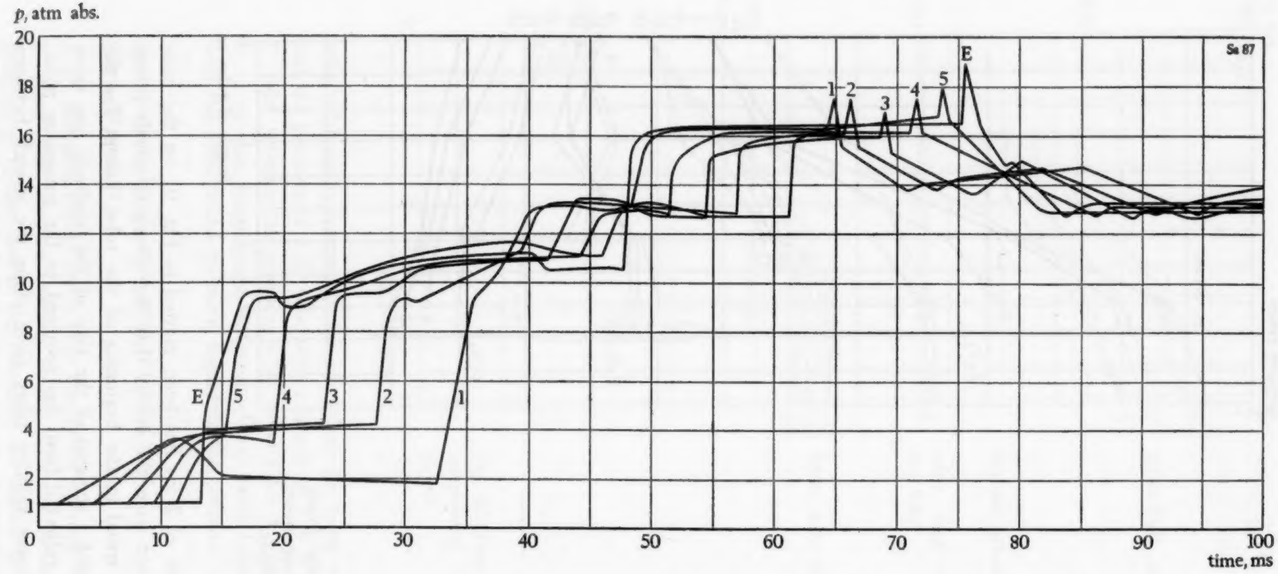

E, 1–5 Measuring points

Fig. 90. Pressure as function of time when measured with M-gauge at various points in arrangement 18 ($p_n = 16$ atm abs.).

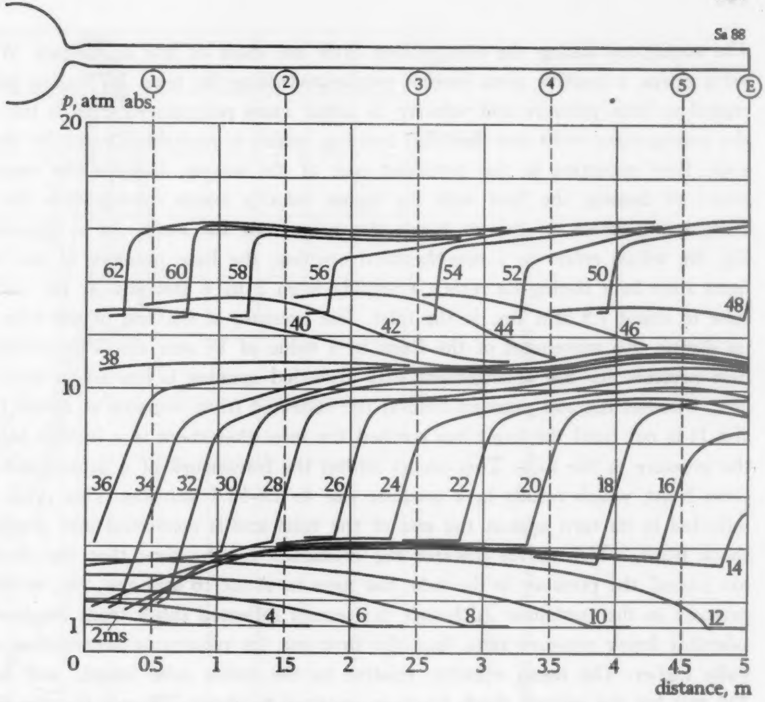

Fig. 91. Pressure distribution along the tube in arrangement 18 as calculated from the curves of Fig. 90.

sure at point 2 and the following ones amounts to about double the value of that at point 1. It does not appear possible to draw any conclusion about whether this transition occurs suddenly, that is to say, in the form of a shock compression, or continuously.

A comparison with Figs. 85 and 86 for the 5-m long 3" tube with the valve arrangement without any throttling means after the valve shows, inter alia, that the pressure at the end of the tube is built up more slowly when the inlet is throttled. In arrangement 18 the throttled cross-sectional area amounts to 43 per cent of the cross-sectional area of the tube. It takes twice as long time to attain the container pressure, 16 atm abs., than with a non-throttled tube (about 50 ms as opposed to about 25 ms). The slower pressure rise at the end of the tube for arrangement 18 is associated with the fact that the tube is not charged here from one single direct and reflected compression cycle followed by an expansion cycle. Instead, the compression cycle takes place in two successive stages. During the first stage the tube is charged to about 2/3 of the container pressure, and during the second stage to approximately the full container pressure. The full pressure in the tube is thus not reached until the front has passed the tube four times, twice forwards and twice back again.

The conditions during the compression cycle are more or less as follows. When the valve opens, a positive press front is propagated along the tube. Its leading part, with regard to both pressure and velocity, is rather more pronounced than is the case for the arrangement with non-throttled opening, which is probably caused by the supersonic flow occurring in the extended part of the nozzle. Despite the considerably lower air density, the flow with the higher velocity exerts consequently the greater compressing effect on the air inside the tube from the start. As is apparent from Fig. 86, which refers to a non-throttled opening, the base pressure of the reflected front rises here during its return gradually from 3 to 4 atm abs. at the end of the tube to about 7.5 atm abs. at the inlet. The pressure at the end of the tube is built up during this movement of the front to a value of 18 atm abs. The corresponding base pressure for the arrangement with throttled opening is limited to about 4 atm abs., whereas the top pressure behind the reflected front remains at about 11.5 atm abs. It is not until the front has reached the inlet that there is a further increase in the pressure in the tube. This occurs within the framework of a superposed positive press front, which results in a pressure rise to 13–13.5 atm abs. This press front is reflected in its turn against the end of the tube and is converted into a superposed shock front, which moves towards the container. By the time that the shock front has passed, the pressure in the tube has risen to about 16 atm abs., i.e., to the initial pressure in the container. Although the second reflected shock front displays a considerably lower pressure ratio than the first one, its velocity is nevertheless substantially higher. The mean velocity, relative to the entire tube length, will be about 335 m/s for the second shock front as opposed to about 220 m/s for the first one. The reason for this difference in velocity is mainly to be found in the lower mass speed ahead of the second shock front, especially in the tube section up to about 1.5 m from the inlet. The first shock front encounters in this section air which partly flows with supersonic speed, and is thus retarded in its propagation. The velocity of the front is, on the average, about 170 m/s within this section. The air ahead of the second shock front hardly attains supersonic speed at any point; a contributory factor to this is that the difference between the container pressure and the tube pressure is probably not sufficient.

Arrangements 19 and 20: 3″ and 2″ tubes in succession
(Figs. 39, 50a, 52 and 53)

The oscillograms recorded with these two arrangements display only insignificant differences between one another. It has therefore been considered sufficient to plot curves for only one of these arrangements. The choice fell on arrangement 20, which is of greater interest for the comparison with arrangement 21 than is the case with arrangement 19.

Arrangement 20 comprises a 5-m long 3″ tube to which is coupled a 3-m long 2″ tube, where the transition between the tubes is formed by a converging nozzle with a

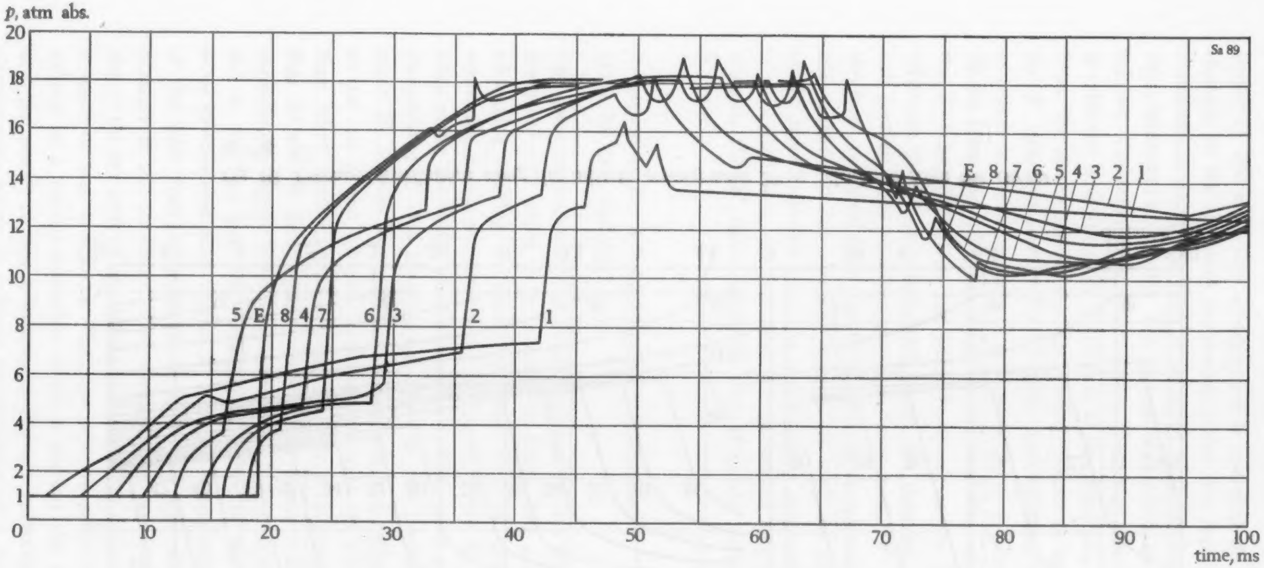

E, 1–8 Measuring points

Fig. 92. Pressure as function of time when measured with M-gauge at various points in arrangement 20 ($p_n = 16$ atm abs.).

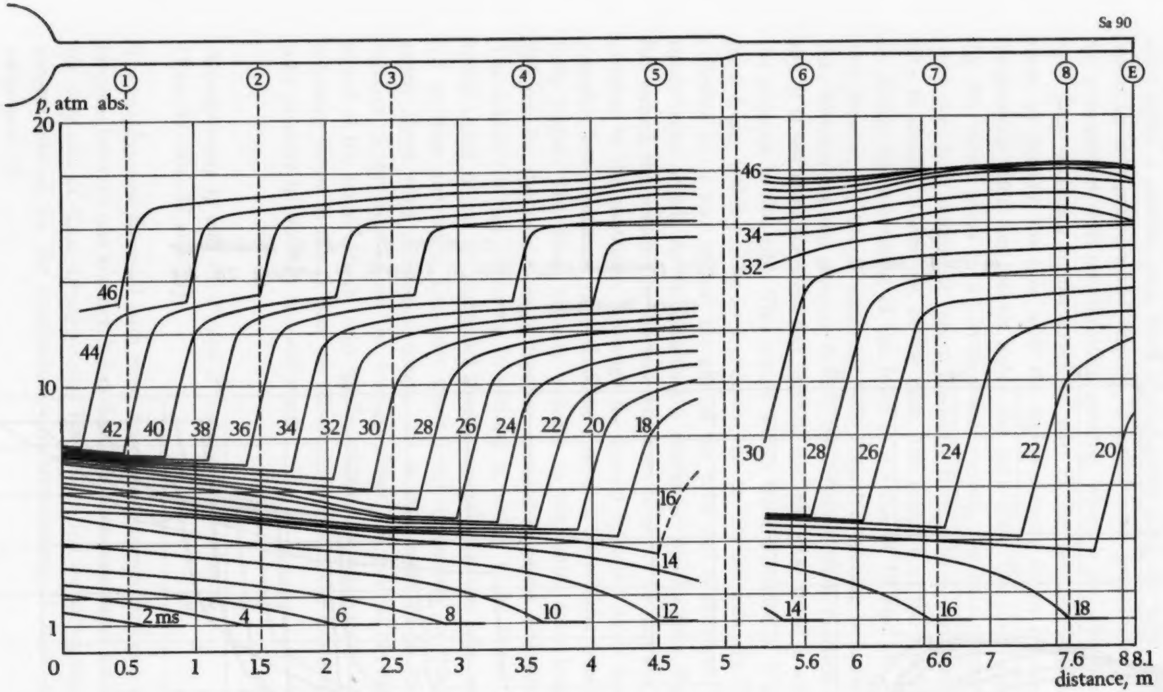

Fig. 93. Pressure distribution along the tube in arrangement 20 as calculated from the curves of Fig. 92.

length of 100 mm. This arrangement is operated by means of a valve. The pressure changes at the different measuring points are reproduced in Fig. 92. The pressure distributions along the duct at intervals of 2 ms have been plotted on the basis of these pressures in Fig. 93. The general characteristics of the wave propagation are as follows. The press front which rushes along the tube after the valve has been opened is reflected both from the restriction at the transition from the 3" to the 2" tube and from the closed end of the duct, which results in two negative shock fronts, one in the 3" tube and one in the 2" tube. Both of these shock fronts travel towards the container at the same time. One of these fronts is located in the middle of the 3" tube 30 ms after the valve has been opened, and the other front roughly at the inlet to the 2" tube. After this, the latter front enters the 3" tube, without any noticeable reflection at the transition, and causes the pressure in the 3" tube to be increased still further. This second superposed front in the 3" tube has a higher velocity than the front reflected from the restriction. As is apparent from Fig. 93, when it reaches the container it has practically caught up with the last-mentioned front. The velocity of the front reflected from the restriction is comparatively low, about 160 m/s. This is associated with the fact that the air behind this front is not at rest, but travels towards the 2" tube, which in fact is in the process of being charged from the 3" tube.

Arrangement 21: 2" and 3" tubes in succession
(Figs. 39, 50b and 53)

The same conical nozzle as in arrangement 20 has been used here, although mounted the other way round to fit in with the tubes. The nozzle thus acts as a Laval nozzle (diverging nozzle), as in arrangement 18. The pressure changes at the different measuring points are reproduced in Fig. 94, while Fig 95 shows the pressure distributions along the tubes at different times. The wave propagation is considerably more complicated in this arrangement than in the previous ones, for example, arrangement 20. Several fronts travelling forwards and backwards occur before the pressure at the end of the tube has had time to reach its maximum value. The pressure rise thus takes almost twice as long as with arrangement 20. A comparison between Figs. 93 and 95 shows that the static flow pressure at the inlet of the duct attains a considerably higher value in arrangement 21 than in arrangement 20. This is probably due to the fact that the damming-up effect in the 2" tube in arrangement 21 is more pronounced than in the 3" tube in arrangement 20. The static flow pressure at the inlet rises in arrangement 20 to 7.7 atm abs. = 48 per cent of the initial pressure in the container. The corresponding pressure in arrangement 21 is 10.5 atm abs. = 66 per cent of the initial pressure. The development of the front movements is more or less as follows. The first positive press front in arrangement 21 is also subject to a partial reflection when it reaches the conical nozzle, despite the fact that the nozzle in this arrangement diverges outwards in the direction of flow. This phenomenon seems to indicate the presence of a stationary shock front behind the

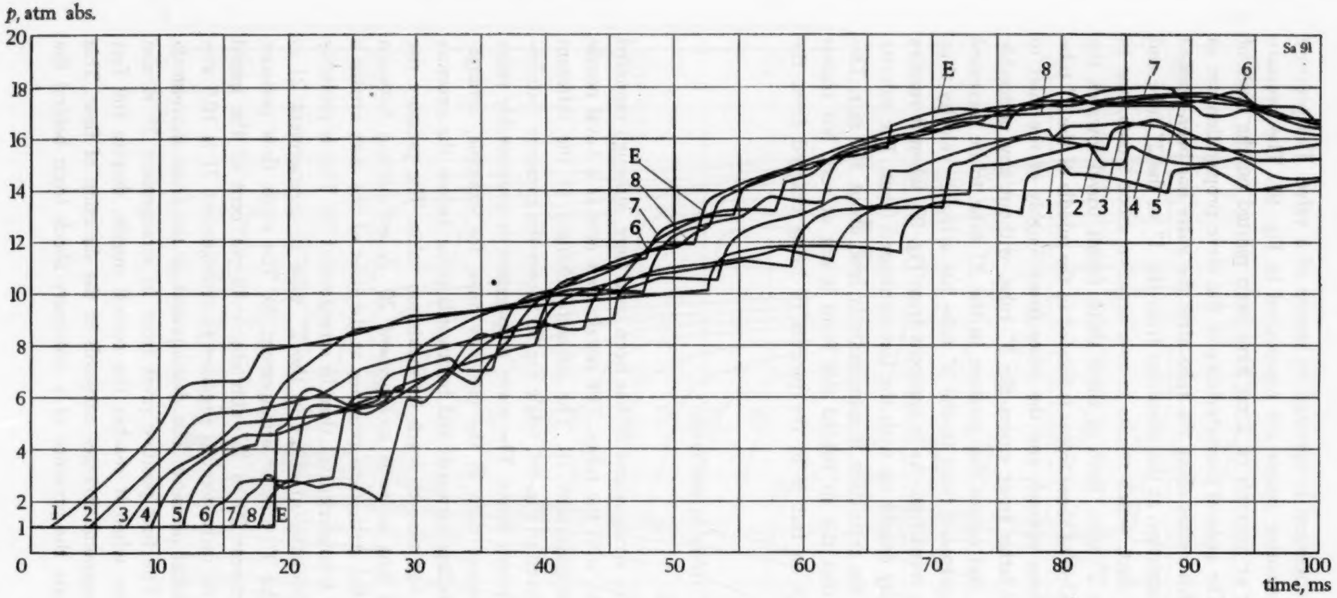

E, 1–8 Measuring points

Fig. 94. Pressure as function of time when measured with M-gauge at various points in arrangement 21 ($p_n = 16$ atm abs.).

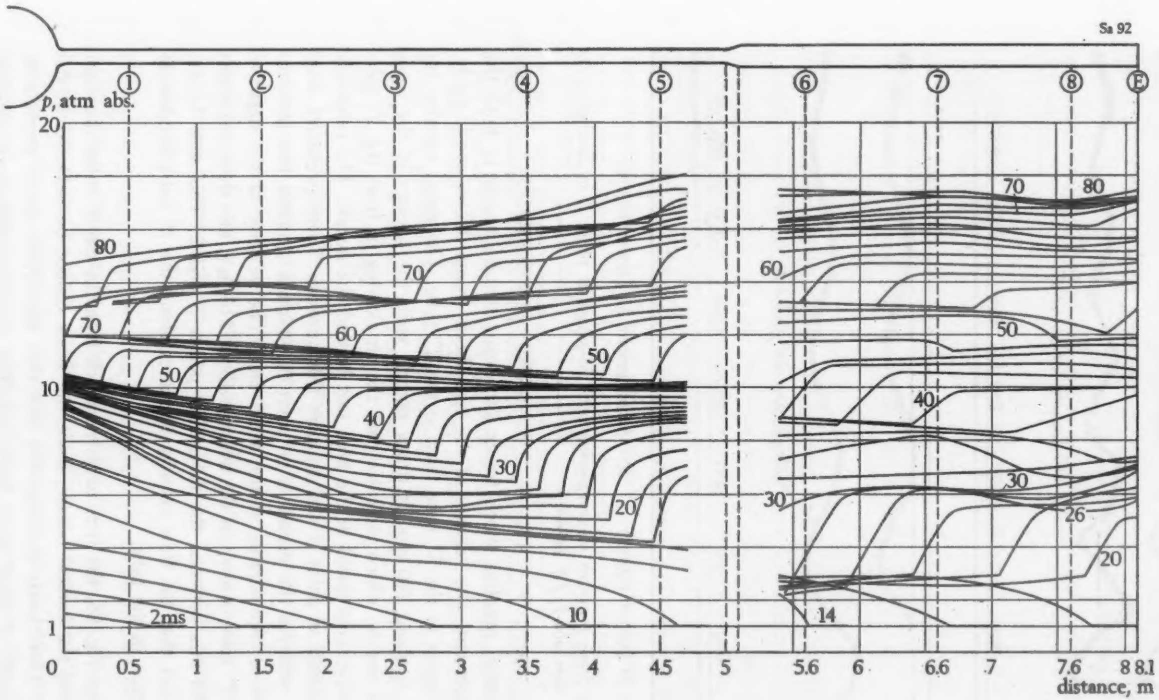

Fig. 95. Pressure distribution along the tube in arrangement 21 as calculated from the curves of Fig. 94.

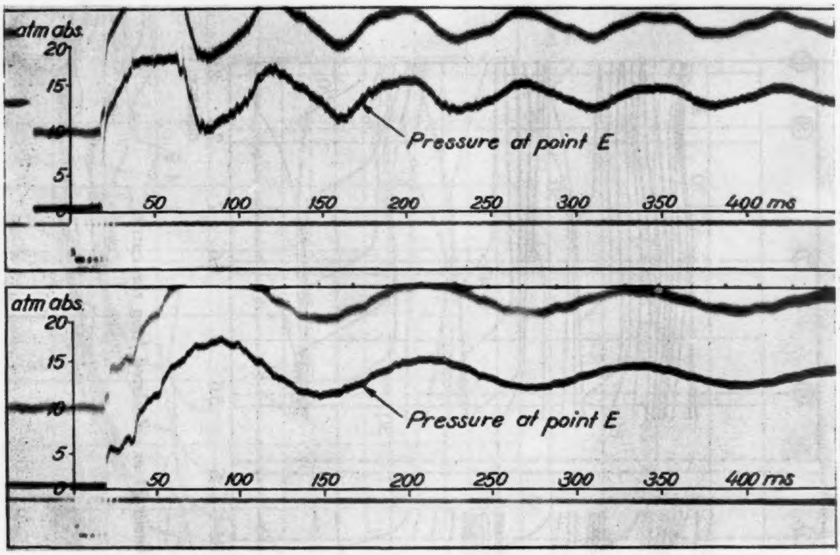

a Arrangement 20 (upper Figure) b Arrangement 21 (lower Figure)

Fig. 96. Oscillograms from pressure measurements with M-gauge at point E in arrangements 20 and 21 ($p_n = 16$ atm abs.). (Z 11783.)

nozzle. For this reason, negative shock fronts also occur simultaneously in both the tubes of this arrangement. The velocity of the two shock fronts differs considerably. It is substantially higher in the 3" tube than in the 2" tube. The mean velocity for the entire 3" tube is about 280 m/s. It drops slightly with the passage of the front towards the conical nozzle, which indicates that the air flowing in from the 2" tube is travelling with supersonic speed in the area just behind the nozzle. The relatively low pressures measured at point 6 also support this surmise. These pressures drop slightly with time, whereas the pressures at point 5, which is situated just in front of the nozzle, increase considerably at the same time. The velocity of the negative shock front in the 2" tube is low, on the average about 118 m/s, and does not reach more than about 93 m/s between the measuring points 3 and 5. This may be associated with the fact that the flow velocity increases along the 2" tube because of heating due to friction in the tube.

As can be seen from Fig. 95, the first negative shock front in the 3" tube does not pass the area around the conical nozzle, since the front cannot be detected at the measuring point 5. This clearly confirms the fact that supersonic speed prevails to the right of the nozzle. A weak press front travelling outwards appears to develop as a result of the reflection, which front in its turn is reflected from the end of the tube and becomes steeper on its path towards the nozzle, as is apparent from the pressure distributions at the time 38–44 ms. When this front passes measuring point 6, it has almost the characteristics of a shock front. On reaching the nozzle, this front causes both a new negative shock front in the 2″ tube and a reflected positive press front in the 3″ tube. The latter front is reflected in its turn from the end of the tube and gives rise at the nozzle to yet another negative shock front in the 2″ tube.

Fig. 96 shows oscillograms of the pressure changes at the end of the tube in arrangements 20 and 21.

Arrangements 22 and 23: 1 ½″ and 1 ¼″ tubes
(Figs. 40, 54a and b)

The experiments with these arrangements were carried out in conjunction with investigations on an air-blast circuit-breaker and have been included in this study because of an irregularity in the behaviour of the flow which might be of some interest. As can be seen from Fig. 54, the flow areas in the valve are ample in comparison with the tube cross-sectional area, which for the 1 ½″ tube is 13.5 cm^2 and for the 1 ¼″ tube 10.1 cm^2, whereas the minimum flow area of the valve is 34 cm^2. The pressures in the 1 ¼″ tube were measured at the beginning and the end of the 8.64-m long tube. In the 1 ½″ tube the pressures were measured also approximately in the middle of the tube. The pressure changes are reproduced in Fig. 97. As can be seen, the pressure increases at the measuring point 0 of the 1 ¼″ tube in the normal manner and is relatively free from superposed oscillations until the shock front reflection from the end of the tube causes a sudden rise in pressure after about 57 ms. In the 1 ½″ tube, on the other hand, the pressure ceases rising after about 8 ms. The pressure then remains constant at about 6.5 atm abs., until it suddenly rises to about 9 atm abs. at about 19 ms. After this, the pressure curve for the 1 ½″ tube continues normally.

It is beyond doubt that the behaviour of the pressure is associated with the test arrangement, since a large number of oscillograms were recorded, which all displayed the same irregularity in the pressure curve for the 1 ½″ tube. A number of measurements made on a 1″ tube display the same uniform characteristics as for the 1 ¼″ tube. The disturbance thus seems to occur when the tube diameter exceeds a certain value.

It is by no means simple to find a suitable explanation of this disturbance, but it is possible that a temporary suspension of the flow from the wall at the inlet of the tube takes place. In other words, a jet effect is experienced with supersonic speed and low pressure behind the minimum flow area, which latter can be considered as lying ahead of the measuring point 0. If it is assumed then that the supersonic state changes over as the result of a compressive shock to a subsonic state and that this compressive shock travels towards the container due to the intensification of the

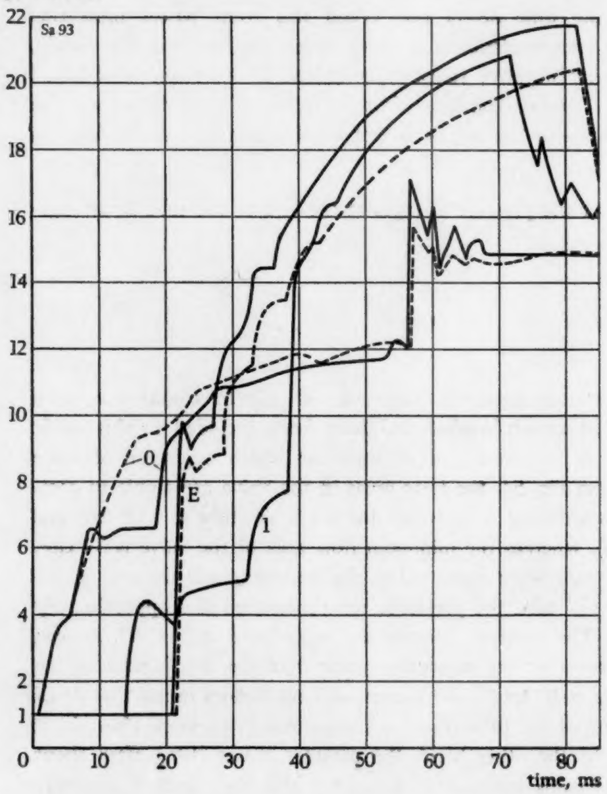

1 ½" tube
1 ¼" tube

E, 0, 1 Measuring points

Fig. 97. Pressure as function of time when measured with M-gauge at various points in arrangements 22 and 23 ($p_n = 16$ atm abs.).

flow, thus passing the measuring point 0, the pressure should behave in approximately the same way as has been recorded.

The front velocities in the 1 ½" tube differ rather considerably in the two halves of the tube. Mean values of about 325 and about 630 m/s, respectively, are obtained for the distances 0–1 and 1-E for the front travelling outwards, whereas the reflected front has the approximate values 230 and 265 m/s, respectively, for the same distances.

M. EXPERIMENTS ON THE ACCELERATION PERIOD OF ESCAPING AIR

Arrangements 24 and 25
(Figs. 41, 55 and 56)

In both arrangements air flowed out from the usual 0.3 m^3 container through a cylindrical 3" connection piece with a length of 100 mm to the atmosphere. A valve (cf. Fig. 55) was inserted between the container and the connection piece in arrange-

The photograph Nos. on the upper abscissa indicate the time spacing of the photographs taken on arrangement 24 with $p_n = 16$ atm abs. (curve 4).

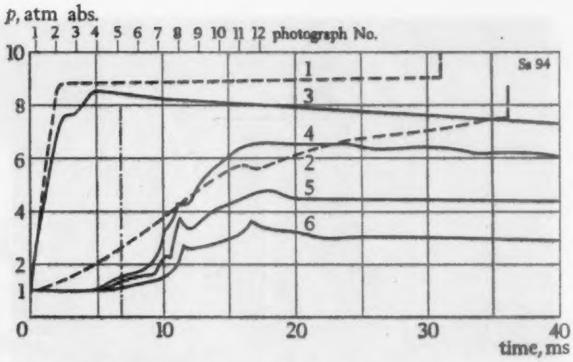

- · - · - Point of time when the valve is fully open

1 Arrangement 8, P-gauge measurements, $p_n = 16$ atm abs.
2 Arrangement 12, M-gauge measurements, $p_n = 16$ atm abs.
3 Arrangement 25, P-gauge measurements, $p_n = 16$ atm abs.
4 Arrangement 24, M-gauge measurements, $p_n = 16$ atm abs.
5 Arrangement 24, M-gauge measurements, $p_n = 12$ atm abs.
6 Arrangement 24, M-gauge measurements, $p_n = 8$ atm abs.

Fig. 98. Pressure as function of time when measured at point 0 in arrangements 24 and 25 (free escape) and arrangements 8 and 12 (5-m tubes).

ment 24, whereas diaphragms (cf. Fig. 56) were used in arrangement 25. The static flow pressure was measured at a distance of 20 mm from the opening of the connection piece by means of an M-gauge in arrangement 24 and a P-gauge in arrangement 25.

The recorded pressure changes are reproduced in Fig. 98. Experiments were carried out on arrangement 24 with the valve at initial pressures of 8, 12 and 16 atm abs. in the container. For the sake of comparison a broken curve (arrangement 12) has been plotted, showing the pressure changes for the same valve arrangement, but mounted on a 3″ tube, 5 m long, in the place of the connection piece. The curves show that it takes a relatively long time to attain a continuous state of flow in the connection piece with the valve arrangement. The static pressure is not reached until about 17 ms have elapsed after the opening of the valve. At this juncture the valve has been fully open for 10 ms. It can be inferred from this that the continuous state of flow through the valve does not commence immediately after its opening, but that a *stabilising period* occurs, the duration of which is obviously dependent on how the valve is shaped from the flow point of view. The pressure curve for arrangement 25, with bursting diaphragms, has quite different characteristics. The delay in the pressure rise is very small here and the duration of the period of stabilisation is clearly only about one third of that observed with the opening of the valve. From

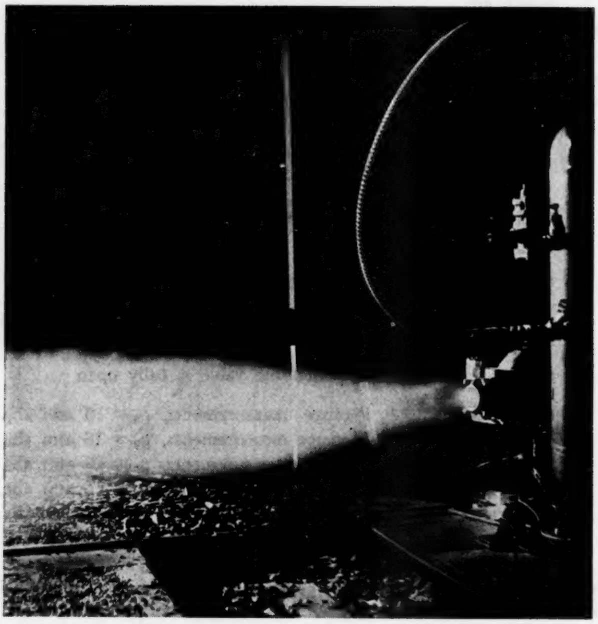

Fig. 99. Jet of compressed air leaving the nozzle of arrangement 24. (Z 11784.)

this it can be inferred that, when using valves, an air passage through the valve as straight as possible should be adopted if particularly rapid charging is required.

The broken pressure curves in Fig. 98, recording the charging of a 5-m tube, show a more rapid pressure rise at the beginning of the cycle. This is due to the frictional resistance in the tube, which has a damming-up effect on the following air. What happens is probably that the air is heated due to friction against the tube walls, which leads to an increase in its specific volume. Its velocity does not rise, however, to the extent corresponding to the increase in volume, and this means that the air from the container is slowed down to a certain extent, that is to say, it flows into the tube with a lower velocity than when flowing direct out into the atmosphere. This corresponds, however, to an increase in the static pressure.

The maximum pressure after the stationary state has been reached is, according to Fig. 98, about 20 per cent lower for the arrangement with the valve than for the arrangement with the diaphragms (at an initial pressure of 16 atm abs.). In the latter arrangement the measured pressure corresponds very well with the theoretical, critical value. The fact that the pressure for the arrangement with the valve lies considerably lower can be attributed to the flow resistance in the valve. Although the effective flow area of the valve is about 50 per cent greater than the cross-sectional area of the connection piece, it is not nevertheless the latter which constitutes the sole

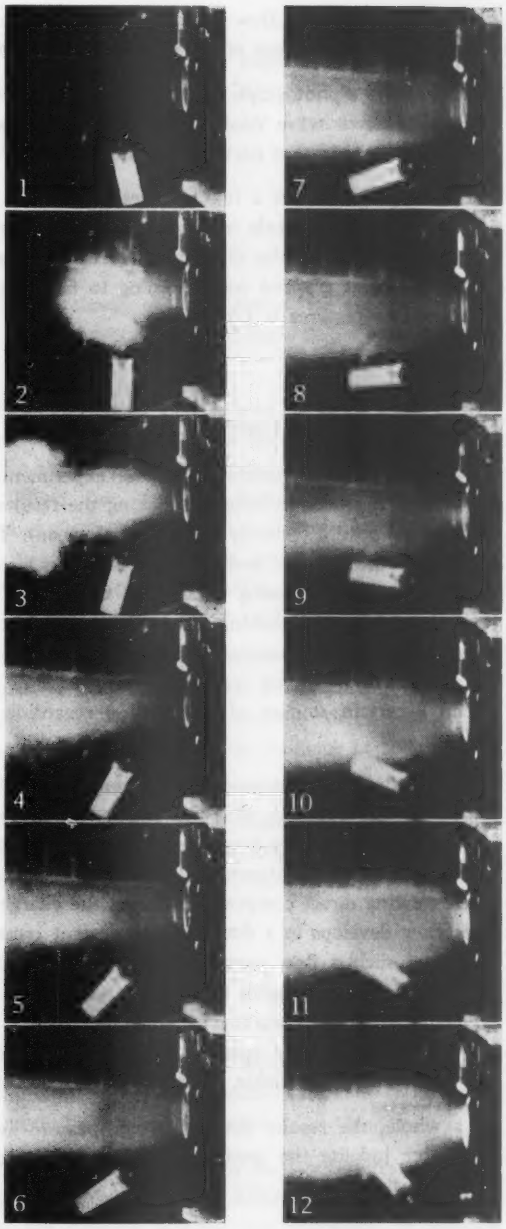
1
2
3
4
5
6
7
8
9
10
11
12

Fig. 100. Slow-motion pictures of jet. The time spacing of the photographs is as indicated in Fig. 98. (Z 11785.)

decisive factor for the flow volume per unit of time. This volume is determined also by the conditions in front of the narrowest part of the outlet.

Fig. 99 shows a photograph of the valve and connection piece with built-on M-gauge. The well-known wave configurations [11] associated with flow at acoustic speed can be observed in that part of the emerging jet of air just in front of the nozzle.

Finally, Fig. 100 shows a few pictures recorded on a film illustrating the jet of air emerging from the nozzle in arrangement 24, where the initial pressure was 16 atm abs. The times when the different pictures were taken are indicated in Fig. 98. The film was run at a speed corresponding to 655 pictures per second, i.e., the interval between two pictures is 1.53 ms.

N. GENERAL CONSIDERATIONS

In the course of the treatment of the experiments described in this treatise, great importance has been attached to making the results obtained from the measurements as lucid as possible, chiefly by graphical means. The interested reader can himself thus study the material and draw his own conclusions about different aspects of the problems. When discussing the results, the author has been obliged to make certain limitations to avoid making this work unwieldy. For this reason, therefore, the major part of the discussion is devoted to the comparison between the measured and the theoretically derived results. In the course of this, it has also been possible to obtain a certain amount of information regarding the influence of the attenuating factors.

From the theoretical viewpoint, this treatise probably presents certain new features. It appears, for example, that the detailed investigation of the reflection phenomena in conjunction with the boundary layer occurring during charging has not previously been described in the literature. The theory in which an expansion front is introduced when treating direct compression during the charging of a duct implies that a supersonic flow develops in a duct with a constant cross-sectional area. The physical possibility of such a flow cannot be appraised directly. Nevertheless, by applying the theory, it has been possible to obtain results which agree well with those from measurements. It would naturally be of value if direct confirmation of the theory could be obtained by making speed measurements. Apparatus for performing such measurements was not available, however, during the investigations.

As a whole, the results obtained from these investigations have proved to be well suited for judging the oscillatory phenomena encountered in high-voltage air-blast circuit-breakers.

ACKNOWLEDGEMENT

The author would like to express his thanks to Mr Nils Jansson for the exemplary way in which he has carried out the measurements, to Mr Algoth Olsson for valuable assistance in obtaining the necessary references, and to Mr Martin Blake for the thorough translation of the Swedish manuscript.

SUMMARY

After treating the basic equations for the theory of elastic waves, the author describes the wave phenomena which occur in conjunction with the rapid filling and discharge of ducts with compressed air.

Wave investigations, which have been performed at the Asea Research Laboratories, Ludvika, with 25 different experimental arrangements are presented and the results obtained from the measurements are reproduced in the form of curves for the pressure variations at different points along the duct. The front movements are then graphically reproduced on the basis of these pressure curves. Comparisons have been made between the estimated and measured results, these generally leading to good agreement during the initial stage of the wave propagation, when the attenuating factors have not yet had time to exert any real influence on the oscillations.

Most of the measurements have been performed with tubes having a diameter of 2" and 3" and lengths ranging between 3 and 11 m. The initial pressure has been as a rule 16 atm abs. – a standard pressure for air-blast circuit-breakers. The experiments were mainly intended to provide information for the designing of such circuit-breakers.

The results of the above-mentioned calculations of wave phenomena have been summarised and plotted in diagrams which can be universally applied. This treatise has been supplemented by a historical survey of the research work into waves in compressible media.

RÉSUMÉ

Après avoir établi les équations fondamentales de la théorie des ondes élastiques, l'auteur décrit les phénomènes ondulatoires qui se produisent lors du remplissage ou de la vidange rapides de conduites à l'aide d'air comprimé.

L'article relate les recherches qui ont été effectuées dans les laboratoires de l'Asea à Ludvika au moyen de 25 dispositifs expérimentaux différents et présente sous forme de diagrammes les résultats des mesures relatives aux variations de pression en différents points de la conduite. Les mouvements frontaux sont alors reproduits

graphiquement en se basant sur ces courbes de pression. Des comparaisons ont été effectuées entre les valeurs estimées et les résultats des mesures. Ces comparaisons ont montré que l'on obtenait une concordance satisfaisante durant le stade initial de la propagation de l'onde, c.-à-d. lorsque les coefficients d'atténuation n'ont pas encore eu le temps d'exercer une influence réelle sur les oscillations.

La plupart des mesures ont été effectuées sur des tuyaux de 2" et 3" de diamètre et sur des longueurs de 3 à 11 m. La pression initiale était en général de 16 atm. abs. – une pression normale pour disjoncteurs à air comprimé. Les expériences avaient surtout pour but de fournir des données aux constructeurs de ce genre de disjoncteurs.

Les résultats des calculs relatifs à ces phénomènes ondulatoires sont rassemblés dans des diagrammes qui sont d'application générale. Ce traité est complété par un examen historique des travaux de recherche concernant les ondes dans les fluides compressibles.

ZUSAMMENFASSUNG

Nach Behandlung der Grundgleichungen zur Theorie der elastischen Wellen werden die Schwingungserscheinungen untersucht, die beim raschen Füllen und Entleeren von Druckluft-Rohrleitungen auftreten.

Die in den Forschungslaboratorien der Asea, Ludvika, an 25 verschiedenen Anordnungen durchgeführten Schwingungsversuche werden beschrieben und die Meßergebnisse als Kurven der Druckänderungen in verschiedenen Punkten entlang der Rohrleitung aufgetragen. Mithilfe dieser Druckkurven werden die Bewegungen der Druckfront graphisch dargestellt. Die Meß- und die Berechnungswerte werden miteinander verglichen. In der ersten Phase des Vorganges ist die Übereinstimmung im allgemeinen gut, da die Dämpfungsfaktoren den Schwingungsvorgang noch nicht nennenswert beeinflussen konnten.

Die meisten Messungen wurden an Rohren mit einem Durchmesser von 2" und 3" und einer Länge zwischen 3 und 11 m vorgenommen. Der Anfangsdruck betrug im allgemeinen 16 ata – ein gebräuchlicher Wert für Druckluftschalter. Die Versuche dienten in erster Linie dazu, Unterlagen für die Konstruktion von Druckluftschaltern zu schaffen.

Die Ergebnisse aus den obigen Berechnungen der Schwingungserscheinungen wurden in allgemein gültigen Schaubildern zusammengestellt. Vervollständigt wurde die Arbeit durch einen historischen Überblick über die Forschungsarbeiten auf dem Gebiet der Schwingungen in kompressiblen Medien.

BIBLIOGRAPHY

1. *Poisson, S. D.*, Mémoire sur la théorie du son. École Polytechnique (Paris), Journal 7(1808), p. 319 ff.

   Lord Rayleigh [26] in his paper of 1910 makes the following comment: "The first step, and it was a very important one, in the treatment of waves of finite amplitude is due to Poisson. Under assumption of Boyle's law, $p = a^2\varrho$, he proved that for waves travelling in one direction (positive) the circumstances of the propagation are expressed by $u = f[x - (a + u)t]$, in which f denotes an arbitrary function."(t = time, x = distance (plane wave), u = mass speed, a = speed of sound.)

2. *Stokes, G. G.*, On a difficulty in the theory of sound. London, Edinburgh and Dublin Philos. Magazine and Journal of Science 23(1848), pp. 349–356.

   Lord Rayleigh [26] makes the following comment: "A closer discussion of the solution represented by Poisson's integral was given by Stokes, who pointed out the difficulty which ultimately arises from the motion becoming discontinuous. It is probable, as suggested by Stokes, that some sort of reflection would ensue."

3. *Earnshaw, S.*, On the mathematical theory of sound. Royal Society (London), Philos. Trans. 150(1860), p. 133 ff.

   An examination of the wave phenomena set up in a tube by an accelerating piston. The wave in front of the piston is expressed as "wave of condensation" and "positive wave", the front to the rear of the piston as "wave of rarefaction" and "negative wave". A positive wave is said to be one in which the motions of the particles are in the direction of wave transmission, whereas in a negative wave the direction of motions of the particles is opposite to that of wave transmission. Earnshaw speaks about a constant change of wave type which leads to a bore, i.e., a tendency to discontinuity of pressure, being formed in the wave front. According to his opinion, however, discontinuity of pressure is a physical impossibility. What happens is described as follows (p. 138): "Nature so contrives that as the discontinuity is in its initial stage of beginning to take place, its actual occurrence is prevented by a gradual (not sudden) prolongation of the wave's front, and by the constant casting off, from its front in a retrogressive direction, of a long continuous wave of a negative character, which will be of greater or less intensity according as the tendency to discontinuity is more or less intense in the original wave."

4. *Riemann, B.*, Über die Fortpflanzung ebener Luftwellen von endlicher Schwingungsweite. Königl. Gesellsch. der Wissenschaften, Göttingen, Abhandl. (Math.) 8(1860), p. 43 ff. Also in Riemann's Collected Works, 2nd ed. 1892, p. 156 ff.

   Riemann proved mathematically that a compression front becomes steeper during propagation and that an expansion front becomes flatter. He found a compression front ultimately to be transformed into a shock front and that this wave type was maintained during the continued propagation. The variations of state within the front were assumed to follow the adiabatic law of Poisson, i.e., the static adiabate. Variations according to this law being reversible, Riemann concluded that shock fronts were able to travel in a retrogressive direction as well (rückwärtslaufender Verdichtungsstoß). Riemann's treatment of the problem of shock compression has been subject to much discussion (see, e.g., Lord Rayleigh [26] and Weber [27]).

   The investigations of other research workers show the impossibility of shock fronts travelling in a retrogressive direction (see, e.g., Zemplén [20]). A front of this type will at once change into an expansion front.

   The papers of Earnshaw [3] and Riemann are of basic importance for the treatment of continuous waves. Riemann deals with the problems in a more general way and obviously was not acquainted with the work of Earnshaw.

5. *Rankine, M.*, On the thermodynamic theory of waves of finite longitudinal disturbance. Royal Society (London), Philos. Trans. A 160(1870) Part II, p. 277 ff.

   This paper contains, as shown by Lord Rayleigh [26] in 1910, a thermodynamic solution of the problem of shock compression. In the work of Hugoniot [10], which appeared about 15 years later, the problem is solved in a mechanical way leading to comparatively simple equations of motion. Rankine's work seems to have been carried out without knowledge of previous investigations in this field. In a supplement, however, references are given to the works of Poisson [1], Stokes [2], Airy and Earnshaw [3].

6. *Mach, E., Sommer, J.,* Über die Fortpflanzungsgeschwindigkeit von Explosionsschallwellen. Math.-naturwiss. Classe d. Kaiserl. Akad. d. Wissenschaften (Vienna), Sitzungsberichte 75(1877), p. 101 ff.

   This paper deals with laboratory experiments on the velocity of explosion waves, using to some extent the Schlieren method of Toepler. (*Toepler,* Beobachtungen nach einer neuen optischen Methode, Max Cohea, Bonn 1864.) Reference is given to the work of Riemann [4] of 1860, which has obviously come to the knowledge of the authors after the completion of the investigations.

7. *Lord Rayleigh,* Theory of sound. Macmillan, London 1877 (Vol. I) and 1878 (Vol. II). (2nd ed. 1894 and 1896. Also an edition in 1929. German edition: Die Theorie des Schalles. Braunschweig 1880.)

   It may be seen from the second edition, Vol. II, p. 36 ff., that Lord Rayleigh in 1896 considered the problem of shock compression as not yet solved. No mention is made of, for example, Hugoniot's work [10] of 1889. Riemann's treatment [4] of shock compression and his theory on the propagation of a discontinuity – mainly its travelling in a retrogressive direction – are criticised. On page 83 ff., wave reflection against a boundary surface between gases of unequal densities is investigated.

8. *Sebert, Hugoniot, H.,* Sur la propagation d'un ébranlement uniforme dans un gaz renfermé dans un tuyau cylindrique. Comptes Rendus Hebdom. Séances Acad. Sciences 98(1884), p. 507 ff.

9. *Lipschitz, R.,* Beitrag zu der Theorie der Bewegung einer elastischen Flüssigkeit. Journal reine u. angew. Mathematik (Crelle's J.) 100(1887).

   Mathematical treatment of wave problems on a broader basis than by Riemann [4]; Earnshaw's work [3] is not mentioned.

10. *Hugoniot, H.,* Mémoire sur la propagation du mouvement dans les corps et spécialement dans les gaz parfaits. École Polytechnique (Paris), Journal 58(1889), pp. 1–125. (See also same Journal 57(1887), p. 3 ff., and also Journal Math. Pures et Appl. 3(1887), p. 477 ff. and 4(1888), p. 153 ff.)

    Probably the most well-known work of early years dealing with shock compression. Investigating the energy conditions, Hugoniot proved that the problem cannot be solved on the basis of the adiabatic law of Poisson. Instead of the "static" adiabate following Poisson's law, it is necessary to introduce the "dynamic" adiabate. The problem, however, is not completely solved by means of the theory of Hugoniot, because the viscosity, i.e., the internal friction, and the heat transfer have not been taken into account. A treatment in this direction was published in 1940 by Bechert [43].

11. *Emden, R.,* Über die Ausströmungserscheinungen permanenter Gase. Annalen Physik u. Chemie (Wiedemanns Ann.) 69(1899), pp. 264–289, 426.

    This paper deals theoretically and experimentally with the stationary waves occurring in a jet leaving a nozzle. Comparisons are made with the theory of Riemann [4]. Lord Rayleigh's criticism [7] with respect to the possibility of the occurrence of shock waves is discussed.

12. *Wolff, W.,* Über die bei Explosionen in der Luft eingeleiteten Vorgänge. Annalen d. Physik 69(1899), p. 329 ff.

    Measurements of wave speed and wave energy at various distances from the point of explosion. The results were found to be in agreement with the theory of Riemann [4].

13. *Vieille, P.,* Étude sur le rôle des discontinuités dans les phénomènes de propagation. Memoires Poudres et Salpêtres 10(1899), p. 177 ff.

14. *Stodola, A.,* Die Dampfturbinen und die Aussichten der Wärmekraftmaschinen. VDI-Zeitschr. 47(1903): 1, pp. 1–10.

    This paper contains the first description of experiments showing by means of pressure measurements the occurrence of a stationary compression shock in a Laval nozzle.

15. *Hadamard, J.,* Leçons sur la propagation des ondes et les équations de l'hydrodynamique. Cours du Collège de France. Librairie scientifique A. Hermann, Paris 1903.

16. *Jouguet, É.*, Remarques sur la propagation des percussions dans les gaz. Comptes Rendus Hebdom. Séances Acad. Sciences 138(1904), p. 168 ff.

17. *Jouguet, É.*, Remarques sur la loi adiabatique d'Hugoniot. Comptes Rendus Hebdom. Séances Acad. Sciences 139(1904), p. 786 ff.

18. *Zemplén, G.*, Besondere Ausführungen über unstetige Bewegungen in Flüssigkeiten. Encyklopädie math. Wissenschaften 4(1905), p. 3 ff.

19. *Zemplén, G.*, Über unstetige Bewegungen in Flüssigkeiten. Encyklopädie math. Wissenschaften 4(1905), p. 281 ff.

    A discussion of shock waves from the thermodynamic point of view is given on p. 306 ff. Riemann's treatment [4] of shock compression is compared with that of Hugoniot [10].

20. *Zemplén, G.*, Sur l'impossibilité des ondes de choc négatives dans les gaz. Comptes Rendus Hebdom. Séances Acad. Sciences 141(1905), p. 710 ff.

21. *Proell, R.*, Strömungsverlauf und Verdichtungsstoß im zylindrischen Rohre. Zeitschr. ges. Turbinenwesen 3(1906), pp. 37–38.

    The author criticises a suggestion by Langrod (same periodical, 2(1905), p. 370 ff.) about the physical impossibility of compression shocks.

22. *Prandtl, L.*, Zur Theorie des Verdichtungsstoßes. Zeitschr. ges. Turbinenwesen 3(1906), 241–245.

    The compression shock is calculated, taking into account the heat transfer but not the viscosity. The thickness of the shock layer is found to be of the same magnitude as the wave length of light (approx. 0.5 μ).

23. *Duhem, P.*, Sur la propagation des ondes de choc au sein des fluides. Zeitschr. physikal. Chemie 69(1909), p. 169 ff.

24. *Kobes, K.*, Die Durchschlagsgeschwindigkeit bei den Luftsauge- und Druckluftbremsen. Österr. Ing.- u. Architekten-Verein, Zeitschr. 55(1910), p. 553 ff.

    The wave velocity was measured in long brake conduits and was shown to be higher than the normal acoustic speed. Kobes investigates the conditions of propagation theoretically as well as experimentally. The work is important and references are frequently made about it in recent literature.

25. *Taylor, G. J.*, The conditions necessary for discontinuous motion in gases. Royal Society (London), Proc. Ser. A, 84(1910), pp. 371–377.

26. *Lord Rayleigh*, Aerial plane waves of finite amplitude. Royal Society (London), Proc. Ser. A, 84(1910), pp. 247–284.

    Concerning Riemann's treatment [4] of shock compression the following statement is given on p. 260: "Commenting on these results in the 'Theory of sound' (1878), I pointed out that although the conditions of *mass* and *momentum* were satisfied, the condition of *energy* was violated and that therefore the motion was not possible; and in republishing this paper Stokes (Collected Works, Vol. 2, p. 55) admitted the criticism, which had indeed already been made privately by Kelvin. On the other hand Burton (London, Edinburgh and Dublin Philos. Magazine and Journal of Science 35(1893), p. 316 ff.) and H. Weber (Die partiellen Differential-Gleichungen der mathematischen Physik, Braunschweig 1901, Vol. 2, p. 496) maintain at least to some extent, the original view. – Inasmuch as they ignored the question of energy, it was natural that Stokes and Riemann made no distinction between the cases where energy is gained or lost. As I understand, Weber abandons Riemann's solution for the discontinuous wave (or *bore*, as it is sometimes called for brevity) of rarefaction, but still maintains it for the case of the bore of condensation."

27. *Weber, H.*, Die partiellen Differential-Gleichungen der mathematischen Physik (nach Riemann's Vorlesungen). 5th ed., Vieweg, Braunschweig 1912. Fortpflanzung von Stößen in einem Gase, Vol. 2, p. 503 ff.

    The following statements given on p. 552 ff. may be of interest: "Riemann hat unter der Voraussetzung eines *adiabatischen Vorganges* das *Poissonsche Gesetz* $p = a^2\varrho^\varkappa$ für die Abhängigkeit des Druckes von der Dichtigkeit hergeleitet, und kommt dadurch im Falle unstetiger Bewegung zu Resultaten, die mit dem Prinzip der Erhaltung der Energie

nicht übereinstimmen. Die Annahme eines konstanten Wertes von $a^2 = p\varrho^{-\varkappa}$ führt zu einem Gesetz, das man die *Erhaltung der Entropie* nennen könnte. Es zeigt sich also, daß die beiden Gesetze, das der Erhaltung der Energie und der Entropie, nicht immer miteinander verträglich sind, daß beim Durchgang eines Gasteilchens durch eine Unstetigkeitsstelle entweder ein *Verlust an Energie* oder ein *Gewinn an Entropie* stattfinden muß. In der Riemannschen Darstellung ist das Energieprinzip preisgegeben, während Hugoniot, Zemplén u.a. die Erhaltung der Entropie fallen lassen.
In betreff der Frage, welche von beiden Annahmen die richtige ist, muß man sich klar machen, daß beide Annahmen nur Annäherungen an die Wirklichkeit darstellen. Das Energieprinzip setzt eine *reibungslose* Bewegung voraus, während das Entropieprinzip jede *Wärmeleitung ausschließt*. Beides entspricht nicht der Wirklichkeit. Es kommt dazu, daß wir ohne weiteres die Gesetze, wie sie bei *ruhenden* idealen Gasen gelten, auf bewegte Gase angewandt haben. Ist es doch sogar zweifelhaft, ob bei bewegten Gasen noch das Boylesche und Gay-Lussacsche Gesetz gilt. Es wäre denkbar, daß der Ausgleich zwischen Druck, Volumen und Temperatur eine gewisse Zeit braucht, die noch nicht verstrichen ist, wenn ein neuer Zustand eintritt."

28. *Rüdenberg, R.*, Über die Fortpflanzungsgeschwindigkeit und Impulsstärke von Verdichtungsstößen. Artillerist. Monatshefte (1916): 113.

29. *Becker, R.*, Stoßwelle und Detonation. Zeitschr. f. Physik 8(1922): 5, pp. 321–362.

30. *Stodola, A.*, Dampf- und Gasturbinen. 6th ed., Berlin 1924.
Compression shocks and expansion waves are dealt with on p. 833 ff.

31. *Hildebrand, F.*, Über unstationäre Luftbewegungen in langen Rohrleitungen und ihre Beziehungen zu den Steuervorgängen der indirekten Luftbremsen. Dissertation. VDI-Verlag, Berlin 1927.

32. *Ackeret, J.*, Gasdynamik. Handbuch der Physik. Springer, Berlin 1927, Vol. 7, p. 289 ff.

33. *Busemann, A.*, Verdichtungsstöße in ebenen Gasströmungen. Aerodynamic lectures, Aachen 1929. Gilles, Hopf und v. Kármán, Berlin 1930. See also: Handbuch der Experimentalphysik, Vol. IV/1, p. 431 ff.

34. *Fay, R. D.*, Plane sound waves of finite amplitude. Acoustical Soc. of America, Journal 3, Part 1(1931), pp. 222–241.

35. *Schardin, H.*, Bemerkungen zum Druckausgleichsvorgang in einer Rohrleitung. Physikal. Zeitschr. 33(1932), pp. 60–64.
This paper deals, for example, with shock waves occurring when a closed evacuated duct is rapidly opened to the atmosphere at one end. It also treats wave fronts occurring when a boundary wall separating air columns of unequal pressures is momentarily displaced.

36. *Schmidt, E.*, Schwingungen großer Amplitude von Gassäulen in Rohrleitungen. VDI-Zeitschr. 79(1935): 22, pp. 671–673.

37. *Mayer-Schuchard, C.*, Schwingungen von Luftsäulen mit großer Amplitude. VDI – Forschungshefte, ed. B, 7(1936): 376, pp. 13–22.

38. *Lettau, E.*, Messungen an Gasschwingungen großer Amplitude in Rohrleitungen. Deutsche Kraftfahrtforschung No. 39, 1939.

39. *Görtler, H.*, Zum Übergang von Unterschall- zu Überschallgeschwindigkeiten in Düsen. Zeitschr. angew. Mathematik u. Mechanik 19(1939), p. 325 ff.

40. *Giffen, E.*, Rapid discharge of gas from a vessel into the atmosphere. Engineering 150(1940), pp. 134–136, 154, 155, 181–183.

41. *Görtler, H.*, Gasströmungen mit Übergang von Unterschall- zu Überschallgeschwindigkeiten. Zeitschr. angew. Mathematik u. Mechanik 20(1940), p. 254 ff.

42. *Bechert, K.*, Zur Theorie ebener Störungen in reibungsfreien Gasen. Annalen d. Physik 37(1940): 5, p. 89 ff., and 38(1940): 5, p. 1 ff.

43. *Bechert, K.*, Ebene Wellen in idealen Gasen mit Reibung und Wärmeleitung. Annalen d. Physik 40(1941): 5, p. 207 ff.

44. *Pfriem, H.*, Die ebene ungedämpfte Druckwelle großer Schwingungsweite. Forschung Gebiete d. Ingenieurwesens 12(1941), p. 51 ff.

45. *Pfriem, H.*, Reflexionsgesetze für ebene Druckwellen großer Schwingungsweite. Forschung Gebiete d. Ingenieurwesens 12(1941), p. 244 ff.

46. *Pfriem, H.*, Zur Theorie ebener Druckwellen mit steiler Front. Akustische Zeitschr. 6(1941), p. 222 ff.

47. *Pfriem, H.*, Zur gegenseitigen Überlagerung ungedämpfter ebener Gaswellen großer Schwingungsweite. Akustische Zeitschr. 7(1942), pp. 56–65.

48. *Pfriem, H.*, Zur Frage des Gasdruckes auf bewegte Wände. Forschung Gebiete d. Ingenieurwesens 13(1942), p. 76 ff.

49. *Pfriem, H.*, Der Einfluß der Kolbenbeschleunigung auf die Verdichtung von Gasen. Forschung Gebiete d. Ingenieurwesens 13(1942), p. 112 ff.

50. *Schultz-Grunow, F.*, Nichtstationäre, eindimensionale Gasbewegung. Forschung Gebiete d. Ingenieurwesens 13(1942), p. 125 ff.

51. *Prandtl, L.*, Führer durch die Strömungslehre, Berlin 1942. Vierter Abschnitt: Strömung mit erheblichen Volumenänderungen. See in particular §§ 1 and 4.

52. *Sauer, R.*, Zur Theorie des nichtstationären ebenen Verdichtungsstoßes. Ingenieur-Archiv 14(1943), p. 14 ff.

53. *Sauer, R.*, Theorie der nichtstationären Gasströmung, I–IV. – Department of Commerce, Office of Declassification and Technical Services (Washington), Publication Board Reports, available as microfilms and photostats.
The following designations refer to abstracts in the Bibliography of Scientific and Industrial Reports.
    I. Ebene, stetige Gaswellen. Original version: PBL 61528 (Techn. Hochschule Aachen, Report No. 1675/1, Sept. 1942). English translation: PB 38050 (Laminar steady gas waves).
    II. Ebene Gaswellen mit Verdichtungsstößen. Original version: PBL 60805 (Techn. Hochschule Aachen, Report No. 1675/2, Dec. 31, 1942). English translation: PB 42757 (Plane gas waves with compression shocks).
    III. Fadenströmung in Rohren veränderlichen Querschnitts, insbesondere Kugel- und Zylinderwellen. Original version: PBL 60806 (Techn. Hochschule Aachen, Report No. 1675/3, March 24, 1943). English translation: PB 75949 (Laminar flow in tubes of variable cross section, in particular spherical and cylindrical waves).
    IV. Ebene Gasströmung mit Reibung, Wärmeleitung und Wärmetönung. Original version: PBL 60807 (Techn. Hochschule Aachen, Report No. 1675/4, July 28, 1943). English translation: PB 75952 (Plane gas flow with friction, heat transfer and temperature differences).

54. *Sauer, R.*, Zur Einführung in die Strömungslehre zusammendrückbarer Flüssigkeiten. VDI-Zeitschr. 88(1944): 23/24, pp. 301–307.

55. *Keenan, J. H., Kaye, J.*, Thermodynamic properties of air. Wiley, New York 1945.

56. *Ackeret, J., Feldmann, F., Rott, N.*, Untersuchungen an Verdichtungsstößen und Grenzschichten in schnell bewegten Gasen. Zürich 1946. English translation: Investigations of compression shocks and boundary layers in gases moving at high speed. National Advisory Comm. for Aeronautics, Techn. Memoranda, Note 1113 (Jan. 1947), pp. 1–34.

57. *Payman, W., Shepherd, W. C. F.*, Explosion waves and shock waves. – IV. The disturbance produced by bursting diaphragms with compressed air. Royal Society (London), Proc. A 186(1946), pp. 293–321.

58. *Weibull, W.*, Ondes planes de pression à front discontinu. VI. Congr. Intern. Méch. Appl., Paris 1946.

59. *Weibull, W.*, Teknisk Fysik. Elastiska vågor med ändlig amplitud. (Elastic waves of finite amplitude.) KTH Föreläsningar No. 104, 1947. (Lectures published by the Royal Institute of Technology, Stockholm. In Swedish.)

60. *Martin, M. H.*, A problem in the propagation of shock. Quarterly Appl. Mathematics 4(1947): 4, pp. 330–348.

61. *Paterson, S.*, La réflexion répétée des ondes de choc. Comptes Rendus Hebdom. Séances Acad. Sciences 224(1947): 12, pp. 891–892.

62. *Hsue-shen Tsien*, Flow conditions near the intersection of a shock wave with solid boundary. Journal Mathematics and Physics 26(1947), p. 69 ff.

63. *Quade, W.*, Über die Theorie ebener, kontinuierlicher Gaswellen endlicher Amplitude. Zeitschr. angew. Mathematik u. Mechanik 25/27(1947), pp. 215–232.

64. *Brinkley, S. R.*, *Kirkwood, J. G.*, Theory of the propagation of shock waves. Physical Review 71(1947): 9, pp. 606–611.

65. *Taub, A. H.*, Refraction of plane shock waves. Physical Review 72(1947): 1, pp. 51–60.

66. *Viaud, L.*, *Benoit, A.*, Sur la mesure des pressions dans un écoulement fluid avec ondes de choc. Comptes Rendus Hebdom. Séances Acad. Sciences 225(1947): 2, pp. 96–98.

67. *Montgomery, L. H.*, *Ward, J. W.*, Measurement of transient hydraulic pressures. Review Scient. Instruments 18(1947), pp. 289–293.

68. *Schultz-Grunow, F.*, Theoretisch und experimentell ermittelter Durchfluß einer nichtstationären Gasströmung. Zeitschr. angew. Mathematik u. Mechanik 25/27(1948), pp. 155–156.

69. *Hudson, A. A.*, Gas-blast circuit-breakers. Preliminary study of aerodynamic conditions near the nozzle contact on no-load. British Electr. and Allied Industries Research Association, Technical Report G/T 220, 1948.

70. *Keenan, J. H.*, *Kaye, J.*, Gas Tables. Thermodynamic properties of air, products of combustion, and component gases and compressible flow functions. New York 1948.

71. *Paterson, S.*, The reflection of a plane shock wave at a gaseous interface. Physical Society (London), Proc. 61(1948), pp. 119–121.

72. *Wild, R. W.*, The electrical measurement of pressure and strain, with particular reference to the testing of circuit breakers. IEE Journal, Part II, 95(1948): 48, pp. 733–749.

73. *Herpin, A.*, La théorie cinétique de l'onde de choc. Revue Scientifique 86(1948), pp. 35–37.

74. *Courant, R.*, *Friedrichs, K. O.*, Supersonic flow and shock waves. Interscience Publishers, New York 1948.

75. *Weibull, W.*, Waves in compressible media. (I. Basic equations. II. Plane continuous waves.) KTH Handlingar No. 18, 1948. (Transactions published by the Royal Institute of Technology, Stockholm.)

76. *Bannister, F. K.*, *Mucklow, G. F.*, Wave action following sudden release of compressed gas from a cylinder. Inst. Mech. Engrs., Proc. 159(1948), p. 269 ff.

77. *Patterson, G. N.*, Theory of the shock tube. Physical Review, 2nd Ser., 75(1949), p. 1294.

78. *Fletcher, C. H.*, *Weimer, D. K.*, *Bleakney, W.*, A shock tube for the study of transient gas flow. Physical Review, 2nd Ser., 75(1949), p. 1294.

79. *Weimer, D. K.*, *Fletcher, C. H.*, *Bleakney, W.*, Transonic flow in a shock tube. Journal Appl. Physics 20(1949): 4, pp. 418–419.

80. *Marlow, D. G., Nisewanger, C. R., Cady, W. M.,* Method for instantaneous measurement of velocity and temperature in high speed air flow. Journal Appl. Physics 20(1949): 8, pp. 771–776.

81. *Jenny, E.,* Berechnungen und Modellversuche über Druckwellen großer Amplituden in Auspuff-Leitungen. Promotionsarbeit. Thesis, Ameba-Druck, Basle 1949.

82. *Huber, P. W., Fitton, C. E., Delpino, F.,* Experimental investigation of moving pressure disturbances and shock waves, and correlation with one-dimensional unsteady-flow theory. National Advisory Comm. for Aeronautics (Washington), Techn. Memoranda, Note 1903 (July 1949), pp. 1–65.

    From Appl. Mechanics Review, 3(1950): 12, p. 414, the following extract may be cited concerning this work: "Pressure disturbances occur frequently in combustion and other related phenomena. While progress has been made in the development of the theory of unsteady flow in one dimension, little experimental verification has been attempted. This report contributes useful experimental information for comparison with theory, and shows that piezoelectric techniques can be successfully used with the shock tube. Schardin's method of calculating flow in shock tubes has been extended to include subsequent reflections and interactions of waves so that a complete time history may be determined. Measurements were made in a shock tube by means of piezoelectric transient pressure recording equipment. It should be pointed out, however, that tests involved relatively weak shock waves."

83. *Pillow, A. F.,* The formation and growth of shock waves in the one-dimensional motion of a gas. Cambridge Philos. Society, Proc. 45(1949) Part 4, pp. 558–586.

84. *Polachek, H., Seeger, R. J.,* On shock wave phenomena: Interaction of shock waves in gases. American Mathematical Soc. (New York), Proc. Symposia appl. Math. 1(1949), pp. 119–144; see also Physical Review 84(1951), pp. 922–928.

85. *Sauer, R.,* Shock waves in one-dimensional unsteady gas flow. Helvetica Physica Acta 22(1949): 4, pp. 467–472.

86. *Jenny, E.,* Eindimensionale instationäre Strömung unter Berücksichtigung von Reibung, Wärmezufuhr und Querschnittsänderung. Brown Boveri Mitt. 37(1950): 11, pp. 447–461.

87. *Mayenfisch, E.,* Plötzliches Vordringen einer bewegten Gassäule gegen eine ruhende. Schweizer. Archiv angew. Wissenschaft u. Technik 17(1951): 4, pp. 119–126.

88. *Schall, R., Thomer, G.,* Röntgenblitzaufnahmen von Stoßwellen in festen, flüssigen und gasförmigen Medien. Zeitschr. angew. Physik 3(1951): 2, pp. 41–44.

89. *Schiller, K. K.,* No-load pneumatic transients in air-blast circuit-breakers. Engineer 192 (1951): 4986, pp. 200–203.

90. *Wallace, F. J.,* The superimposition of plane waves of finite amplitude. Engineering 172 (1951): 4471, pp. 423–425.

91. *Zoller, K.,* Zur Struktur des Verdichtungsstoßes. Zeitschrift f. Physik 130(1951): 1, pp. 1–38.

92. *Forwald, H.,* Elektriska tryckluftsströmbrytare, särskilt ur pneumatisk synpunkt. (Air-blast circuit-breakers, particularly from a pneumatic point of view.) Tryckluft 6(1951): 1–2, pp. 1–8. (In Swedish.)

93. *Frederiksen, E.,* Luftpulsationer i rörsystemer. Teoretiske og experimentelle undersögelser paa basis av impedansbegrebet. (Air waves in tube systems. Theoretical and experimental investigations based on the conception of impedance.) Thesis, Institute of Technology of Denmark, Copenhagen 1954. (In Danish.)

94. *Rudinger, G.,* Wave diagrams for nonsteady flow in ducts. Nostrand, New York 1955.

95. *von Mises, R.,* Mathematical theory of compressible fluid flow. Academic Press, New York 1958.

This paper was received in August, 1959, and has been published in Asea Research No. 5, 1960.

[illegible]

[illegible]

[illegible]

[illegible]

[illegible]

[illegible]

[illegible]

[illegible]

[illegible]

[illegible]

[illegible]

[illegible]

[illegible]

[illegible]

[illegible]

[illegible]

[illegible]

[illegible]

THE LAST VOLUMES OF ACTA POLYTECHNICA PHYSICS INCLUDING NUCLEONICS SERIES

(The predecessor of Acta Polytechnica Scandinavica)

Volume 3

Nr 1 Svartholm, N: *Two Problems in the Theory of the Slowing Down of Neutrons by Collissions with Atomic Nuclei.* Acta P 177 (1955), 15 pp, Sw. Kr. 5: 00 UDC 539.185.7

Nr 2 Bolinder, F E: *The Relationship of Physical Applications of Fourier Transforms in Various Fields of Wave Theory and Circuitry.* Acta P 189 (1956), 22 pp, Sw. Kr 6: 00 UDC 517.512.2:621.37

Nr 3 Brundell, P-O, and Enander, B: *The Neutron-Proton System with a Central Exponential Potential. II.* Acta P 190 (1956), 13 pp, Sw. Kr 2: 00 UDC 530.145:539.185

Nr 4 Bäckström, M: *Einfache Theorie der Gaszirkulation in Sorptionskälteapparaten nach v. Platen und Munters.* Acta P 195 (1956), 71 pp, Sw. Kr 8: 00 UDC 621.575

Nr 5 Granström, S A: *Loading Characteristics of Air Blasts from Detonating Charges.* Acta P 196 (1956), 93 pp, Sw. Kr 10: 00 UDC 624.042.3:533.6.011.72

Nr 6 Strandell, N: *A Photographic Method of Studying the Spread of Trochoidal Electron Beams.* Acta P 204 (1956), 13 pp. Sw. Kr 2: 50 UDC 621.385.16.537.533.7.087.5

Nr 7 Zimen, K E: *Diffusion von Edelgasatomen die durch Kernreaktion in festen Stoffen gebildet werden (Edelgasdiffusion in Festkörpern 1)*
Inthoff, W, und Zimen, K E: *Kinetik der Diffusion radioaktiver Edelgase aus festen Stoffen nach Bestrahlung (Edelgasdiffusion in Festkörpern 2)* Acta P 206 (1956), 7+15 pp, Sw. Kr 6: 00 UDC 533.15:546.29-16:539.17

Nr 8 Bäckström, M: *Entropy-Enthalpy Diagram for Water Vapour and Liquid Extended to Higher Temperatures and Pressures.* Acta P 207 (1956), 23 pp, Sw. Kr 5: 00 UDC 536.722:536.75:621.1.01(084 21)

Nr 9 Meyer, N I: *Switching Time in P-N Junction Diodes with Built-In Drift Field* Acta P 210 (1957), 32 pp, Sw. Kr 5: 00 UDC 537.311.33

Nr 10 Olsen, H, Romberg, W and Wergeland, H: *Reaction of Sound Waves and its Application for Absolute Measurement of Intensity* Acta P 226 (1957), 13 pp Sw Kr 7: 00 UDC 534.61

Nr 11 Andersson, B J: *Studies on the Circulation in Organic Systems with Applications to Indicator Methods.* Acta P 229 (1957), 19 pp, Sw. Kr 3: 00 UDC 612.13:532.574.8

ACTA POLYTECHNICA SCANDINAVICA PHYSICS INCLUDING NUCLEONICS

Ph 1 Fant, C G M: *Modern Instruments and Methods for Acoustic Studies of Speech.* (Acta P. 246/1958), 83 pp, Sw. Kr 7: 00 UDC 534.154:612.789.

Ph 2 Stubb, T: *The Measurement of Conductivity in Semiconductors with the aid of Microwaves.* (Acta P 259/1959) 14 pp, Sw. Kr. 7.00 UDC 537.311.33

Ph 3 Stubb, T: *Untersuchung über die Lebensdauer der Minoritätsträger in Germanium.* (Acta P 269/1960) 17 pp. Sw.Kr. 7.00 UDC 537.311.33

Ph 4 Roos, Matts: *Approximate gamma ray flux calculations outside a reactor core.* (Acta P. 273/1960) 24 pp. Sw. Kr. 7.00 UDC 539.122:621.039.538

Ph 5 Härlin, A: *Elementary Analysis and Heat Values* and Widell, T: *Enthalpy Diagram for Flue Gases.* (Acta P. 275/1960) 28 pp. Sw. Kr. 7: 00 UDC 536.662 + 536.722

Ph 6 Cyvin, Sven J: *Mean Amplitudes of Vibration in Molecular Structure Studies.* (Acta P. 279/1960) 226+6 pp, Sw. Kr. UDC 539.19

Ph 7 Jensen, Erling: *General Theory on Spin Echoes for Any Combination of any Number of Pulses. Introduction of a simple «Spin-Echo Diagram».* (Acta P. 283/1960) 20 pp, Sw. Kr. 7: 00 UDC 539.143.4

Ph 8 Mørch, K. A.: *Measurement of Total Acoustic Power of Sources of Sound in a Reverberation Chamber.* (Acta P 286/1960). 25 pp, Sw. Kr. 7:00. UDC 534.62

Ph 9 Jääskeläinen, P.: *On Microwave Conductivity, Noise, and Oscillations of Gas Discharge Plasma.* (Acta P. 291/1960). 24 pp, Sw. Kr. 7:00. UDC 537.562:621.391.822.2

Ph 10 Forwald, Haakon: *Wave Phenomena in Compressed-Air Ducts.* (Acta P. 292/1961). 147 pp. Sw. Kr. 14:00. UDC 533.17:534.213.4-13:621.315.54

Price Sw. Kr. 14: —

UPPSALA 1961
APPELBERGS BOKTRYCKERI AB